UNIVERSIDAD DE CANTABRIA

ESCUELA TÉCNICA SUPERIOR DE INGENIEROS INDUSTRIALES Y DE TELECOMUNICACIÓN

TESIS DOCTORAL

Desarrollo de nuevos dispositivos y técnicas para espectroscopía inducida por láser

Autor: **FRANCISCO ANABITARTE GARCÍA**
Directores: **JOSÉ MIGUEL LÓPEZ HIGUERA**
ADOLFO COBO GARCÍA

SANTANDER, 2012

UNIVERSIDAD DE CANTABRIA

ESCUELA TÉCNICA SUPERIOR DE INGENIEROS INDUSTRIALES Y DE TELECOMUNICACIÓN

DEPARTAMENTO DE TECNOLOGÍA ELECTRÓNICA, INGENIERÍA DE SISTEMAS Y AUTOMÁTICA

TESIS DOCTORAL

Presentada por: Francisco Anabitarte García
Ingeniero de Telecomunicación

Para acceder al título de: Doctor por la Universidad de Cantabria

Dirigida por: José Miguel López Higuera
Doctor Ingeniero de Telecomunicación

Adolfo Cobo García
Doctor Ingeniero de Telecomunicación

Santander, 2012

Tesis Doctoral: **Desarrollo de nuevos dispositivos y técnicas para espectroscopía inducida por laser**

Autor: **Francisco Anabitarte García**
Aspirante a Doctor Ingeniero de Telecomunicación

Directores: **José Miguel López Higuera**
Catedrático de Universidad
Universidad de Cantabria
Adolfo Cobo García
Profesor Titular de Universidad
Universidad de Cantabria

Tribunal que juzgó la Tesis Doctoral:

Presidente: ……..

……..

Vocal 1: ……..

……..

Vocal 2: ……..

……..

Vocal 3: ……..

……..

Secretario: ……..

……..

El tribunal acuerda otorgarle la calificación de:……

Santander, a…… de…… de 2012

A Iratxe

De vez en cuando vale la pena salirse del

camino, sumergirse en un bosque.

Encontrará cosas que nunca había visto.

Alexander Graham Bell

Preface

This thesis has been carried out in the Photonics Engineering Group of the Electronics Technology, Systems and Automation Engineering Department in the University of Cantabria. I would like to express my gratitude to the supervisors of this thesis, José Miguel López-Higuera and Adolfo Cobo García for their invaluable guidance and supervision throughout this thesis work. Furthermore, I would like to thank all my colleagues at this research group for their support and collaboration.

In addition, I would like to express my sincere thanks to Prof. Michael S. Angel for his supervision and help during my 3-month stay at Department of Chemistry and Biochemistry of University of South Carolina (USC), United States. I am also grateful to Dr. Vincenzo Palleschi for allowing me to spend 3 months at Istituto di Chimica dei Composti Organometallici of Consiglio Nazionale delle Ricerche (CNR) of Pisa, Italy. Janna Register from USC and Lorenzo Pardini from CNR as well as coworkers at USC and CNR are gratefully acknowledged for their support and help.

The funding of this work has been provided by the Spanish Government's Ministry of Education, culture and sports through the grant AP2007-02230. I am also grateful for support from the Spanish Government's Ministry of Science and Technology through the project TEC2010-20224-C02-02.

Acknowledgements

Una vez terminas de escribir todo el cuerpo de la Tesis, notas como te quitas un peso de encima. Al final de todo, por lo menos en mi caso, se escriben los agradecimientos, y lo que parecía una labor baladí, se puede transformar en un auténtico reto debido a un motivo muy conciso; El número de personas a las que tienes que agradecer cosas durante este periodo es enorme. Espero que en esta vorágine de gratitud, no se me olvide regalarle el oído a alguien importante, pero voy a intentar no dejar a nadie en la cuneta.

Las personas que más cerca han estado durante este trabajo han sido, obviamente, los miembros del Grupo de Ingeniería Fotónica. Empezamos juntos en los antiguos laboratorios de la escuela y ahora estamos en una nueva localización, y durante ambos periodos hay gente que permanece y otros que se han ido. De los que quedan me gustaría destacar a mis directores de Tesis, José Miguel y Adolfo por su apoyo incondicional y por conseguir que el barco llegue finalmente a puerto. No me quiero olvidar por supuesto de Luis que lo mismo te puede ayudar con un grating que con una botella de whisky, ni tampoco dejo en el tintero a Chus, con el que he compartido publicaciones y trabajos. Olga, Marian y Fran son las tres personas con las que he compartido docencia; muchas gracias por dejarme trabajar con vosotros. También agradezco los momentos compartidos a los compañeros que están actualmente compartiendo despacho conmigo, Hany, Rubén, Ángel y Alma y a todos los que han pasado por aquí, como Manu, Alba, Carlos, Pedrito o Manu el sevillano. De todos estos que han pasado agradecer especialmente a Ana, Bea, Paula y Junior, por su ayuda y por ser mis amigos este tiempo. Tampoco se me olvidan los chicos de desarrollo, especialmente Bubka por su ayuda y Rober por ser “especial”, así como María por hacernos las cosas difíciles fáciles. Solo quedan algunos profes, pero no por ser los últimos son menos importantes. Gracias Antonio y Mauro ya que sin todos vosotros y vuestra ayuda, esto no estaría escrito.

Otras personas que merecen una mención especial son Sara y Bea, nuestras secres, y todos los demás miembros del departamento TEISA. Al final, todos ponen un granito de arena en este trabajo.

Además de las personas de la Universidad de Cantabria, hay personas en otras partes del globo que merecen estar aquí. Gracias a Vince y a Mike, mis supervisores en Italia y EEUU, por enseñarme un enorme porcentaje de lo que sé sobre LIBS y por acogerme en vuestros laboratorios. Gracias a Janna especialmente y a Chris, Nate y Oscar, por compartir laboratorio, combates y cervezas, mis días en Carolina del Sur fueron más cómodos con vosotros. En Italia dejo también amigos, como Diego, mi amigo argentino, Stefano o Giulia, pero mención especial merece Lorenzo por su apoyo totalmente desinteresado tanto en Italia como desde la lejanía.

Después del mundo laboral, toca agradecer al entorno familiar. Gracias sobre todo a mis padres y a mi hermana, por apoyarme y animarme tanto a empezar esta andadura como a desarrollarla y terminarla. Estas personas siempre han aportado todo lo necesario para que yo alcanzara todo lo que quisiera académicamente y esto ha supuesto un gran sacrificio que solamente pago con mi gratitud y cariño. Gracias a todos mis familiares por vuestro apoyo, sois unos cuantos y no voy a escribir todos los nombres para evitar olvidos embarazosos. También sé que hay algunas personas que ya no están con nosotros y que hubieran disfrutado viendo este trabajo. A todos ellos va un pedazo de mi recuerdo y si en ese pedazo hay otro de mi memoria, podréis ver cómo este trabajo ha finalizado.

Muchas gracias también a todos mis amigos. Ellos están en su gran mayoría desconectados de mi trabajo, pero el mero hecho de poder quedar con ellos para desconectar aporta el equilibrio necesario para todo esto.

Finalmente, aunque probablemente sea esta la persona más importante de todas, gracias Iratxe, que empezó todo esto como mi novia y lo acaba como mi mujer, y ha soportado tanto los buenos momentos como los pozos de los que hay que salir durante estos años. Muchas gracias, esto te lo dedico especialmente a ti.

No sé si se me olvida alguien, pero teniendo en cuenta la calidad de mi memoria para este tipo de cosas, puede ser que con las personas que se me olvidan pudiera escribir un texto del tamaño de este documento. A todos vosotros, gracias y no os enfadéis.

Abstract

Light-matter interaction can provide rich information about the nature of matter. Spectroscopy is the science that studies this interaction in a wavelength-resolved manner, and has become a very valuable tool for optical characterization of any kind of material.

Laser Induced Breakdown Spectroscopy (LIBS) is a kind of laser spectroscopy. LIBS uses a high energy pulsed laser to extract constituent elements and charges from a small amount of the sample, inducing the formation of plasma. This ionized gas emits optical radiation during its cooling process, having these light spectral features of each chemical element which composes the sample, thus allowing their identification.

LIBS can work with samples in different states (solids, liquids and gases) without any or an easy sample preparation. The identification of elements and its quantization is possible with a fast analysis. LIBS ablates the sample, but only a crater of several micrometers is created. For that reason LIBS is considered as a microdestructive technique. These features and the developments of better laser sources, detectors or algorithms explain the increasing of the scientific and industrial interest on LIBS despite the fact that the equipment is still expensive and there are other spectroscopic techniques with better detection limits.

The first part of the document is an introduction to this thesis work. Accordingly, a brief state of the art about Laser Induced Breakdown Spectroscopy (LIBS) is presented. The aim of this state of the art is to give a brief LIBS background and to identify fields where new research lines can be started. The objectives to be reached are then established and finally, the structure of this thesis work is exposed.

The second part shows different contributions to the development of the LIBS technique. These contributions are related to the design of new sensors for the detection of acoustic LIBS signal based on optical fibers using different kind of

transducers and techniques. Besides, contributions to new algorithms for LIBS quantitative analysis or for blind sample classification are presented. The last section of this part is devoted to real applications of LIBS for real fields, specifically for archaeology and the industry.

The third part shows the conclusions of this thesis work and the open research lines. Finally, the fourth part is devoted to the bibliography and shows the list of published works as a result of this PhD period.

Acronyms

AAS: Atomic Absorption Spectroscopy.

ANN: Artificial Neural Networks.

APD: Avalanche PhotoDiode.

CCD: Charge Coupled Device.

CF-LIBS: Calibration Free Laser Induced Breakdown Spectroscopy.

CNR: Consiglio Nazionale delle Ricerche.

DP-LIBS: Dual Pulse Laser Induced Breakdown Spectroscopy.

ETA-AAS: ElectroThermal Atomization – Atomic Absorption Spectrometry.

FBG: Fiber Bragg Grating.

FOC: Fiber Optic Cables.

FPS: Frames per second.

FTIR: Fourier Transform InfraRed spectroscopy.

HAZ: Heat Affected Zone.

He-Ne: Helium-Neon.

ICCD: Intensified Charge Coupled Device.

ICP: Inductively coupled plasma.

ICP-AES: Inductively Coupled plasma – Atomic Emission Spectrometry.

ICP-MS: Inductively coupled plasma – Mass Spectrometry.

ICP-OES: Inductively Coupled plasma – Optical Emission Spectrometry.

IPCF: Instituto per i Procesi Chimico-Fisici.

IPDA: Intensified Photodiode Array.

IR: Infrared.

Knn: K nearest neighbors.

LASER: Light Amplification by Stimulated Emission of Radiation.

LDA: Linear Discriminant Analysis.

LIBS: Laser Induced Breakdown Spectroscopy.

LSC: Laser Supported Combustion.

LSD: Laser Supported Detonation.

LSR: Laser Supported Radiation.

LTE: Local Thermodynamic Equilibrium.

LTSD: Lens to Sample Distance.

MODI: Mobile Dual-Pulse Instrument.

MOiCO: Moment Of inertia of the Co-Occurrence matrix.

MSL: Mars Science Laboratory.

Nd:YAG: Neodymium-doped Yttrium Aluminum Garnet.

OC-LIBS: Optical Catapulting Laser Induced Breakdown Spectroscopy.

PCA: Principal Component Analysis.

PCF: Photonic Crystal Fibers.

PDA: Photodiode Array.

PMMA: Poly(Methyl Methacrylate).

PMT: PhotoMultiplier tube.

POF: Plastic Optical Fiber.

Ppb: Parts per billion.

Ppm: Parts per million

PSO: Particle Swarm Optimization.

Py-GC/MS: Pyrolysis Gas Chromatography Mass Spectrometry.

RC: Real Composition.

RSD: Relative Standard Deviation.

SFFS: Sequential Floating Forward Selection.

ST-LIBS: Stand-Off Laser Induced Breakdown Spectroscopy.

SVM: Support Vector Machines.

THSP: Temporal History of Speckle Pattern.

TL: ThermoLuminescence analysis.

UV: Ultraviolet.

XRF: X-Ray Fluorescence.

Index

Part I

Preliminary

This part is introduction to this thesis work. Accordingly, a brief state of the art about Laser Induced Breakdown Spectroscopy (LIBS) is presented. The aim of this state of the art is to give a brief LIBS background and to identify fields where new research lines can be started. The objectives to be reached are them established and finally, the structure of this thesis work is exposed.

Chapter 1

Introduction: Brief History of Laser Induced Breakdown Spectroscopy (LIBS)

Since early 1800's, researchers realized that there were different elements which emits light with different colors. Atomic theory helped scientist to discover that these colors or wavelengths were different for each element and the information was a "fingerprint" which allowed them to identify them. It was the beginning of spectrochemical techniques based on atomic emission.

The first sources of atomic emission spectra where the sun, the flames or gas discharges, and other kind of sources developed more recently, like inductively coupled plasmas (ICP). These sources were plasmas, and researchers tried to discover new ways to induce plasmas in different kind of samples, in order to analyze the light emission and identify the elements which compose the sample.

Laser sources were employed to induce plasmas in 1963 for the first time when the production of sparks in air using a pulsed ruby laser was observed. The main problem at the beginning, between 1960's and 1980's, was that the production of laser sparks was in its infancy due to the development of laser sources in these years and the capability of detection was too poor for the analysis of these sparks. Laser sources were used to vaporize a small amount of material which was analyzed using techniques like conventional electrode spark (Moenke and Moenke-Blankenburg, 1973). A few time after, tunable dye lasers were developed, allowing the use of a laser wavelength which was resonant with an atomic transition of the species under analysis. The absorption of the laser light or the intensity of the laser-induced fluorescence was used to measure the presence of this element. These

techniques need to tune the laser for each specie and are less adaptable and flexible than a hot plasma in which a large number of species can be excited and analyzed at the same time.

The acronym of Laser Induced Breakdown Spectroscopy (LIBS) has a history which has passed parallel to the acronym LASER (Light Amplification by Stimulated Emission of Radiation). The first real use of sparks as a source of spectral information was in 1983 when D. A. Cremers and L. J. Radziemsky at Los Alamos National Laboratory in U.S.A. proposed a tool for both quantitative and qualitative chemical analysis based on laser-produced plasmas. They named this technique Laser Induced Breakdown Spectroscopy and in *Laser Induced Plasma & Applications,* published in 1989, they summarized all the process and physics of laser produced plasmas. They described LIBS as a useful tool for chemical analysis with a light sample preparation and predicted a widespread use of this technique due to the development of lasers and detectors in the future.

This prediction was successful thanks to the development during 1990's of more reliable lasers with improved features and reduced cost and size, miniaturized spectrographs which allowed the detection of broadband spectra, and detectors with better signal-to noise ratio. These devices were the tools that LIBS needed to grow.

LIBS has developed like a major analytical technology. The main feature which allows this is that a LIBS set-up is easy to prepare in comparison with other kind of spectrochemical techniques. One has only to focalize a pulsed laser beam in or on the sample and acquire the plasma light with a spectrometer attached to a detector. The sample can be a gas, a solid or a liquid, and no sample, or a very easy sample preparation, is required. These features allow in situ analysis and the small amount of ablated material enable the analysis of valuable samples. However, despite the fact that the technique is easy to use, the processes involved in plasma formation and evolution are not simple and a big amount of parameters are involved in the process. For that reason, LIBS is a technique difficult to adjust in order to obtain the best performance. LIBS researchers are trying to solve these disadvantages, changing set-up parameters like laser wavelength, developing new statistical

algorithms to extract more information from LIBS spectra or creating new algorithms in order to allow an accurate quantitative chemical analysis.

Nowadays, LIBS is introduced in a wide range of applications in different fields. Human tissues, teeth or bones are being analyzed using LIBS for different purposes, like the detection of tumor cells or other kind of diseases. Pollen or bacteria are being analyzed trying to identify them using LIBS. Applications for homeland security, like the detection of traces of explosives, are also being tested. Besides, LIBS is beginning to be a useful tool for industrial applications, like the detection of impurities for quality control. Even at the same time that the author of this Thesis work is writing it, a spacecraft is arriving to Mars to analyze its surface and one of the analytical tools that this probe uses is LIBS.

Chapter 2

State of the art of Laser Induced Breakdown Spectroscopy.

LIBS is an atomic emission spectroscopy technique which uses highly energetic laser pulses to provoke optical sample excitation [1]. The interaction between focused laser pulses and the sample creates plasma, composed of ionized matter [2]. Plasma Light emissions can provide “spectral signatures” of chemical composition of many different kinds of materials in solid, liquid or gas state [3]. LIBS can provide an easy, fast and in-situ chemical analysis with a reasonable precision, detection limits and cost. Additionally, as there is no need for sample preparation, it could be considered as a “put & play” technique suitable for a wide range of applications [1]

Considerable progress has been made during the last few years on very different and versatile applications of LIBS, including remote material assessment in nuclear power stations, geological analysis in space exploration, diagnostics of archaeological objects, metal diffusion in solar cells, etc [4]. Today, LIBS is considered an attractive and effective technique when a fast and whole chemical analysis at the atomic level is required.

Some of the established techniques for analytical atomic spectrometry are Inductively Coupled Plasma-Atomic Emission Spectrometry (ICP-AES), Electrothermal Atomization-Atomic Absorption Spectrometry (ETA-AAS) and Inductively Coupled Plasma-Mass Spectrometry (ICP-MS) [5]. However, development on LIBS during recent years has reduced its gap in performance with respect to these other well-known approaches [5].

This chapter begins with a brief explanation of the physics involved in plasma induction and the features of this plasma in LIBS, and is then followed by a description of the basic devices which compose a LIBS set-up. These devices will be described associating their features with the properties of the induced plasma. Moreover, different kinds of analysis algorithms will be introduced in order to go beyond the “spectral signatures” obtained with the technique. Finally, some key LIBS applications will be described, and the main research challenges that this approach faces at the moment will be discussed. It is important to notice that this chapter has another important goal. Different fields where research efforts should be carried out will be exposed in order to detect and identify the research lines which have been followed during this PhD.

1. Fundamentals of plasma physics and its spectra

Understanding the plasma physics of LIBS is essential to provide an optimized setting for LIBS measurements. A large number of environmental factors affect the plasma life time and features, changing the spectral emission and the performance of this technique for chemical analysis at the atomic level.

1.1 Laser ablation and plasma physics of LIBS

Laser-matter interactions are governed by quantum mechanics laws describing how photons area absorbed or emitted by atoms. If an electron absorbs a photon, the electron reaches a higher energy quantum mechanical state. Electrons tend to the lower possible energy levels, and in the decay process the electron emits a photon (de-excitation of the atom). The different energy levels of each kind of atom induces different and concrete photon energies for each kind of atom, with narrowband emissions due to the quantization, with an uncertainty defined by Heisenberg uncertainty principle. These emissions are the spectral emission lines [6] found in LIBS spectra and their features associated with energy levels are well known for each atom [7].

If the energy applied to the atom is high enough (overcoming the ionization potential), electrons can be detached by the atom inducing free electrons and positive ions (cations). Initially, the detached electron is the most external one (the furthest with respect to the nucleus) because it has the lowest ionization potential, but with higher energy supply it is possible to detached more electrons overcoming the second ionization potential, the third and so on. These ions can emit photons in the recombination process (cations absorbs a free electron in a process called free-bound transition) or in the de-excitation process (the cations and the electrons lose energy due to kinetic process in a process called free-free transition). These emissions can be continuum due to the different energies of the ions and the different energy transitions, however cations de-excitation has discrete (or quantized) set of energy levels which characteristic emission lines for each kind of element, allowing its identification together with the atomic emission lines [7] .

The plasma induced by the interaction pulsed laser-sample, emits light which consists of discrete lines, bands and an overlying continuum. These discrete lines, which characterize the material, have three main features; wavelength, intensity and shape. These parameters depend of both the structure of the emitting atoms and their environment. Each kind of atom has some different energy levels which determine the wavelength of the line. Besides, the identification of the elements in the sample, that is, the calculation of the amount of each element in the sample from the line intensities, is possible, but considering different necessary conditions fixed by local thermodynamic equilibrium (LTE condition) or problems related with matrix effects which can reduce the accuracy of quantitative analysis [8, 9].

On the other hand, the intensity and shape of the lines depend strongly on the environment of the emitting atom. For not too high plasma densities, both the natural broadening (due to Heisenberg's uncertain principle) and the Doppler broadening[1] dominate the linear shape [10]. For high plasma densities, atoms in the plasma are affected by electric fields due to fast moving electrons and slow moving ions, and these electric fields split and shift the atomic energy levels. As a consequence of these perturbations of the levels, the emission lines are broadened and they change

[1] Doppler Broadening is due to the thermal motion of the emitters, the light emitted by each particle can be slightly red- or blue-shifted, and the final effect is a broadening of the line

their intensity and shape. This effect is known as the Stark effect [10] and it dominates the line shape for dense plasmas. This broadening together with the different parameters of spectral lines (intensities and shapes) and even the continuum radiation features can be useful to determine plasma parameters, such as electron temperature, pressure and electron density [2, 7]. These parameters are very important to characterize the plasma, giving information about its physical state. Moreover the calculation of these parameters is necessary because the set-up has to be tuned to ensure LTE, key condition for an accurate quantitative analysis [11].

Basically, there are three stages in the plasma life time (Figure 1). The first one is the ignition process. This process includes bond breaking and plasma shielding during the laser pulse, depending on laser type, irradiance and pulse duration.

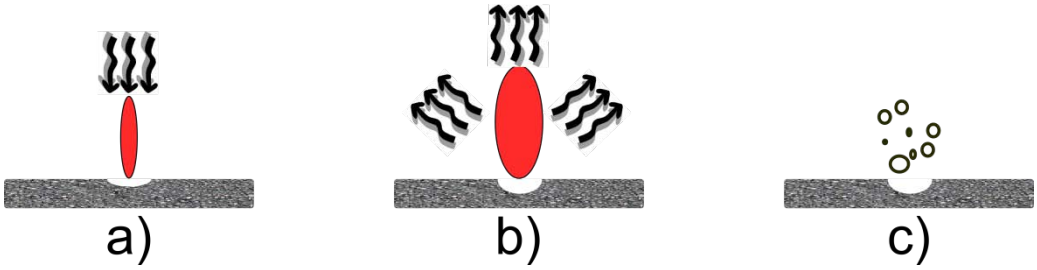

Figure 1: Plasma life stages: a) Plasma ignition, b) plasma expansion and cooling and c) particle ejection and condensation [7].

If the selected laser is a femtosecond one, non-thermal processes will dominate the ionization. The pulse is too short to induce thermal effects; hence other effects should ionize the atoms, depending of the kind of sample. The pulse has a huge amount of energy, and effects like multi-photon absorption and ionization, tunneling and avalanche ionization, excite the sample. With this amount of energy, the electron-hole created will induce emission of x-rays, hot electrons and photoemission. This will create highly charged ions through a process called Coulomb explosion [7]. The absence of thermal effects creates a crater with highly defined edges without melted or deposited materials.

In contrast, nanosecond lasers induce other effects. The electron-lattice heating time is around $10^{-12}s$, much shorter than the pulse time. This causes thermal effects to dominate the ionization process. Briefly, the laser energy melts and vaporizes the

sample, and the temperature increase ionizes the atoms. If the irradiance is high enough, non-thermal effects will be induced too, and both will ionize the sample. Between $10^{-9}s$ and $10^{-8}s$, plasma becomes opaque for laser radiation, thus the last part of the laser pulse interacts with the plasma surface and will be absorbed or reflected, hence it will not ionize much more material. This effect is called plasma shielding and is strongly dependent on environmental conditions (surrounding gases or vacuum) and experimental conditions (laser irradiance and wavelength) [12, 13]. This shielding reduces the ablation rate because the radiation does not reach the sample surface. To Summarize, this kind of laser induces a crater with melted and deposited material around it but at the same time the plasma is re-heated and the lifetime and size of plasma is higher [13, 14].

The next step in plasma life is critical for optimization of LIBS spectral acquisition because the plasma causes atomic emission during the cooling process. After ignition, the plasma will continue expanding and cooling. At the same time, the electron temperature and density will change. This process depends on ablated mass, spot size, energy coupled to the sample and environmental conditions (state of the sample, pressure, etc.).

If the plasma is induced in a vacuum, the plasma-plume expands adiabatically and the expansion of the ablated material can be described by the Euler equations of hydrodynamics [15]. In contrast, if the surrounding medium is a gas or a liquid, the plume will compress the surrounding medium and produce shockwaves. In this situation the plasma plume is a mixture of atoms and ions from both vaporized material and ambient gas. The shockwave expansion can be described by Sedov's theory [7, 16].

Plasma temporal evolution changes with pulse duration. For pulses longer than about 5ps, the laser-plasma interactions result in plasma heating and the plasma temperature increases with pulse duration [17]. For short times (below 30 ns), fs-induced plasma emission intensity decays while ns-induced plasma becomes hotter [18]. The last part of the nanosecond laser pulse is absorbed by the plasma, reheating it, elongating its lifetime and increasing line emission, but at the same time, the background is higher and this decreases the sensitivity for nanosecond set-ups.

A way to improve the performance has been proposed [19]: a femtosecond laser is used to ablate the sample and nanosecond or picosecond pulses reheat the plasma afterward.

The last stage of the plasma life is not interesting for LIBS measurements. A quantity of ablated mass is not excited as vapor or plasma; hence this amount of material is ablated as particles, creating condensed vapor, liquid sample ejection or solid sample exfoliation, and this mass does not emit radiation. Moreover, plasma becomes cold after their emission stage and nanoparticles are created in the recombination process between free ions and electrons which compose this plasma.

1.2 Plasma emission spectra

The emission lines from the atomic species can be hidden by continuum radiation that is caused by two processes. The first one is due to radiative recombination. Both continuum and line photons can be produced in such a recombination event as the electron passes from the free state into the upper bound levels of the ion and then cascades down to form a ground state ion. The other effect involved in continuum radiation is called Bremsstrahlung. This effect is related to free-free transitions corresponding to loss of kinetic energy by an electron in the field of an ion. The electron loses energy in the deceleration process when it travels into the field of the ion, emitting photons in different wavelengths, depending on the gap between its kinetic energy after and before the deceleration process. Continuum emission can hide atomic emission peaks, thus this effect should be avoided.

The continuum emission depends of both temperature and density of plasma. These parameters are too high in the initial stages of plasma, especially in the ignition. For this reason, the time control unit has to delay the acquisition window in order to avoid this continuum. For femtosecond lasers, the continuum emission is observed within one nanosecond after the laser ablation; hence the delay with these lasers should be greater than this time. For nanosecond lasers, atomic emission occurs after 1 microsecond and molecular emission occurs at later times from recombination of species in the plasma [2, 7, 14]. Inside this acquisition window, the initial stages of plasma life are characterized by a higher temperature and electron density. These

parameters provide a better emission of ionic lines, for that reason these initial stages are better to acquire ionic lines despite the continuum emission. These optimal acquisition windows depend strongly on the sample material and both environmental and experimental conditions, but the values given above can be interesting as a starting point for each kind of laser [20].

Lifetime for femtosecond induced plasmas is shorter and with less background. For that reason, the acquisition window size should be shorter for short pulses and femtosecond lasers are better for non-gated measurements because the background is weak and the LIBS sensitivity improves [14].

Generally, femtosecond lasers are a better choice to obtain highly accurate craters and for non-gated measurements, using delays of a few nanoseconds and small acquisition windows that can improve LIBS sensitivity. Nanosecond lasers create a melted crater and need delays of a few microseconds and larger windows with the advantages of low complexity in the laser system. There are other kinds of lasers, such as picosecond lasers, for which the time pulse is between a femtosecond and a nanosecond, hence the features are between the two [7].

2. Environment

The plasma size, propagation speed, energy and emission properties are related to the ambient gas into which the plasma expands. The ambient gas can help to prevent the plasma shielding. For example the gas can shield the sample from the laser beam if a gas breakdown occurs before sample vaporization [21]. These undesirable effects are less important for gases and aerosols, but they can be important for solid samples.

Gas pressure can influence plasma expansion. Low pressures increase energy losses and uniformity of the plasma energy distribution. The plasma expands almost freely at low pressures (less than 1 Torr) and the external part is colder because the higher energy loss. An increasing of pressure around 1 Torr reduces this energy loss and produces a more uniform temperature distribution on plasma volume [7]. In addition, different gases have different behaviors at different pressures [21].

The gas which surrounds the sample can change the plasma properties. Sdorra and Niemax [22] compared the effect on plasma parameters of different surrounding gases (argon, neon, helium, nitrogen and air) using a Nd:YAG laser on a copper sample. Argon atmosphere increased plasma temperature, electron density and emission intensity and reduced ablation rate and plasma temperature decay. This temperature behavior is due to argon low thermal conductivity, and the higher heat efficiency of argon induced a buffer plasma which shielded the sample surface and reduced the ablated mass. This shielding appeared with lower laser energy for argon atmosphere. Contrarily, Helium induced a lower temperature, density and emission intensity. Argon yielded the highest analyte emission intensity, except at high pressures with the best performance for neon.

At the same time, argon atmosphere offers other important effect. This gas reduces the generation of compounds like oxides from excited atoms which reduce the analyte emission intensity. Wisbrun et al. [23] found a higher emission intensity of Zn and better reproducibility due to the argon atmosphere.

Some kind of ambient gases can be necessary to obtain proper spectra. The observation of UV emission range is difficult. UV is commonly broken up into three rough groupings called UV-A, UV-B, and UV-C. Oxygen and nitrogen absorb UV-C. Besides, oxygen forms ozone. Ozone absorbs UV-C and some UV-B. Ozone also absorbs UV-B and re-radiates it randomly. This effect reduces the emission in UV range in atmospheric environment and an inert gas is necessary to obtain UV emission.

3. LIBS set-up components and main parameters.

The main devices involved in a LIBS analysis are shown in Figure 2. A high energy pulsed laser (usually in the nanosecond range), is directed at the sample [2]. This light energy vaporizes the sample and induces the plasma.

The spectrometer is in charge of diffracting the light collected, with a more or less complex optical system, in order to obtain the spectral signature. Then, the light is detected by using devices such as a photomultiplier tube (PMT), a photodiode array

(PDA) or a charge-coupled device (CCD) [2, 7]. Finally, the acquired spectrum is processed by a computer for further analysis. LIBS set-ups need an accurate time control to avoid some plasma life stages and to improve the spectral signature [2, 3, 7]. The choice of the laser combined with the set spectrometer-detector and time control, adapted to environmental conditions, can determine the success or failure of the experiment.

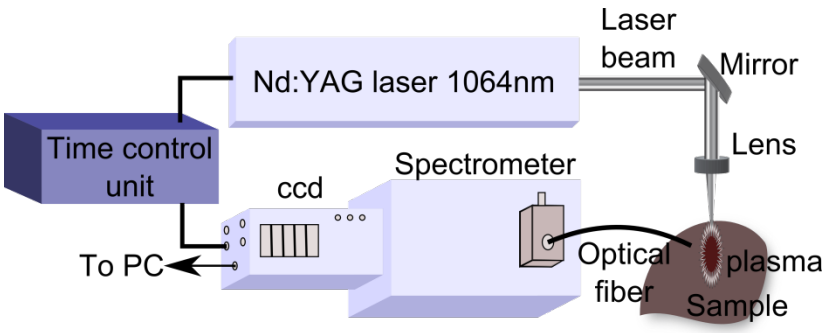

Figure 2: Typical LIBS set-up

3.1 Laser configurations for LIBS

The main device of LIBS is the laser. It generates the energy to induce the plasma and mainly determines the plasma features. The main parameters related to the laser are the pulse time (explained above), the energy per pulse, the wavelength and the number of pulses per burst [24]. Obviously, each application works better with a combination of these parameters. Nanosecond pulsed lasers are the most common for LIBS. Therefore, the most of this section is related to this kind of laser.

3.1.1 Laser wavelength

The wavelength influence on LIBS can be explained from two points of view; the laser-material interaction (energy absorption) and the plasma development and properties (plasma-material interaction).

When photon energy is higher than bond energy, photon ionization occurs and non-thermal affects are more important. For this reason, the plasma behavior depends on wavelength in nanosecond LIBS set-ups. In the same way, the optical penetration is shorter for UV lasers, providing higher laser energy per volume unit of material. In

general, the shorter the laser wavelength, the higher the ablation rate and the lower the elemental fractionation[2] [25].

The plasma ignition and its properties depend of wavelength. The plasma initiation with nanosecond lasers is provoked by two processes; the first one is inverse Bremsstrahlung by which free electrons gain energy from the laser during collisions among atoms and ions. The second one is photoionization of excited species and excitation of ground atoms with high energies. Laser coupling is better with shorter wavelengths, but at the same time the threshold for plasma formation is higher. This is because inverse Bremsstrahlung is more favorable for IR wavelengths [26].

In contrast, for short wavelengths (between 266 and 157 nm) the photoionization mechanism is more important. For this reason, the shorter the wavelength in this range, the lower the fluence necessary (energy per unit area) to initiate ablation [27]. In addition, when inverse Bremsstrahlung occurs, part of the nanosecond laser beam re-heats the plasma. This increases the plasma lifetime and intensity but also increases the background at the same time. Longer wavelengths increase inverse Bremsstrahlung plasma shielding, but reduce the ablation rate and increase elemental fractionation [28].

The most common laser used in LIBS is pulsed Nd:YAG [29]. This kind of laser provides a compact, reliable and easy way to produce plasmas in LIBS experiments. The fundamental mode of this laser is at 1064 nm and the pulse width is between 6-15 ns. This laser can provide harmonics at 532, 355 and 266 nm, which are less powerful and have shorter time pulses (between 4-8 nm) [2, 7]. The fundamental and the first harmonic are the most common wavelengths used in LIBS. These harmonics can be useful to work with different wavelengths in the same environmental conditions, because a lot of Nd:YAG lasers can produce all of them. Other kinds of lasers can be used in LIBS, such as CO_2 or excimer lasers to work in far IR or UV ranges respectively. Lasers based on fiber or dye technology can reduce the pulse width if the user is attempting to work with picosecond or femtosecond pulses.

[2] Elemental Fractionation is the redistribution of elements between solid and liquid phases which modifies plasma emission

3.1.2 Laser energy

The energy parameters related with laser material interaction are fluence (energy per unit area, $\mathrm{J/cm^2}$) and irradiance (energy per unit area and time, $\mathrm{W/cm^2}$). Ablation processes (melting, sublimation, erosion, explosion, etc.) have different fluence thresholds [30]. The effect of changes in the laser energy is related to laser wavelength and pulse time. Hence, it is difficult to analyze the energy effect alone. In general, the ablated mass and the ablation rate increase with laser energy.

The typical threshold level for gases is around $10^{11}\,\mathrm{W/cm^2}$ and $10^{10}\,\mathrm{W/cm^2}$ for liquids, solids and aerosols [2]. These values are for guidance and depend strongly on laser pulse time and environmental conditions, reaching up to around $10^{15}\,\mathrm{W/cm^2}$ for nitrogen at 760 Torr with a Nd:YAG laser, 1064 nm, 7 ps [2].

3.2 Acquisition time and delay.

The first stages of LIBS induced plasma are dominated by the continuum emission. The time gate of decay of this continuum radiation change with a wide range of experimental parameters, such as laser wavelength and pulse time, ambient pressure or sample features. Besides these experimental parameters fixes the time periods of atomic emission, the most interesting stage of LIBS plasmas.

Plasma evolution using an IR (Nd:YAG) and a UV (excimer) lasers has been analyzed to discover differences induced by laser wavelength [31]. The plasma continuum emission stage was around 400 ns for UV laser and several microseconds for IR lasers. Laser wavelength can affect the selection of delay time (gate delay) and integration time (gate window), and these parameters are essential to optimize the signal to background ratio. The analysis of plasma evolution for Zn and Cd in sand has been analyzed in other works, with an optimal gate delay of 0.5 µs and a gate window of 1.5 µs [23].

This analysis of optimal gate delay and window can be achieved optimizing the signal to background ratio and the repeatability of this parameter. For a Nd:YAG laser at the fundamental wavelength with power density of approximately 2 GW/cm^2, the best compromise between lower relative standard deviation (R.S.D.) and higher

signal-to-background ratio was found at a delay of approximately 6 μs. The integration time was fixed at 15 μs [20].

Actually, there are different points of view to optimize the gate delay and window and the big amount of experimental parameters involved in plasma evolution make it difficult to recommend valid values for these parameters. The selection should be determined case by case in order to achieve a compromise between high line intensity and low background. Briefly, for Nd:YAG lasers, both times for gate delay and gate window are in the order of microseconds but this values can change if another kind of results are sought.

3.3 Sequences of pulses: double pulse LIBS

Proposed twenty-eight years ago to improve the detection limits of some elements [32], dual pulse LIBS (DP-LIBS) configuration consists on the sequence of two laser pulses temporally spaced in the order of few nanoseconds or microseconds (depending on laser pulse time, the larger the pulse time, the larger the time delay between pulses). These two pulses can excite the same area and create two temporally spaced plasmas or the second pulse can reheat the plasma induced by the first one. Cremers et al. [32] were the pioneers using this technique in dissolved species in an aqueous solution. Enhanced emission from dissolved species was reported due to the formation of a bubble by the first laser pulse into which the second laser pulse was focused to create the plasma. Uebbing et al. [33] began to use DB-LIBS on solid samples. First pulse was used to ablate the material, and the second one was parallel to sample surface in order to reheat the ablated material. An increase in Mn and Al emission and less dependence on the matrix in which the element was found were observed in steel samples and glass. Sattman et al. [34] used bursts of pulses from the same flashlamp and found higher ablation rate for the sequence of pulses than for a pulse with the same energy that the sum of all the pulses of the burst. Later, the same research group used multi-pulse LIBS on steel in vacuum ultraviolet and detection limits of less than 10 μg/g for phosphorus, sulfur and carbon were reported [35]. Sturm et al. [36] obtained emission enhancements of 5 to 10 times using a dual pulse configuration with a 1064 nm and 266 nm laser

pulses. Angel et al. [37] found emission enhancements of 10 to 30 times using a pre-ablative orthogonal configuration.

Using DP-LIBS, atomic emission, signal-to-noise ratio and limit detection can be improved. Conversely, DP-LIBS can complicate the LIBS set-up, although the benefits can justify this complication. These improvements provide better detection limits than single pulse configurations due to the induced atomic emission enhancement. Figure 3 shows the most common dual pulse configurations.

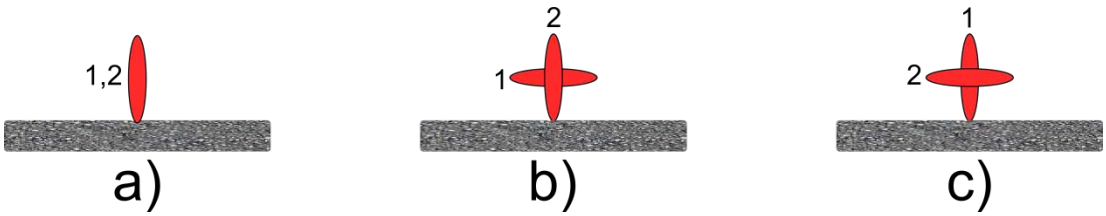

Figure 3: dual pulse configurations: a) shows collinear configuration; the first pulse ablates the sample and the second one reheats the plasma [34]. b) is an orthogonal pre-ablative configuration; the first pulse creates a spark on the surrounding media and the second one ablates the sample [14, 38]. c) shows the same idea as a), but the plasma is reheated in an orthogonal way [33].

The signal emission enhancement is due to different factors in these dual pulse configurations. This enhancement in collinear and orthogonal reheating is due to energetic issues. In collinear configurations, the second pulse increases the ablated material and, mainly, reheats the plasma, increasing its volume and its emission, but if the time between laser pulses is enough to allow the fading of the plasma, the second pulse interacts with the sample and ablates more material across the reduced atmosphere induced by the first pulse. In the orthogonal configuration, the second pulse does not ablate more material, but reheats the plasma and re-excites the material ablated by the first pulse. Other authors have given reasons for the signal enhancement on pre-heating orthogonal configurations, such as a reduction in density or pressure of the surrounding media due to the first pulse [37-40].

Other interesting way to use DP-LIBS is to combine laser pulses with different pulse times like a femtosecond and nanosecond pulses. Femtosecond laser pulses for single-pulse LIBS produce better ablation precision and better reproducibility between emission spectra of different pulses compared with nanosecond pulses

[41]. Consequently, it seems interesting to combine femtosecond and nanosecond dual pulse configuration in order to obtain an increasing of precision of DP-LIBS. Due to the improved ablation process using femtosecond lasers, the re-heating combination with a nanosecond laser to re-heat and a femtosecond laser to ablate should improve DP-LIBS performance. Very large enhancements were seen by using this configuration when the femtosecond pulse was used to ablate and a nanosecond pulse was used to re-heat, with a delay between them of ~5 μs and orthogonal configuration. This enhancement was about 80-fold for aluminium and 30-fold for copper with respect the same elements using a single femtosecond pulse [3]. Though, not clear results have been reported for orthogonal pre-ablative configuration. Signal enhancement has been observed for aluminum using a nanosecond pre-ablative spark and a femtosecond ablative pulse, but this enhancement was not reported for copper [3].]. Nanosecond ablation with a femtosecond pre-ablation spark obtained 4-fold enhancements for copper compared with nanosecond single-pulse LIBS. This improvement was reported using a delay between pulses of 6 μs and a 1 mm air spark height above the sample surface, although no signal enhancement was reported for aluminium [3].

3.4 Spectrometers and detectors.

The spectrometer or spectrograph is a device which diffracts the light emitted by the plasma. There are different designs, such as Littrow, Paschen-Runge, Echelle and Czerny-Turner [42, 43]. The Czerny-Turner spectrograph is the most common device in LIBS. This spectrograph is composed of an entrance slit, two mirrors and a diffraction grating. The light comes through the slit and reaches the first mirror which collimates the light, directing it onto the grating. Light is reflected at different angles according to its wavelength. The second mirror focuses the light on the focal plane where the detector is placed.

In recent years, the Echelle spectrograph has been used more extensively [43]. The Echelle spectrograph uses a diffraction grating placed at a high angle, producing a large dispersion in a small wavelength range in each order. As the orders are spatially mixed, a prism is used to separate them. The orders are stacked vertically on the focal plane. For that reason, Echelle devices need a two-dimensional

detector. Each vertical portion of the detector contains a part of the spectra and the software composes the whole spectrum.

Different kinds of detectors are used in LIBS, depending of the application. To measure light intensity without spectral decomposition, the photomultiplier tube (PMT) or avalanche photodiode (APD) can be used. On the other hand, for one-dimensional spatial information, the researcher can combine a spectrograph and a photodiode array (PDA), or an intensified photodiode array (IPDA) for time-resolved measurements.

If two-dimensional spatial information is required, the most common devices are charge coupled devices (CCD) and intensified CCD (ICCD). A CCD detector provides less background signal, although ICCD improves the signal-to-noise ratio and is better for time-resolved detection using integration windows of a few nanoseconds [44]. Another problem related to ICCDs is the price, which is much higher than conventional CCDs.

3.5 Collecting and focusing light: Geometrical set-up

The shape and emission intensity profile of induced plasma is a function of the laser power density and other parameters. Accordingly, a proper selection of experimental parameters can optimize the acquired spectra, and this set of parameters should be adjusted together.

There are two main parts related to light acquisition and focusing. Typical laser spots currently must be focused to increase the irradiance to induce plasma formation. Light from plasma must then be collected using devices such as optical fibers, lenses or combinations of both in order to guide it to the spectrometer.

3.5.1 Focusing laser pulses with lenses.

As the laser beam width from the majority of solid-state lasers is of the order of 6-8 mm, the most common lenses used to focus laser pulses have diameters of 25 or 50 mm and focal lengths between 50 and 150 mm. There are other applications such as stand-off set-ups where a multi-lens system or different lenses are required. The

material of the lens should have maximum transmission at laser wavelength and they must be coated with anti-reflection layers to minimize transmission losses[3].

Lens shape can improve the performance of the laser beam focalization. Eppler et al. [45] compared the precision to focalize the laser beam on a solid sample surface using spherical and cylindrical lens, obtaining a better precision with cylindrical one.

For solid samples usually the laser is focalized perpendicular to sample surface and the induction of plasma in the air above the sample surface is a common phenomenon which can shield the sample surface and reduce the ablation rate. This problem can be reduced fixing the distance between the lens and the sample a little shorter than the focal length of the focalization lens [46]. For liquids, a perpendicular focalization pattern can be a problem due to the ejection of droplets induced by plasma shockwave. These droplets stain the lenses and reduce the performance of LIBS set-up. Fichet et al. [47] proposed an angled configuration with an angle of 75º between laser beam and the perpendicular of sample surface which avoids stains on lenses.

3.5.2 Collecting light

A common set-up to acquire plasma light is shown in Figure 4. The first lens collimates the emitted light to improve the focalization of the second one into the fiber probe and to optimize the ratio of acquired light. This set-up can be adapted to different systems using only one lens, a multi-lens device and even only the fiber probe positioned in front of the spark. The features of lenses used to focus the plasma light are useful for this purpose, adapting them to different environmental features or set-ups. This configuration is perpendicular to the laser axis and the distance from the collection axis to the sample surface is critical because it usually integrates only a fraction of the light from the plasma plume. Lee et al. [48] studied the spatial features of plasma plumes induced on metallic samples. They measured the emission intensity along the axial direction perpendicular to sample surface and noted that plasma plume extension was about 2 mm for copper and 5 mm for lead, with a maximal emission 1 mm and 2 mm above sample surface. Thermal

[3] The laser beam can lose around 8% of its energy passing through an uncoated lens. Anti-reflection coatings can reduce this ratio to around 0.5%.

conductivity among other factors of sample material can affect this spatial distribution. For that reason is important to analyze the distance between collecting axis and sample surface for this kind of configuration.

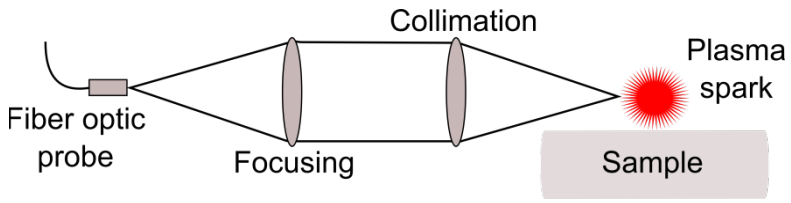

Figure 4: Typical perpendicular light acquisition system

Other kind of acquisition set-up is positioned axially to laser beam, that is, the plasma light is acquired from the same path that the laser pulse hits the sample. This configuration has less sensitivity to lens to sample distance and reduces the collection instabilities due to the increasing crater depth on a sequence of laser pulses over the same area, which increases this lens to sample distance [49]. For that reason the focal length of lenses used to acquire the plasma light on LIBS is keep large, at least several centimeters.

3.5.3 Optical fibers

Sometimes, the sample is far from the detection system, from the lasers or from both of them, and so a system based on lenses like the one shown in Figure 4 is unpractical [50]. In these situations or when the environment is too aggressive or the access restriction makes it difficult to induce the plasma or acquire the light, fiber optic cables (FOCs) or bundles are used [51-53]. This feature is especially useful in remote measurements in industrial environments. An optical fiber can be positioned near to plasma plume (few millimeters far to avoid thermal problems) to acquire plasma light. A comparison between the performance of a FOC and a collection set-up based on lenses has been carried out and the detection limits were very similar for both systems [52]. Although the most common optical fibers in LIBS are made of fused silica (with diameters between 50 µm and 1 mm), different kinds of fibers such as photonic-crystal fibers (PCF) are used too [54]. Approaches using these coiled

fibers (including plastic optical fiber (POF) ones) placed around the plasma plume are also used [55]. FOC bundles can be used to acquire the light from different parts of plasma plume simultaneously [56] or to deliver the laser pulse using one fiber and the others to acquire plasma light [57].

Optical fiber technologies can be used to detect other significant signals from plasma such as shockwaves [58]. Plasma compresses the surrounding media and generates a shockwave. This shockwave can be detected with classical microphones [58, 59]. However, shockwaves can also be detected using other devices based on optical fiber such as Fiber Bragg Grating [60]. In addition, with this technology based on periodical refractive index changes in the fiber core, temperature or strain, among other factors, can be detected and measured [61].

Optical fibers can be used for a wide range of purposes and LIBS uses FOC only to direct the laser beam or to detect plasma light. It is possible to use optical fibers as sensors, for example, to monitorize the ablation process at the same time than the plasma light is acquired. The detection of the acoustic soundwave generated by the plasma, using fiber optic sensors, is another possibility that could help to reduce the effect of the intrinsic instabilities of the plasma process. This is an interesting research field that needs to be followed in order to design new devices based on FOC to detect and measure the induced shockwave, the plasma light of both of them simultaneously.

3.6 Remote LIBS

Laser beams can be directed anywhere, allowing the researcher to work near to the sample or far from it, for instance explosives detection [62] in Stand-off configurations. A Stand-Off LIBS (ST-LIBS) is defined as a LIBS set-up which allows a remote, non-contact material detection-characterization over a distance of at least several meters [63]. This feature of LIBS enables flexible set-ups adapted to dangerous environments or samples.

There are mainly three ways to use ST-LIBS set-ups. In an open path ST-LIBS, the laser beam is directed and focalized from the distance across the ambient (gas or vacuum) and the plasma light is acquired from the distance too. This configuration

allows working in dangerous or forbidden areas focusing the laser and acquiring the spectra far away from the sample and even across a transparent window. The next ST-LIBS configuration uses a FOC or a FOC bundle to direct the laser beam to the sample and collect the plasma light. This set-up reduces the optical requirements with respect to open path ST-LIBS which needs several special features of laser and collection/ focalization optics. Besides, a direct line of view is not required, allowing the acquisition of spectra in places of difficult access. At the same time, the distance to the sample can be larger than for an open path configuration. The last configuration is called compact probe fiber optics LIBS. The main feature of this set-up is that the laser is positioned close to the sample, and the light is acquired using an optical fiber and directed to the remote measurement system. With this approach, a high quality and density laser beam can be delivered to the sample without special optics requirements, and a large distance to the instrumentation can be achieved.

4. Algorithms for quantitative and qualitative analysis

The main goal of LIBS is to achieve a chemical analysis at the atomic level, either qualitatively (i.e., to assess the presence of particular elements) or quantitatively, in which the relative amount of different elements in the sample is quantified from the processing of the acquired spectra. At the moment, the accuracy of LIBS quantitative analysis is limited, but the gap with respect to other spectrochemical techniques is getting closer. Research efforts should be carried out in order to improve the current algorithms and specially to develop new algorithms which can improve the quantitative analysis.

For both qualitative and quantitative analysis, a key step is the proper identification of each emission line of a particular element in a neutral or ionized state [2]. If the sample composition is known approximately, the set-up can be adapted to find the optimal spectral range where the emission lines of the elements under analysis are expected, or to discard emission lines of elements outside the sample. At the same time, it is interesting to know the expected relative intensity of each line. If there are doubts about one line that could belong to different elements with very close

emission wavelengths, the most probable element can be inferred from the relative intensity and other theoretical and empirical information about emission probabilities [64]. By the same token, the ionization stage is important too. If two elements in different ionization stages are possible for the same emission line, the element in neutral stage should be more likely. Even more, experimental conditions can determine the emission lines in the spectral signature. For example, lines from Fe(I) and Fe(II) are possible in air, but in vacuum, Fe(III) is possible too because the ionization potential of second ionization stage is lower in this medium.

The latest research in LIBS has tried to improve the accuracy of quantitative chemical analysis. Quantitative analysis has to provide the concentration of species in the sample (parts per million), the absolute mass of species (ng in a particle) or a surface concentration (ng/cm^2). This analysis usually finishes in a calibration curve, but this curve is strongly dependent on experimental conditions. A calibration curve is a method for determining the concentration of a substance in an unknown sample by comparing the unknown one with a set of standard samples of known concentration. For this reason, the conditions should be the same when a new sample is analyzed, and sometimes this is difficult because there are many factors that can change them. An averaging of many acquired spectra can attenuate the variation of spectral emission for the analysis, but the pulse-to-pulse variation can be too high to attempt quantitative analysis.

These factors involve aspects both from the LIBS set-up and environmental and sample conditions. Changes in laser pulse energy, repetition rate and detector gain and linearity, as well as lens-to-sample distance (LTSD) can render useless the calibration curve [65, 66]. Calibration curves can be affected by environmental conditions like changes in the atmosphere around the sample or in the light path [67]. At the same time, uniformity in sample composition, surface roughness or matrix effects affect the accuracy [45]. All these effects induce the variation of the emission intensity between spectra of the same sample.

Matrix effects, that is, the changes in the emission intensity of some elements when the physical properties or composition of the sample vary, greatly affect the accuracy of quantitative estimations in LIBS. For instance, the emission intensity of silicon in

water or in soil changes, even if the concentration in both samples is the same. There are two kinds of matrix effects. The first one is called physical matrix effect and is related with the fact that physical properties of the sample can change the ablation parameters. These changes alter the amount of ablated mass; hence the emission intensity changes although the concentration is the same in different matrices. Chemical matrix effects, on the other hand, occur when the emission features of one element are altered by the presence of another one.

One common solution is to use calibration curves obtained from materials of known composition. The result is a curve composed by values for the desired quantity as a function of values of sensor output (in LIBS, emission peaks of the element under analysis obtained from LIBS spectra). The curve is created with the measurements of known concentrations and an unknown concentration of a new sample can be predicted using the measurement obtained using its LIBS spectrum. However, many calibrated samples within the expected range of composition variation are required. Another technique, internal standardization, is based on a particular element whose concentration in the sample is constant (it can be added to the sample if needed), and its measurement is used to correct the response to other elements [68]. On the other hand, the impact of other effects (such as unwanted changes in shot-to-shot laser pulse parameters) on the accuracy of the quantitative analysis can be reduced by the so-called external standardization. In this case, an indirect physical magnitude is used to correct (i.e., to normalize) the spectra. For example, it has been observed that during plasma expansion, a shockwave is induced in the surrounding media, and the energy of this shockwave is related to the plasma energy and can be used to reduce the unwanted variations of the spectra [49, 59]. This shockwave can be acquired with a microphone [59] or with other kinds of detectors, such as optical fiber pressure sensors based on Fiber Bragg Gratings or Speckle interferometry.

Furthermore, there is a technique that solves the problem related to the calibration of LIBS, called calibration-free LIBS (CF-LIBS) [9, 69]. This procedure applies an algorithm in order to avoid matrix effects and the use of calibration curves, providing a fast and accurate quantitative analysis. This algorithm assumes that plasma is LTE, mandatory condition for all kind of quantitative analysis using LIBS, the radiation source is thin, and the plasma composition represents the sample

composition, typical conditions for LIBS plasmas. The algorithm calculates the line integral intensity between two energy levels of an atomic species, and using different lines at different energy levels, it can calculate the concentration of each element in the sample without calibration from these lines' integral intensities. Theoretically, this algorithm can calculate the concentration of all the elements in the sample up to the detection limit of the method [9].

4.1 Sample Classification algorithms

The capability of LIBS to detect and discriminate atomic emission from different chemical elements enables an accurate qualitative analysis. However, there are applications where this kind of analysis is not necessary, for example, if two different materials need to be distinguished and classified. In this case, the raw spectra provided by LIBS can be processed by classification algorithms (i.e., classifiers) for distinguishing between different samples. LIBS can provide "spectral fingerprints" of each material and this signature could identify it uniquely. This research line is not very exploited and is an interesting field which can open new ways in applications such as industrial processing or biomedical research if a proper research effort is accomplished.

Algorithms such as artificial neural networks (ANN) [70, 71], support vector machines (SVM) [71, 72] or K-nearest neighbors (Knn) [73, 74] belong to this group. These algorithms need a large training dataset to obtain an accurate classifier and need time to train (SVM and ANN) or need time to classify but not to train (Knn), but the results are usually excellent. These algorithms and other ones can provide a "chemometric" analysis (Powerful statistical signal-processing techniques which provide the automatic identification of chemical information, like spectral fingerprints).

An important aspect of the spectral data provided by LIBS and many other spectroscopic methods is that each spectrum contains a lot of redundant information. In LIBS, in particular, only a few emission lines at particular wavelengths may be interesting to perform the required classification. Redundancy can reduce the

accuracy of classifiers and sometimes needs to be avoided. In addition, classification or training time is reduced if the input dataset has less information.

There are two different kinds of algorithms that discard redundant information. The first group is composed of algorithms which select the most discriminating features. These algorithms, such as Sequential Floating Forward Selection (SFFS) [75] or Linear Discriminant Analysis (LDA) [76] select the best features of the input dataset in order to improve the classification ratio (in LIBS, the best wavelengths). The second group includes algorithms which extract features, such as principal component analysis (PCA) [77]. These algorithms combine the features of the input dataset and generate new features. Both groups, conveniently adjusted, improve the capability of classifiers.

These algorithms and other ones such as supervised learning algorithms or genetic algorithms have recently been applied to LIBS [78, 79]. These works analyze samples ranging from metallic alloys, soils, heavy metals in water to toxins in toys, and can classify them or detect traces of a particular element, automatically.

A great research effort is being devoted to going beyond a mere spectra-capturing device. With the powerful algorithms described above, an integrated and portable device based on LIBS that can induce the plasma, acquire the spectra and automatically discriminate or detect materials is feasible. It could result in an essential instrument in many real applications, like the ones that are being explored today and are described in the following section.

5. LIBS applications

LIBS is useful in a wide range of fields, namely, those which can benefit from a quick chemical analysis at the atomic level, without sample preparation, or even in the field. This paragraph compiles the most important applications at this moment.

5.1 LIBS in archaeology and cultural heritage.

Samples with archaeological or cultural value are sometimes difficult to analyze. These samples cannot usually be moved or destroyed for analysis, and some

chemical techniques to prepare the sample or a controlled environment in a laboratory are needed. In the first place, portable LIBS devices can be used, solving the problem when the sample cannot be moved. In the second place, LIBS does not need contact to analyze the sample, avoiding damage in valuable samples. Although LIBS ablates an amount of the sample, the crater is nearly microscopic and practically invisible to the eye. In addition, this microscopic ablated surface improves the spatial resolution, providing accurate spatial analysis and even a depth profile analysis of the sample. The sample does not need to be prepared; hence the analysis is clean and fast. Besides, LIBS probes based on optical fibers allow the analysis of samples with difficult access. Despite these facts, LIBS is a microdestructive technique and the researcher should pay attention to experimental parameters in order to avoid critical damage in valuable samples. Many cultural heritage artifacts can be analyzed with the right LIBS set-up.

LIBS is feasible with virtually all types of materials, for instance ceramics, marble, bones or metals, usually applying quantitative analysis. The most common analysis attempts to determine the elemental composition of the sample in order to help to date it [80-83], but indirect information can also be extracted, such as the estimation of the diet from minerals in bones [81]. LIBS has been used with delicate samples such as Roman coins [84] or other metallic alloys like bronze [80], even under water [85]. In the field of painting, it can determine the elements that compose the pigments. This analysis of pigments can help to date and authenticate frescos or paintings [86]. Moreover, LIBS can be used, combined with other techniques, in order to sum the potential of them, such as Raman or X-Ray fluorescence (XRF) [84, 87, 88]. LIBS offers some advantages for cultural heritage analysis and this field is an interesting way for LIBS, but it is necessary and useful to use LIBS with other complementary techniques, in order to provide a large set of tools for spectrochemical analysis. These mixed techniques are being tested today, and there are a lot of developments to see in this field.

5.2 LIBS in Biomedical applications.

Biomedicine and LIBS are fields that have not been working together for long. For that reason, this field may provide a large number of new developments in a few

years. LIBS can analyze chemical compositions of biological samples such as human bones, tissues and fluids [89].

LIBS can help to detect excess or deficiency of minerals in tissue, teeth, nails or bones, as well as toxic elements [89, 90]. In the same way, cancer detection is possible with LIBS and it can provide a surgical device which can detect and destroy tumor cells at the same time [91]. In addition, classification of pathogenic bacteria or virus is possible too [92, 93].

The analysis of samples from plants has also been proposed. The analysis of this kind of samples is difficult with other techniques due to the difficult sample preparation. LIBS in this case can provide a fast analysis tool with easy sample preparation, for instance in micronutrient analysis of leaves [94].

5.3 LIBS in industry.

LIBS has been targeting many industrial processes for many years, because it is a fast analytical tool well suited to controlling some manufacturing process. Moreover, LIBS can work at a large range of distances, allowing analysis of samples in hazardous and harsh environments. For example, remote detection of explosives has been assessed with LIBS [95], even at trace levels [96]. One of the best ways to grow LIBS is to focus on industrial applications because the research would be transferred to economically profitable tools. For that reason, LIBS should be more associated with the industrial field and research efforts have to be carried out in order to create this kind of devices.

For example, in the nuclear energy industry, the effects of radiation on living beings and devices are widely known. LIBS can work far away from nuclear waste or reactors, using stand-off configuration or with fiber optic probes, avoiding dangerous radiation levels [57, 97].

In the metallurgical industry, smelters and final products can reach high temperatures, and LIBS can analyze the alloy compositions in production line or detect impurities in other production sectors, such as the automotive industries [98-100].

LIBS can also be useful to detect toxic products like heavy metals in industrial wastes [101]. These waste products should be recycled or stored, and knowing the elements in them can provide key data to reduce the environmental impact of the process.

In the renewable energy field, analysis and detection of impurities in solar cells can be a useful tool to improve the manufacturing processes or to achieve high efficiency solar panels. There are recent research works in this field [102] although there is a huge amount of work to do.

5.4 LIBS and geological samples: towards extraterrestrial limits.

Analysis of some kinds of minerals is possible using LIBS, in particular, of soils and geological samples in situ [103]. Sample features can strongly affect the experimental conditions and reduce the accuracy, but quantitative analysis is still possible [104]. LIBS analysis can detect traces of toxic material in soils, rocks or water without sample preparation and in the natural environment of the sample.

LIBS can work in a wide range of environmental conditions and with different atmospheres, from air to vacuum. This feature, coupled with the capability to analyze soil samples and the possibility to build a portable set-up, enables the possibility to work in the space. Recently, a spacecraft has been launched to Mars to provide spectral analysis of Mars geological samples. This spacecraft contains, among other instruments, a hybrid LIBS-Raman spectrometer [67, 105].

6. LIBS challenges

Probably, the main challenge that LIBS needs to address is its recognition as a standard in chemical quantitative analysis. Calibration-free algorithms offer a good approximation to this goal, but the results are not perfect yet [106]. There are different research lines with the goal of a standard quantitative analysis, attempting to improve the calibration-free algorithm or add new capabilities to it. There are recent works based on spectral normalization to improve the final result [106] or to

detect the elements in the sample automatically [107]. This goal may be the most important and could place LIBS definitively among the most widely used spectrochemical techniques.

In order to widen its use in real applications, new advanced and cost-effective instrumentation is required. Currently, a cumbersome and expensive set-up is needed to achieve accurate analysis, and works are in progress to reduce the size and complexity of LIBS set-ups. The technique of micro-LIBS or improvements in laser sources can enable a compact and accurate set-up which makes it feasible in field work [106]. A recent ("hyphenated") approach combines LIBS with other spectrochemical techniques in order to unite the features of them. The hybrid LIBS-Raman Mars Science Laboratory (MSL) is a good example of this [67, 105].

Advances in new techniques and approaches for LIBS analysis, such as optical catapulting and molecular LIBS are being explored. Optical catapulting LIBS (OC-LIBS) [108, 109] uses a pulsed laser below the plasma threshold energy on the sample surface to create a solid aerosol which is analyzed with LIBS. Molecular LIBS, on the other hand, analyzes the emission of molecules resulting from sample ablation or from the recombination between target elements and ambient air [106]. LIBS can improve its performance with this ability and so enable the analysis of organic samples [110].

7. Conclusions

LIBS is a useful spectrochemical technique that can provide chemical analysis in situ without sample preparation, in a quasi-non destructive way, which can be used in a wide range of environments.

Nevertheless, advances in key optical components, pre-processing and post-processing algorithms in LIBS are essential to go beyond the spectral signatures. Therefore, additional research effort is required to meet the aforementioned challenges and to obtain useful, cost-effective, portable LIBS instrumentation.

Chapter 3

Objectives

This thesis work does not intend to be develop new physics models for to LIBS. This work uses the LIBS background in different applications and tries to join this background with the knowledge in other research areas in order to use interesting components or algorithms from other fields which could improve the LIBS technique. These improvements are then tested and applied to real applications in different fields such as archeology or industry. This thesis intends to be an engineering one, contributing to the advance of LIBS technique.

The main objectives of this work are derived from some of the aspects identified in the previous state of the art that need further research effort, and can be summarized as follow:

1. **To design and to develop new sensors based on Optical Fiber**. These sensors will measure the shockwave induced by plasma plume using different devices, like Fiber Bragg Gratings or effects into the fiber such as speckle. Besides, hybrid sensors will be designed, with the capability to detect the shockwave and acquire the plasma light simultaneously. These sensors can quantify the shockwave energy and this energy is related to plasma features and ablation process. This quantification could be useful to normalize the plasma emission and to improve quantitative analysis and control of the ablation process. This ablation process is related to geometrical parameters like lens to sample distance and these sensors could be a tool for correcting lens to sample distance and consequently focalization errors of the laser on sample surface.

2. **To apply different algorithms to LIBS spectra**. These algorithms will have several purposes. One group of algorithms will try to classify raw LIBS spectra to distinguish different samples. This approach avoids the problem of identification of chemical elements and the uncertainty associated to this identification. Second group is a new approach to quantitative LIBS analysis. A new algorithm based on particle Swarm Optimization (PSO) will be used to carry out a semi-quantitative analysis of sample composition. This work includes a preliminary stage of this algorithm which can become a tool for accurate quantitative analysis.

3. **To use LIBS in real applications**. This application will be divided in two main groups. First one is related with LIBS applications for archeological purposes. This work includes analysis of metallic statues or ceramic vessels and even the content of these vessels. This works use LIBS and compare it with different spectrochemical techniques in order to apply the best technique for each sample or obtain a complementary analysis using the features of each technique. Second group includes LIBS analysis of industrial samples, specifically metallic samples, with the goal of detecting specific coatings or precious metals in waste materials.

Concluding the first part with the formulation of the objectives to be reached, in the next part the three main groups of obtained contributions are included. Chapter four is devoted to new sensors and devices based on optical fiber. Chapter five includes the contributions on algorithms for LIBS and finally, chapter six is dedicated to experimental applications in industrial and archeological environments. The third part is devoted to the conclusions and future lines. Finally the fourth part includes a summary of the references employed during the research part of this PhD and the papers that have been published and submitted for publication in the framework of this thesis work.

Part II

Contributions

This part shows several contributions to the development of the LIBS technique. These contributions are related to the design of new sensors for the detection of acoustic LIBS signal based on Optical fibers. Besides, contributions to new algorithms for LIBS quantitative analysis or for blind sample classification are presented.

Chapter 4

New devices and techniques

As explained in the part I, it is difficult to perform accurate quantitative analysis of the sample composition using LIBS. A combination of diverse phenomena contribute to a significant uncertainty in some of the information that can be obtained about the sample from the emission spectrum, in particular, the relative amount of atomic elements of the sample's constituents calculated from intensities of the emission lines. Among others, chemical and physical matrix effects between the different atomic species [1], shot-to-shot fluctuations of the laser pulse parameters (energy, duration, etc.) [2], influence of particles ejected from previous pulses [3], variations in the spatial shape of the plasma plume that affects the light collection efficiency of the spectrometer, and changes in surface conditions of the sample and the experimental setup and its environment in general have been identified as potential sources of errors in the quantitative sample evaluation [4].

Furthermore, laser-induced plasma emission seems to be a chaotic process in the sense that the overall intensity of the resulting optical spectrum is highly dependent on the initial conditions. It is not uncommon, in an experiment with a series of laser shots with constant parameters and a strict control of the experimental conditions, that some pulses do not produce plasma emission at all. For that reasons, several consecutive laser shots are averaged or integrated into a single spectrum. However, the quantitative analysis accuracy still suffers from variations of experimental parameters, mainly, the laser energy and the beam focusing over the target material.

In order to mitigate this problem, several normalization techniques have been proposed [5]. One simple possibility is so-called internal standardization, already

discussed in the very first paper proposing the LIBS technique [6]. This solution is based on the intensity of the emission line of the element to be quantified being divided by the intensity of a weak spectral line of another element whose concentration is known or at least is constant among samples, as this ratio has been found to vary to a much lesser extent than the absolute intensity. However, not all pairs of lines are suitable candidates and they must satisfy certain thermodynamic criteria: similar excitation potential, intensity differences smaller than 10 times, and spectral proximity have provided good results [5]. Therefore, depending on the sample, it is not always possible to find suitable lines for this internal standardization within the captured spectral range.

External standardization, on the other hand, is based on the use of an external signal derived from the ablation process as the reference for normalization. One possibility is the acoustic wave generated by the plasma: Plasma evolution induces a compression in the surrounding medium and a shock wave which evolves to a sound wave. There are applications which use this shockwave induced by a laser, such as laser shock cleaning [7] or shock wave lithotripsy [8]. For that reason, a deeper analysis of shockwave evolution and the parameters involved in this process is needed. Some authors have proposed a theoretical model to shockwave propagation such as Murray and Wagner [9] or more recently, Rui et al. [10].

Other authors have captured and analyzed this acoustic emission in a different way. Diaci and Mozina discussed the signal recorded during plasma formation with a microphone using the shock wave solution of the point explosion model [11]. Stauter et al. demonstrated a relationship between acoustic emission acquired with a microphone and the ablation rate [12]. Laserna et al. studied the spectral content of acoustic emission and the changes of this spectrum with different irradiances and samples, using a microphone or the laser beam deflection technique to acquire the shockwave [13, 14]. The intensity of the acoustic wave has proven to be linearly related to the amount of mass ablated in the sample by each laser pulse, and therefore, it is a valid signal for normalization [14]. Acoustic emission is usually detected with standard microphones in the human acoustic detection range, allowing the measurement of the acoustic signal from distances up to several meters from the target. At the same time, this shockwave changes with the lens to sample distance

(LTSD) and this distance could be tuned using the acoustic detection to improve the laser focalization on sample surface.

The use of a bare polymer optical fiber is proposed as an acoustic sensor for normalization purposes, based on the sensing principle of speckle interferometry [15]. The optical fiber, coiled around the point of plasma formation, also acts as the light capturing element for the spectrometer. Plasma emission is usually collected by means of a large-core silica optical fiber coupled with a lens system pointed to the zone where the plasma plume is expected to be [16, 17]. This is an efficient system that captures the maximum amount of light from the plasma, but it is difficult to align and its efficiency suffers from the fluctuations in the spatial position and shape of the plasma plume [18]. Instead, in the proposed approach, the light is captured through the fiber's cladding on the inner part of the coil and propagated within the core to the spectrometer, thus performing a spatial integration of the optical emission that does not require alignment [19].

Another possibility is the use of Fiber Bragg Grating (FBG) acoustic transducers, which are made of optical fiber and are immune to electromagnetic fields and chemically inert. In addition, it could be possible to attach the FBG to a fiber optic cable (FOCs) or bundle LIBS head [20] which can emit the laser light and detect both the optical and acoustical emission in places of difficult access or in aquatic environments. For that reasons, a FBG transducer can be an interesting and a complementary option to extend and improve the possibilities for the detection of plasma induced shockwave. This kind of device is used in the second part of this chapter to acquire the acoustic signal and its performance is compared with a standard microphone. Besides, this device is employed to measure the LTSD in order to provide a system to correct this distance and control the ablation rate.

1. Plasma shockwave evolution

Plasma formation is induced by thermal and/or non-thermal effects, depending on laser wavelength, irradiance and pulse time [21, 22]. The sample absorbs energy from the laser source and it is re-emitted during plasma life stages. Mainly, plasma evolution follows three paths depending on laser irradiance: Laser-supported

combustion (LSC) wave for irradiances lower than 10^7 W/cm^2, laser-supported detonation (LSD) wave for irradiances up to 10^9 W/cm^2 and laser-supported radiation (LSR) wave for irradiances larger than this level. These effects can be studied from different points of view, but the limits between them are not clearly fixed [12, 14].

Regardless the plasma expansion model, the shockwave evolution follows more or less the same process, with different times, propagation speeds or pressures fixed by plasma expansion features. When the laser pulse begins to irradiate the sample, it absorbs the energy and a small amount of material is ablated, inducing plasma. This plasma compresses the surrounding medium and induces an abrupt shockwave (blast wave) which travels at a supersonic speed “A” with a spherical pattern (for nanosecond scale lasers). The air behind the shockwave reaches a speed “a”. The plasma is induced before the laser pulse finishes (using nanosecond scale lasers) and the ablated material absorbs the last part of laser pulse energy. The re-absorption induces a new compression wave which travels at speed “A+a”, faster than the shockwave. The compression wave reaches the shockwave and increases its pressure. This phenomenon occurs while the laser pulse irradiates the sample, increasing the pressure more and more. When laser pulse finishes, the compression wave decays although it can still increase the shockwave pressure until it overlaps the plasma shockwave, and the ablated material is cooled very fast. Then the shockwave reaches the steady propagation stage, with a constant pressure because the pressure shockwave has disappeared. This cooling of the plasma induces a rarefaction wave which travels at speed “C+a”, faster than the shockwave. This rarefaction wave overtakes the shockwave and it is attenuated and decreases its pressure. After a few time, the shockwave decays to an acoustic wave [10, 23].

This shockwave evolution depends of time, and for that reason depends of distance from the ablated spot. Close to the ablated spot the shockwave will be a pure shockwave, but far to this area, the shockwave will evolve to a sound wave. Laser energy can change this stages times and distances, but if the sensor which detects shockwave (a FBG transducer, a coiled fiber or a microphone in this work) is far to the plasma plume (in the order of few millimeters) it will detect a sound wave.

2. External normalization based on coiled plastic optical fiber

The proposed device is based on a coiled plastic optical fiber positioned around the plasma emission and above the surface of the material under study by the LIBS setup (Figure 5). A short length of poly(methyl methacrylate) (PMMA) optical fiber, without any protective coating, and core and cladding diameters of 980 and 1000 micron, respectively, has been coiled with a coil diameter of a few centimeters. The light from a Helium-Neon (He-Ne) laser is inserted in one end of the fiber, while the other end is split in two optical outputs using a bifurcated fiber. One of the output fibers is connected to a spectrometer to obtain the spectrum from the plasma emission, while the other is connected to a conventional video camera to visualize the speckle pattern created over the CCD surface. An optical bandpass filter, centered at the He-Ne laser wavelength, is placed between the CCD and the fiber to remove any light contribution from the plasma entering the camera that could interfere with the speckle pattern. The aim of this configuration is to collect and analyze the plasma emission with the spectrometer, and simultaneously, to record the speckle pattern with the camera to estimate the acoustic emission from the plasma.

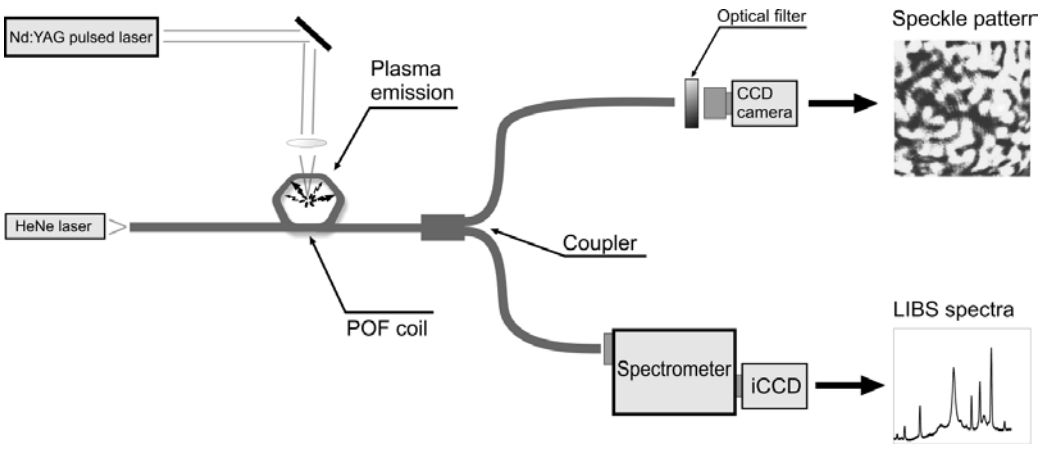

Figure 5: Sensor device based on a coiled plastic optical fiber to simultaneously collect the light emission from the plasma and to detect its acoustic shockwave.

Several designs of the coil patterns and sizes were tested, in particular, coils with circular, square and hexagonal shapes. They were built using a rigid cast of PMMA with the intended shape to coil the plastic optical fiber. One of the mechanisms that enable the light entering the fiber through the cladding to be collected and guided is the presence of scattering centers in the core-cladding interface due to the manufacturing process [24] despite it is primarily the presence of small-radius curvatures in the coil. It was found that the hexagonal pattern, with six sharp curvatures per turn, is the most efficient design. It was also found that the number of turns is not critical in the light capturing capability, because light is also radiated by the sharp curvatures. Thus, a single-turn coil has a collecting efficiency similar to a many-turn design. The coil diameter was also investigated, and, as expected, small coil diameters have better collection efficiency. However, the coil diameter should be large enough to be safely placed around the plasma plume without the optical fiber being degraded by the high temperatures and projections. For this work, a single-turn hexagonal coil with a diameter of 10 mm has been chosen.

This device design enables the simultaneous measurement of the acoustic emission from the plasma. As the fiber's coil is placed very close to the plasma emission, it is exposed to the pressure waves originating from it. The acoustic waves induce strain changes in the optical fiber, which can be detected with different approaches. In this work, the light from a highly-coherent laser is launched into the optical fiber, propagating through the coil, where it is projected over the camera's CCD surface. The induced strain can be easily detected from the perturbation of the speckle pattern captured by the camera. Several processing schemes for the analysis of the speckle images have been proposed as estimators of the physical magnitudes which induce the speckle variation [25]. In particular, the best algorithm for the estimation of the shockwave's acoustic energy from the strain-induced speckle variations has not been previously addressed in the literature. In this work, three processing schemes have been considered. Firstly, the absolute difference between two consecutive frames, i.e., the sum of the intensity value of all pixels from the subtraction image of every two consecutive frames ("differential" processing). Secondly, "contrast" processing, which is calculated as the variance of all the pixel values divided by the mean value, for each image. And finally, the calculation of the

moment of inertia of the co-occurrence matrix derived from the temporal history of the speckle pattern (“MoICO” processing) [26].

The maximum frame rate of the camera can be a serious limitation for shock waves with high-frequency content. For example, differential processing produces an estimation of the acoustic wave limited to frequencies up to half the frame rate, which for conventional cameras, can be as low as tens of Hertz. In the same way, the “MoICO” scheme needs several consecutive temporal images to generate a single estimation of the degree of speckle variation and therefore the dynamic discrimination of the induced strain is even more restricted. On the other hand, the contrast processing is an intra-frame algorithm based on the principle that increasing speckle variations (that is, movement of dark and light spots) within the integration time of a single acquired frame reduces the contrast of the captured image, so its frequency response is twice the one of the differential processing. Moreover, the measurement of contrast is an estimator of the source of speckle disturbances (the acoustic pressure applied to the optical fiber) with higher dynamic range and better linearity to accommodate to different acoustic intensities [25]. Therefore, contrast processing seems more suitable for this particular application.

In the next section, experimental results regarding the light capturing capabilities and acoustic wave estimation of this setup are presented.

2.1 Acquiring plasma light by means POF coiled sensor

The behavior of the proposed design as a plasma light collector has been experimentally tested. A Nd:YAG pulsed laser was used to generate the plasma plume. The light was captured by a spectrometer coupled to an ICCD detector. The laser beam was focused onto a plate of a leaded brass alloy used as a target. This material was chosen because there are six intense emission peaks from zinc and copper at wavelengths around 500 nm, and if the relative amount of these elements is known, this target could act as a calibration element for the LIBS setup.

The plasma emission was collected with the proposed optical fiber coil and with standard collecting optics as a reference for comparison purposes, the latter based on volume lenses and a short silica optical fiber with a 400-micron core diameter.

The reference collecting optics has been focused and aligned to maximize the amount of captured light. The coiled fiber was placed over the brass plate (a few millimeters over the surface) with one end coupled to a He-Ne laser with a wavelength of 632.8 nm and 5 mW power, while the other was attached to a bifurcated optical fiber. One output port of the bifurcated fiber was attached to the spectrometer slit entrance and the other end to the CCD camera.

A first experiment has been carried out to compare the spectra captured by both techniques. It is known that the PMMA fiber has a stronger absorption coefficient than the silica, and different absorption peaks due to carbon-hydrogen vibrational overtone modes and OH^- ions in the visible range [18]. In Figure 6, the captured spectra for a pulse energy of the laser of 22 mJ (26 J pump) are shown. They have been normalized to the maximum value. It can be seen that there are no appreciable differences in the captured wavelength range from 470 to 530 nm. The spectrum using the coiled fiber is noisier due to the fact that the collecting efficiency is lower. From the integration of the intensity of both spectra, the capturing efficiency of the coiled fiber can be calculated as 6% with respect to the volume optics reference setup. However, this low figure is compensated by the fact that no alignment is needed with this approach. Additionally, the previously mentioned natural variations in the plasma plume's spatial shape in different laser shots greatly affect the capturing efficiency of the volume optics setup, as it is focused on a small spatial point above the target's surface. The spatial integration of the emitted light performed by the coiled fiber reduces this variability.

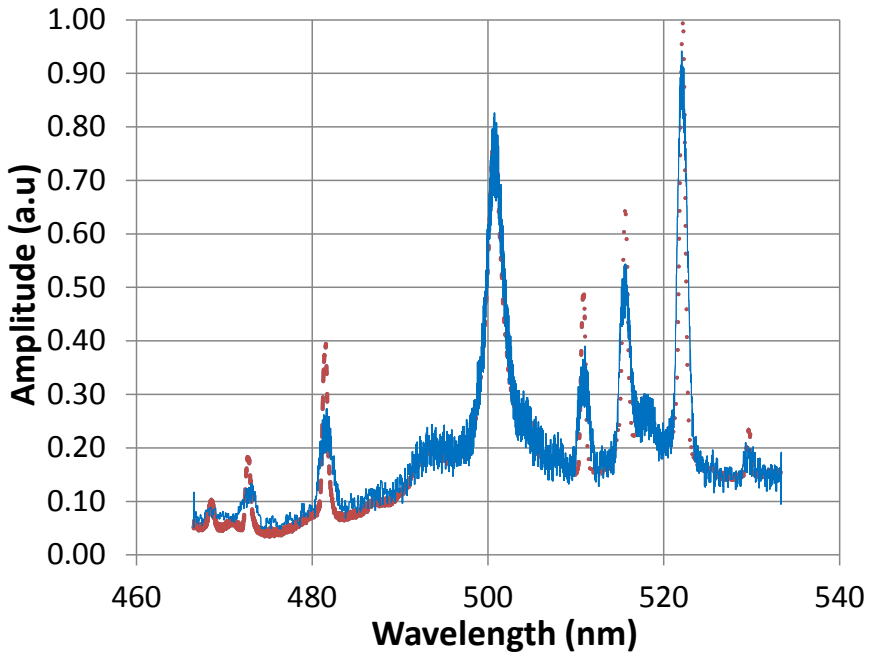

Figure 6: Spectra from the LIBS plasma captured by a standard volume optics setup (dashed line) and the proposed coiled plastic optical fiber (solid line).

To analyze how the collecting efficiency of the coiled fiber varies with the position of the coil with respect to the plasma plume, several experiments were carried out. It is expected that light entering the optical fiber at high angles with respect to the normal to the cladding's surface will be better captured and guided, as it can more easily fulfill the total internal reflection condition in the curved fiber. For this reason, the amount of collected light should increase when the coil is not centered on the laser's focal point and the plasma plume's horizontal position. Figure 7 shows the relative capturing efficiency when the center of the fiber coil is shifted in a radial direction from the laser focal point. As was expected, the capturing efficiency increases for a de-centered position, and it doubles for a 3 mm offset, still a safe position with no appreciable fiber degradation due to the plasma generated. This fact can be used to further increase the capturing efficiency if required.

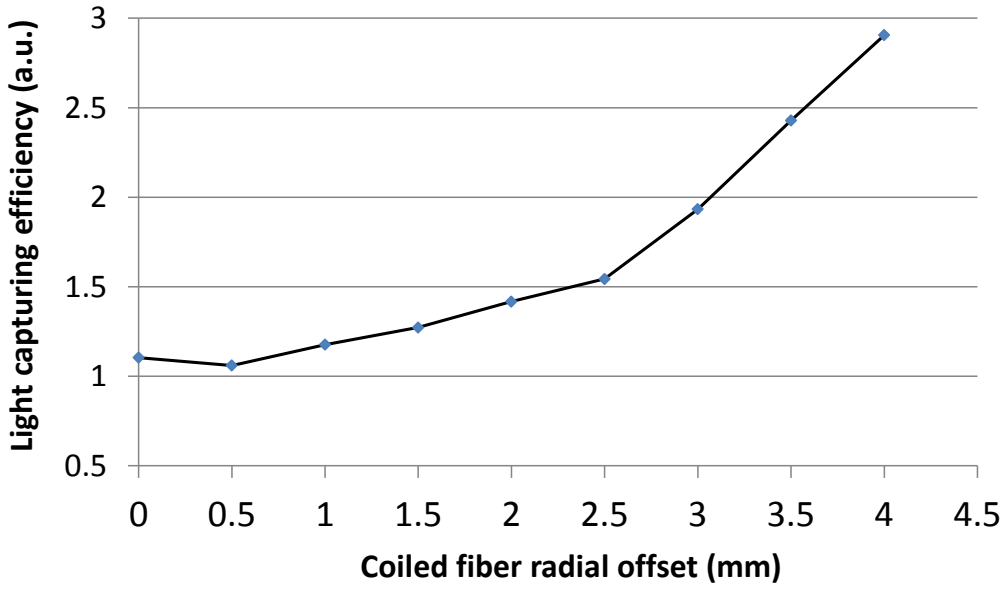

Figure 7: Light capturing efficiency of the coiled plastic optical fiber for positions de-centered from the plasma plume.

2.2 Measurement of acoustic wave

The speckle pattern at one end of the optical fiber was analyzed to obtain an indirect measurement of the acoustic energy emitted by the plasma. The optical spectra with the emission lines from the chemical elements in the sample can then be normalized against the estimated energy to reduce the error in the quantitative estimation of the sample composition.

The speckle pattern was formed simply by pointing one output port of the coupler at the CCD surface (without any optics) of a CCD camera. Images with 256 levels of gray and sizes of 64x64 pixels were acquired at the frame rate of 510 frames per second (FPS). A band-pass optical filter centered at the laser wavelength was inserted between the optical fiber and the CCD camera, in order to remove any contribution from the emitted plasma that could affect the speckle pattern generated by the He-Ne laser. For comparison purposes, a conventional moving-coil microphone was pointed at the plasma emission at a distance of about 15 cm. Its signal was recorded at a sampling rate of 44100 Hz with 16-bit resolution. Despite the optical fiber coil and the reference microphone being situated at different distances from the plasma emission (a few millimeters versus 150 mm), both

sensors are far from the ‘blast wave region’ and within the acoustic domain [19], so they should offer a similar measurement of the acoustic emission.

The plasma emission spectra and the acoustic signals have been recorded at different Nd:YAG laser pump energies from 28 J to 37 J in steps of 1 J. In this range, the laser pulse energy ranges from 86 mJ to 345 mJ and is linearly related with the laser pump energy. For every energy setting, 40 laser shots have been delivered to the sample over the same surface point. All the measurements (pulse energy, LIBS spectra, and acoustic energy from the microphone and from the optical fiber’s speckle signal) have been averaged for the 40 consecutive shots to obtain a single value for every energy point. Due to this averaging process, which reduces the shot-to-shot variability, it is expected that the intensities of the emission lines and the acoustic energy follow the pulse energy. For this reason, the main performance figure of the proposed speckle-based sensor system is its ability to obtain an estimation of the acoustic signal similar to the one provided by a conventional microphone, and to reduce the variations of the emission lines’ intensities at different laser energies using the acoustic signal provided.

The acoustic energy has been estimated using the following procedure: for the microphone, the root-mean-square (RMS) of the acoustic signal has been calculated using a sliding window of 8 samples, and then the RMS signal is integrated around the peak corresponding to each laser shot where the RMS amplitude is above 10% of the maximum value of each peak.

The acoustic energy has been estimated from the speckle signal using the three previously mentioned procedures. The differential processing scheme performs the pixel-by-pixel subtraction of two consecutive speckle images, the energy being estimated as the sum of all the pixel values in the differential image. The contrast processing scheme calculates the ratio between the spatial standard deviation and the mean value of all pixels in every image, the energy estimation being the inverse of this contrast value. Finally, the “MoICO” method firstly extracts a 1x64 pixel horizontal strip from the center of every image, and the rows are concatenated to form the temporal history of the speckle pattern (THSP). Then a co-occurrence matrix with 8 levels of gray is calculated from a 4x64 sliding matrix (4 pixels in the

temporal axis) of the THSP, and the moment of inertia of every co-occurrence matrix is obtained. The energy estimator with this method is the value of the moment of inertia. For all the methods based on the speckle signal, and due to the relatively low sample rate, a clear maximum of the estimated energy is obtained at the precise time of the laser shot, which is considered to be the acoustic energy emitted by the plasma. It should be noted that these procedures obtain not absolute but relative values of the acoustic energy that cannot be compared with different methods; only the comparison of energy values obtained with the same processing scheme for different laser shots is meaningful.

In Figure 8, the acoustic energy from the reference microphone is shown for a laser shot of 135 mJ. The speckle images are displayed for illustration purposes before, during and long after the plasma emission. The different images at the peak maximum and after pulse extinction, with respect to the speckle image at rest, show how the speckle pattern is significantly modified by the shockwave and then returns to its original configuration.

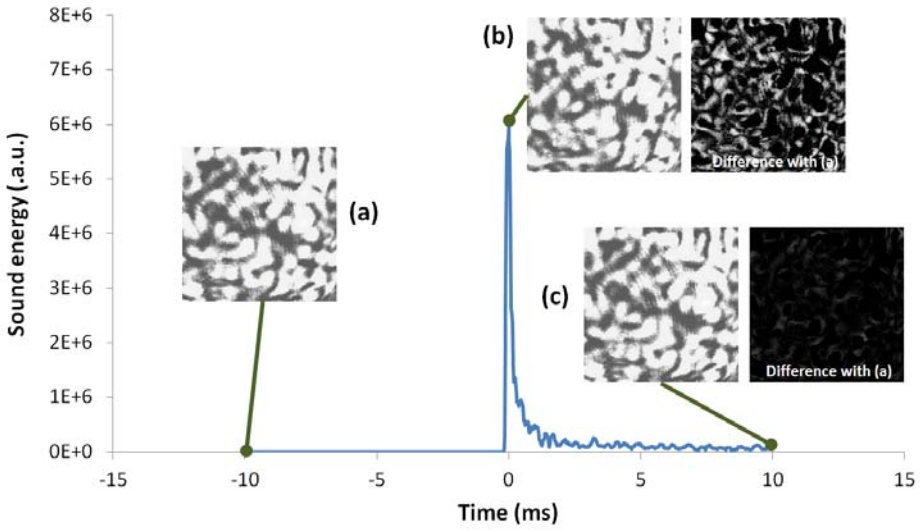

Figure 8: Acoustic pulse from the reference microphone showing the speckle images obtained before (a), during (b) and 10 ms after the laser shot (c).

Firstly, the capacity of the acoustic energy, estimated with the proposed method, to follow the pulse energy, has been analyzed. Figure 9 shows the dependence of the

acoustic energy calculated from the reference microphone, and from the speckle analysis, against the pulse energy. The laser energy sweep corresponds to pump energies from 28 J to 37 J, well above the pump threshold and within the linear range of the Nd:YAG laser. The acoustic energies for each method have been normalized to a maximum value of 1, as they are relative estimations. It can be seen that the microphone has a linear dependence and is able to predict the laser energy delivered to the sample with a correlation value of R^2 = 0.996 and a maximum deviation of 3.2 %. For the speckle analysis, it can be seen that only the contrast method produces a good linear relationship between the acoustic energy and the laser energy. As has already been explained, this method works better with high-frequency disturbances of the speckle signal that are not easy to analyze with this approach due to the low frame rate compared to the sound pressure dynamics.

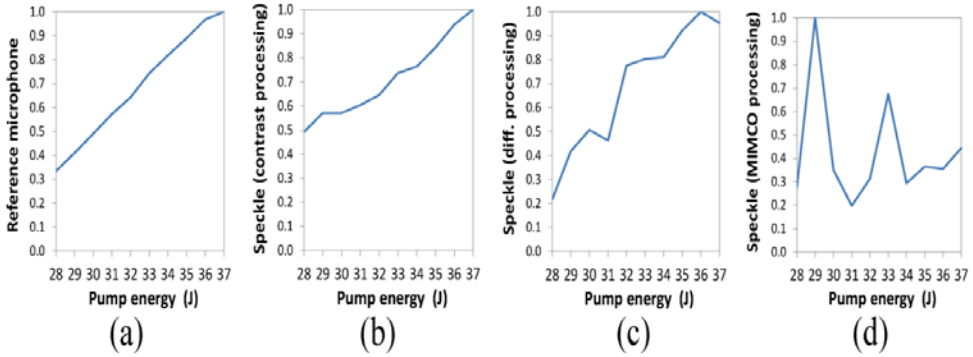

Figure 9: Acoustic energy estimation from the reference microphone (a), and the speckle pattern analysis using the proposed processing schemes of contrast (b), differential (c) and MIMCO (d).

The ability of the acoustic signal to improve the accuracy of the composition analysis of the sample at different laser energies has also been explored. In Figure 10, three LIBS plasma spectra from the leaded brass sample are shown, corresponding to laser energies of 86, 190, and 345 mJ. Six emission lines are visible: three lines of zinc at 468.0, 472.2 and 481.0 nm; and three lines of copper at 510.5, 515.3 and 521.8 nm. As the intensity of these lines increases with the increasing laser energy, the spectra must be normalized to obtain an estimation of the sample composition.

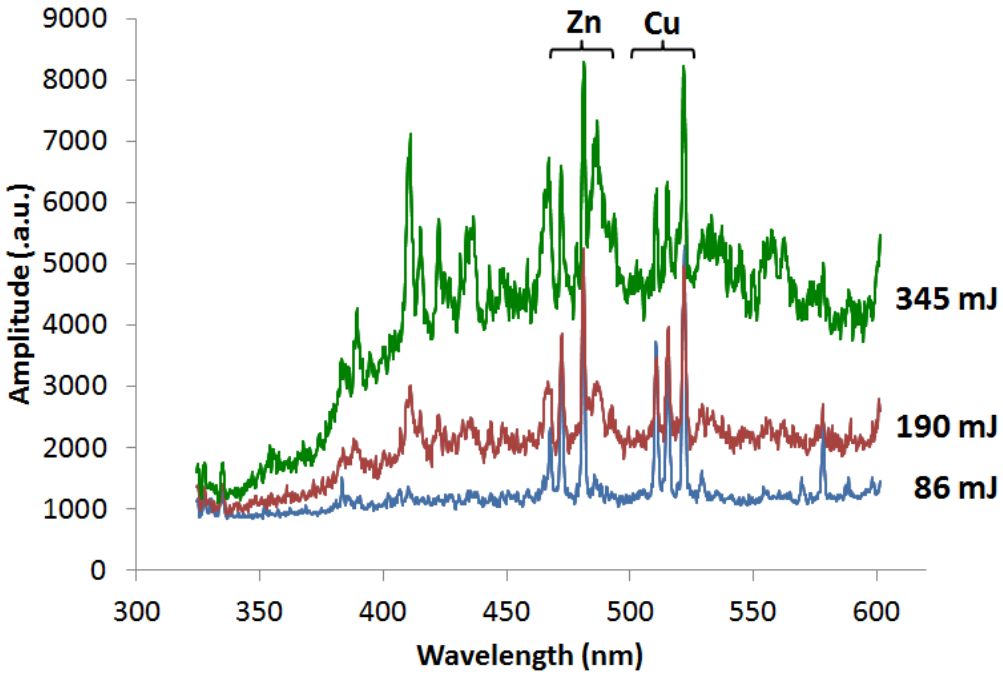

Figure 10: Plasma emission spectra at three different laser energies.

One possible method calculates the ratio of intensities of two lines of different elements, in this case, copper and zinc. The plot of two pairs of lines against the laser energy, which should be constant as the sample composition does not vary during the experiments (58% copper, 39% zinc, 3% lead), is shown in Figure 11. Although some variation still remains, it can be seen that the ratio is fairly constant, despite the 1:4 change in the energy delivered to the sample.

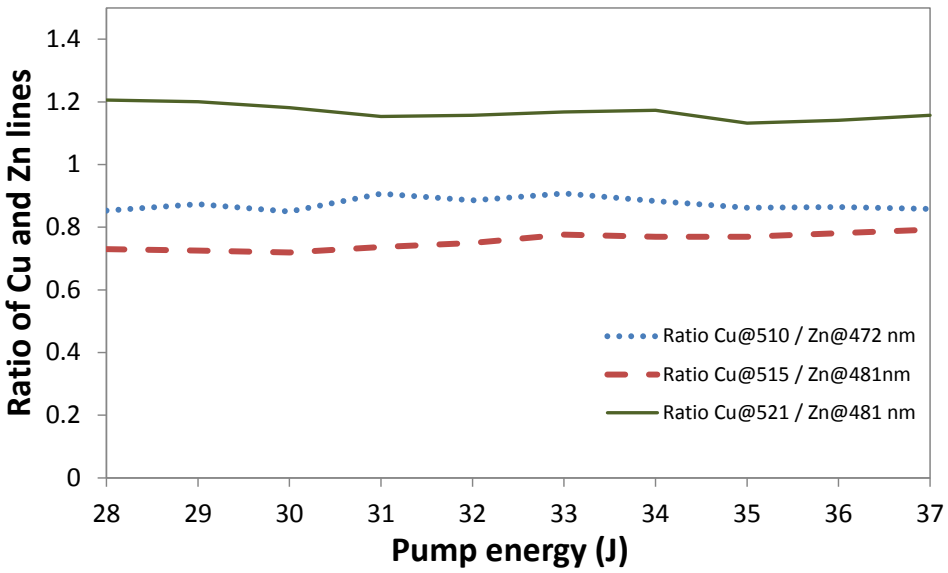

Figure 11: Ratio of three pairs of emission line intensities against the laser pulse energy.

However, depending on sample composition and intended analysis, it is not always possible to find a good line candidate to calculate the ratio. For this reason, the external (i.e., acoustic) normalization can be useful when a suitable line pair of two elements is not available. In Figure 12, the absolute intensity of the copper emission line at 510.6 nm is plotted against the pump laser energy. It can be seen (top graph) that the acoustic normalization using the contrast processing of the speckle signal is able to reduce its variation from 33 % down to 20% for the entire range of energies. In the same way, the unwanted variations of the emission line of zinc at 481.1 nm (bottom graph) are reduced from 33 % to 24 % if the absolute intensity is divided by the acoustic signal. Similar results can be found for other emission lines.

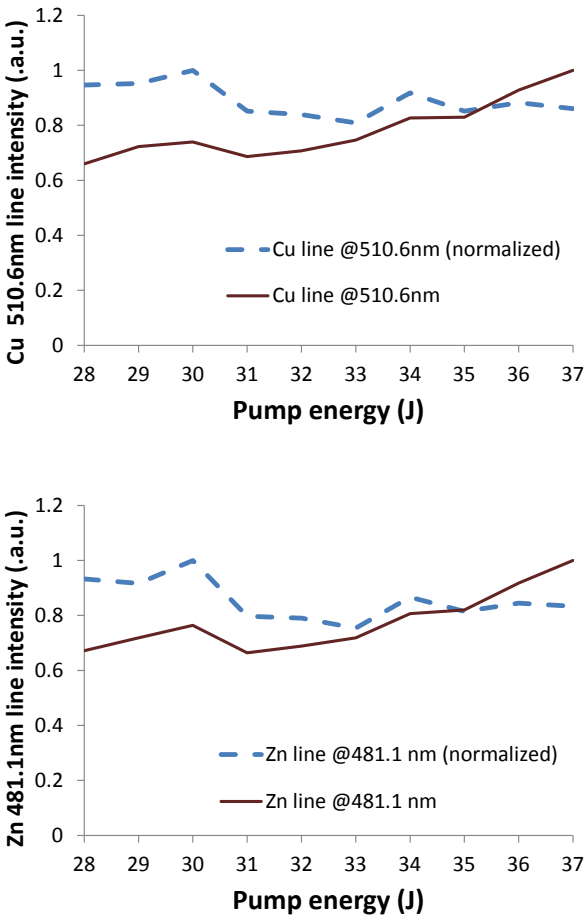

Figure 12: Normalization capability of the acoustic signal (contrast processing of the speckle images) for two emission lines of copper (above) and zinc (below).

3. Shockwave detection: Fiber Bragg Grating transducers

A transducer based on FBG technology has been used in this work and compared with the performance of a standard microphone for the detection and estimation of the induced shockwave. Basically, a FBG is a periodic variation of the refractive index in the optical fiber core that reflects concrete wavelengths [27, 28]. The reflected wavelengths are centered on the Bragg wavelength and this parameter is defined by $\lambda_{Bragg} = 2n_{eff}\Lambda$, where n_{eff} is the effective index (constant) in the fiber core and Λ is the period of the variation of the refractive index. By elongating the FBG, Λ is increased and, thus the central wavelength (λ_{Bragg}) changes. So, by measuring the central wavelength, the strain of the holder structure in which the FBG is attached can be determined. This principle has been widely used for structural health monitoring [29] in very different fields such civil engineering or renewable energies [30]. This elongation can be induced by temperature changes hence FBG is used to measure temperatures in different environments. However, the same optical fiber can contain more than one FBG, allowing measurements in different points (quasi-distributed measurements). Figure 13 shows the operation of an FBG.

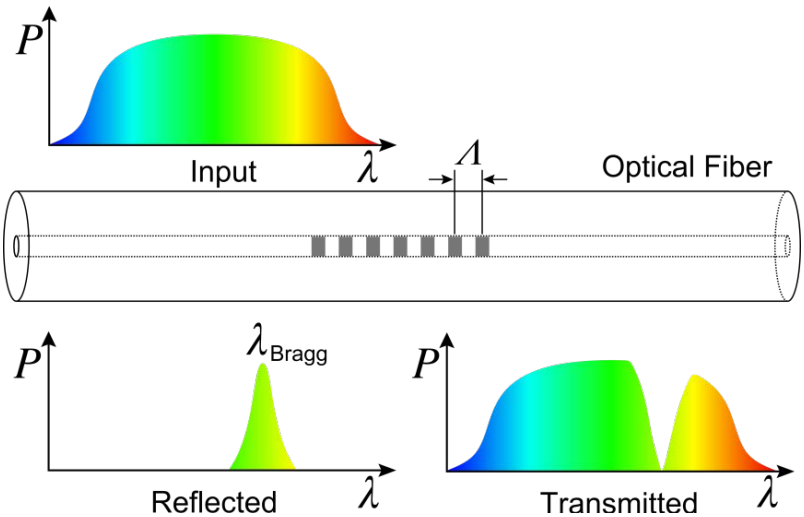

Figure 13: Fiber Bragg Grating basic operation

This kind of transducers needs an interrogation unit which sends light and measures the center wavelength reflected by the FBG. Some of them use a tunable laser which sweeps a wavelength range (this range determines the possible λ_{Bragg}'s) and measure the reflected wavelength. When the laser wavelength coincides with λ_{Bragg}, the reflected wavelength will be maximal. The difference between the reflected wavelength with and without strain determines the displacement. The interrogation unit used in this work allows sample rates up to 10000 samples per second, so signal bandwidth is limited to about 5 KHz. The proposed algorithm analyzes the energy or the peak to peak value of the dynamic strain signal, magnitudes that are related to shockwave intensity. The spectral range of this signal acquired with a standard microphone is between 0-25 Khz, so some frequency components will be lost, too. However, this does not affect the capability of the proposed technique to estimate the acoustic shockwave intensity.

3.1 Focal position detection based on Fiber Bragg Gratings

Plasma features are strongly dependent of different factors like matrix effects [31], LTSD [32] or laser pulse energy. All these factors and others are related to each other, inducing different plasma features for each set of them. A wrong focalization on the sample surface can change the irradiance on the sample, reducing the ablation rate and the spectral emission performance [32]. The optimal LTSD can be found easily in a standard LIBS set-up with easy access to the sample and laser focalization lens, but if the distance between the sample and the LIBS set-up is in the order of several meters, like in ST-LIBS configurations [33], it can be difficult to find. The measurement of the acoustic wave generated by the plasma has been proposed as a monitoring signal of the ablation process, as its intensity or spectral content can be related to the plasma emission. It is found that after the laser pulse-sample interaction, the intensity of the induced shockwave varies with the focal position, which can be used to obtain an error signal to reach optimums LTSD´s. The focal displacement induces a small irradiance change and the capability of FBG transducer to measure this irradiance changes can be useful for this application. It is important to notice that for a given set-up and sample, the spectrum of acoustic

signals from plasma expansion depends mainly of the irradiance, independently if this irradiance changes with varying laser energy or spot size [13].

3.2 Experimental set-up for Fiber Bragg Grating transducers

The FBG transducer scheme is shown in Figure 14. A FBG (λ_{bragg}= 1541 nm) has been fixed to an acetate sheet 10 mm width and 20 mm length in order to improve the mechanical response to the sound waves with a larger contact surface and without adding a heavy weight. This acetate sheet allows the detection of the shockwave because works like an “eardrum”, vibrating with the shockwave and inducing strain variations in the FBG. The optical fiber has been glued to a PVC frame (27 mm width 140 mm length) with the fixing points as close as possible to the end of acetate sheet (28 mm between them) to improve its frequency response. Different distances have been tested, but the longer the distance of fixation points, the worse transducer’s spectral response. This transducer design is dominated by mechanical effects hence a larger distance between fixation points causes a slower mechanical vibration. Plasma expansion shockwave is a fast phenomenon with a small lifetime and a wide spectral range and a slower mechanical vibration can act as a low pass filter, deteriorating the quality of the detected signal.

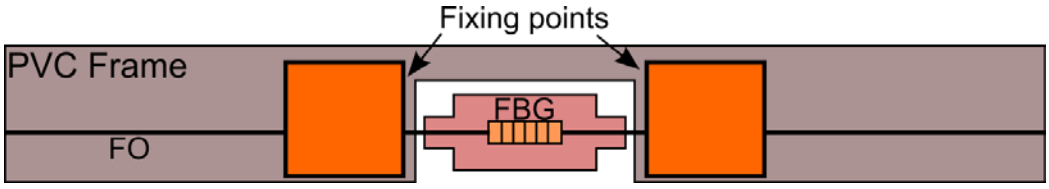

Figure 14: FBG transducer detailed

The LIBS set-up used on these experiments is shown on Figure 15:

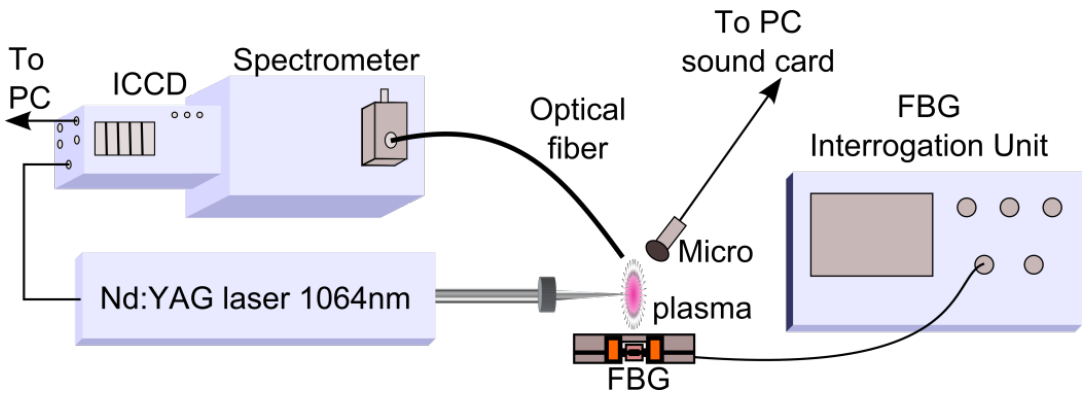

Figure 15: LIBS set-up used in this work

A pulsed Nd:YAG laser source, with a wavelength of 1064nm, is used to induce the plasma. A lens of 75 mm of focal length is used to focus the laser on the sample surface. The sample is placed on a linear stage to provoke the focalization or the de-focalization of the laser beam on its surface. An optical fiber with a core diameter of 600 µm is positioned in front of the plasma to capture and drive the light into the spectrometer. The spectrometer is coupled to an iCCD equipped with a time control unit which triggers the laser and acquires the spectrum with a proper delay in order to avoid the continuum radiation. The laser pulse energy was acquired for each pulse using a beamsplitter positioned in the beam path. This beamsplitter extracts 8.5% of laser energy and this beam sample was measured by a laser energy meter.

The sample material was a brass sheet and different sets of sample spectra were acquired to test the capabilities of the FBG transducer. The first set of samples consists of a sweep of laser irradiance on the sample surface. The laser energy was swept between 36 mJ and 178 mJ per pulse. The induced crater had a diameter of 170µm which results in a range of irradiances between 2.68 and 13 GW/cm^2. 220 spectra per laser irradiance were acquired in order to obtain a good accuracy in the results. The first 50 spectra of each set of 220 were rejected to avoid undesired results due to sample surface impurities, and the remaining 170 spectra were averaged.

The second experiment tries to analyze the capability of FBG transducer to detect focalization errors of laser beam on sample surface. In order to simulate these focalization errors, the brass sample was attached to a Z-axis linear stage and moved up and down with respect the theoretical focal position (75 mm). The

displacement was 10 mm above and 7.5 mm below lens focal length distance. The number of spectra per each focal position and the rejected spectra for each group were the same than in the previous experiment.

3.3 Acquisition of shockwave signal by means Fiber Bragg Grating Transducers

Two different analyses have been done in this work. The first of them is the analysis of time response of FBG sensor compared with the performance of a microphone acquiring the same signal and applying the same post-processing to both signals. A microphone has been selected because is a device previously employed for the detection of plasma expansion induced shockwaves and shows a tested performance [12-14]. The second analysis is the frequency behavior of both sensors.

3.3.1 Temporal analysis of FBG and microphone signals

The induced signal both in microphone and in FBG transducer is shown in Figure 16. FBG signal (left) has a larger lifetime and a higher noise level. Both sensors have been isolated from the sample and each other to avoid the detection of undesired vibrations hence this noise level is not induced by these spurious signals (mainly standing waves and vibrations from other instruments in the laboratory). Basic concepts about FBG transducer and FBG interrogation units have been explained above, but in brief, the interrogation unit measures the wavelength deviation which is induced by the shockwave with respect the rest position. The employed unit was working with a high sample rate (10000 samples per second) and the instability of measurements due to fast and small changes in interrogation unit light source at this high frequency induces this noise level. Another difference between the two signals is the life time. The signal from the microphone lasts for about 1.2 milliseconds, while the FBG signal lasts much longer (about 25 milliseconds). The induced shockwave is a fast pressure wave with a lifetime closer to the microphone signal. This FBG transducer behavior is due to its mechanical properties. In fact, the pressure wave hits the acetate sheet and induces a damped vibration on the piece of fiber between the fixation points. This vibration needs time to relax itself and this time is directly related with the length of this piece of free optical fiber and during this time the FBG suffers a deformation measured by the interrogation unit. For that reason, the

distance between the fixation points of the optical fiber to the PVC frame has been reduced to shorten this relaxation time and to close the behavior of FBG transducer to the microphone, an optimized device for the detection of this kind of pressure waves.

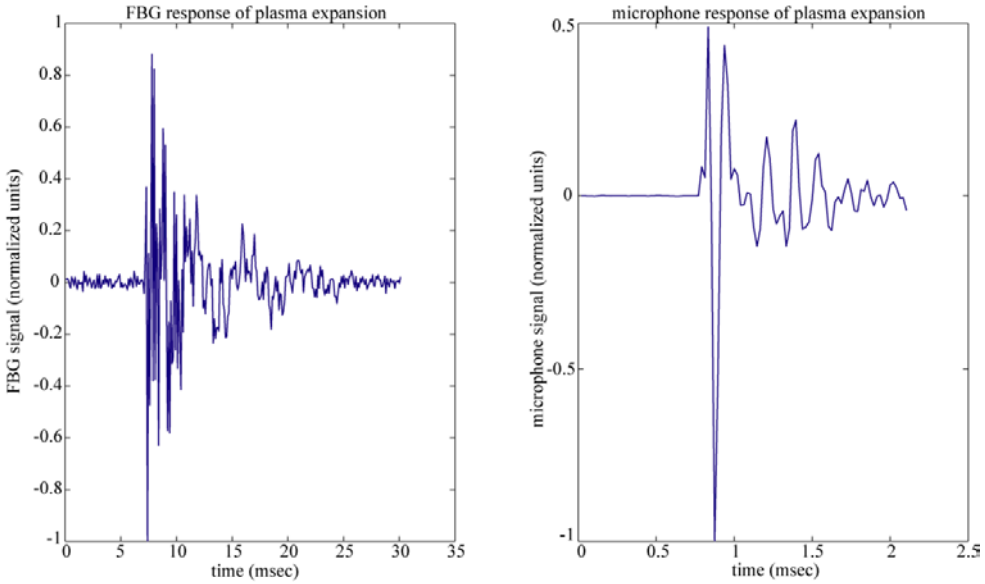

Figure 16: comparison between FBG (left) and microphone (right) temporal response to a plasma shockwave

Two different processing schemes have been applied in order to test the capability of the FBG transducer to follow the changes in the irradiance from the acquired temporal pulses. The first one is based on the calculation of the peak to peak value, as the difference between the maximum and the minimum values of the temporal pulses. The other processing is based on the calculus of the energy of the pulse. The results of both processing schemes using FBG transducer temporal pulses compared with the same regards using the microphone signals is shown in Figure 17.

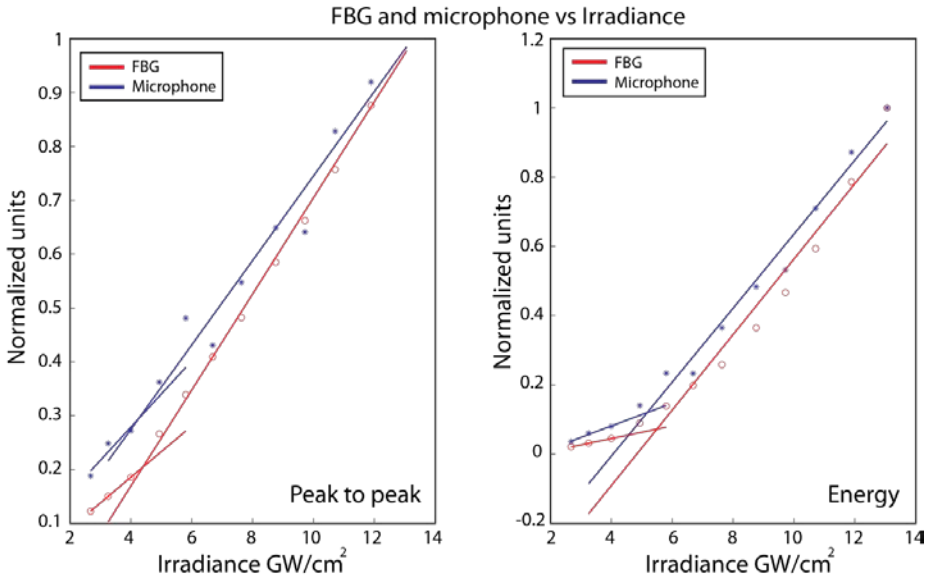

Figure 17: FBG (red circles) and microphone (blue asterisks) behaviors with irradiance evolution. Two different treatments of temporal pulses have been employed; the peak to peak excursion of each pulse (left) and the calculus of the energy of each one (right)

The three mechanisms that plasma expansion can follow have been already explained. The range of laser irradiances was 2.68-13 GW/cm^2 for these experiments and the transition between LSD wave and LSR wave is for irradiances about 10^9 W/cm^2. The transition between this two effects and its influence on the signal acquired with a microphone or even with another kind of devices were well described previously [14, 34, 35]. Laserna et al. recorded a change in the slope of linear trend of microphone signal energy on about 4.8 GW/cm^2 due to this transition between LSD and LSR waves [14]. The laser irradiance sweep was selected to record this transition with FBG transducer previously reported using a microphone [14] and this slope change is clear with the two processing methods for both sensors.

The analysis of pulse energy for the microphone records this transition around 5 GW/cm^2, close to the value described in previous works [14]. FBG transition is less clear for the pulses energies due to the worse linear behavior compared with the microphone, but despite this fact the first three irradiances show a behavior close to microphone results, with a transition between expansion waves about 5.5 GW/cm^2. For this analysis, the microphone has a better linear trend (R^2=0.989 for microphone

and R^2=0.979 for FBG) though both of them have a good performance to follow the laser irradiance and to detect the wave expansion transition.

The performance of both sensors changes with the peak to peak analysis. The wave expansion transition is clearer for FBG and the measured laser irradiance level is about 4.5 GW/cm^2. The linear trend for FBG transducer signals is the best off all analysis (R^2=0.998 for FBG and R^2=0.979 for microphone). The wave transition for microphone is not clear with similar slopes for both of them.

This temporal analysis shows that the performance of FBG transducer to detect the induced shockwave due to plasma expansion is similar to a microphone. Despite the fact that there are differences between them in terms of frequency range and mechanical properties, FBG transducer has a high performance for the detection of laser irradiance changes, even higher than the performance of the microphone due to the better linearity. The higher performance of FBG transducer using the peak to peak analysis is probably due to these mechanical properties. The shockwave, whose intensity is proportional to laser irradiance, hits the FBG and induces the vibration, and this first excitation, perfectly recorded by the peak to peak exclusion, is better for the FBG. Probably, the mechanical response of this FBG transducer, dominated by resonance frequencies, is better for this primary detection, but at the same time the slower relaxation time of FBG transducer due to its own physical properties and dimensions changes the energy of the pulses, distorting the results.

3.3.2 Focal position detection based on temporal analysis

This capability of FBG transducer to measure laser irradiance could be useful to detect errors in the focalization of laser beam. These changes in LTSD imply a change in irradiance on sample surface which the FBG transducer can estimate. For each LTSD the same processing techniques (peak to peak exclusion and energy of the signal) have been used, and two set of measurements with the same parameters have been acquired in order to test the repeatability of the measurements. Both microphone and FBG exhibit different behaviors, shown in Figure 18. FBG shows all the maxima responses for each signal processing and set of measurements centered about 2.5 mm below the lens focal plane and the microphone response peaks are around 3 mm above the lens focal plane, but the difference between these

response peaks is larger than FBG peaks, which means that FBG results are less dependent of processing technique and more repetitive. At the same time, FBG maximum is clearer and acuter. FBG shows better accuracy and repeatability and despite the facts that the maximum is not the initial focal position, the error is small with respect the lens focal length. The LTSD changes the irradiance and these changes in the irradiance change the plasma shape [14]. The plasma size and shape are related to the compression of the surrounding medium and this compression changes the induced shockwave. The larger the irradiance, the higher the plasma plume and the shockwave. When LTSD is reduced, the sample surface irradiated by the laser is larger and consequently the irradiance is lower. This effect reduces the induced shockwave. Contrarily, if LTSD is increased the plasma is induced above the sample surface. This reduces the ablated material but the laser is correctly focalized above the sample. Then, the laser ionizes the air and in theory the plasma is induced in the focal position with the maximal irradiance. This effect should induce a higher plasma plume and shockwave due to a perfect focalization which induces a higher irradiance but at the same time the breakdown threshold (the irradiance that a material needs to be ionized) of the air is larger due to the atmosphere absorbs less laser energy , generating a small plasma plume and shockwave.

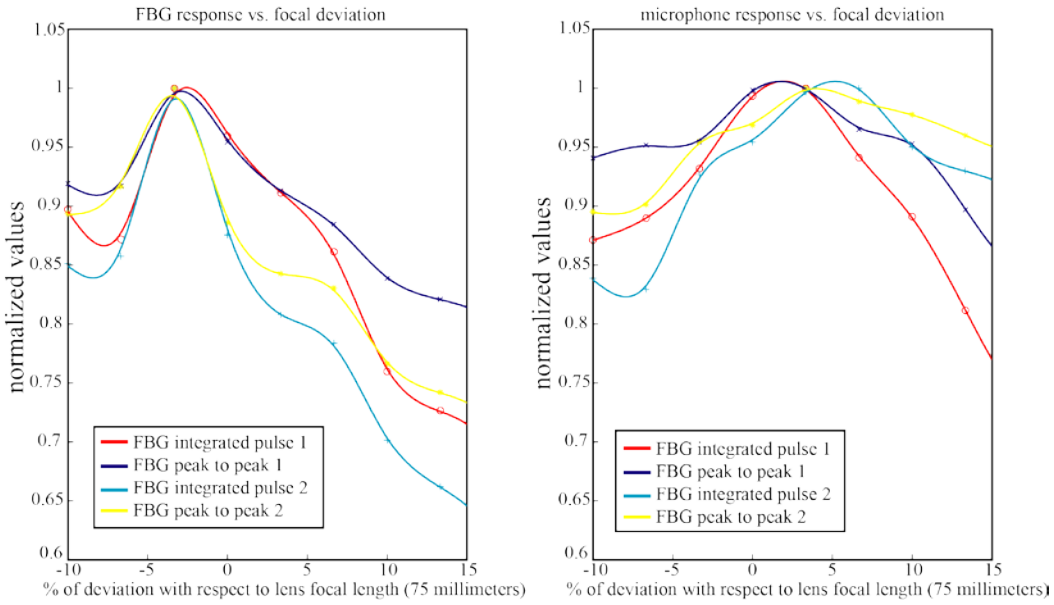

Figure 18: FBG (left) and microphone (right) behaviors with focal displacements

3.3.3 Frequency analysis of FBG and microphone signals

The second analysis carried out in this work in order to test the performance of FBG transducer is a spectral analysis of the induced signals by plasma shockwave using both sensors. Spectral evolution of both sensors related with laser irradiance is shown in Figure 19 for the lowest and the highest irradiances. All the acquired spectra have been filtered using a high pass filter for both sensors. Microphone spectra have been filtered (cutoff frequency of 1400 Hz) to avoid standing waves which can distort the original signal. These standing waves are signals at a stationary position with a pattern of deep hills and valleys which arise as a result of echoes of original signal at concrete frequencies which depends of room dimensions and original signals harmonics. FBG signal has been filtered using a high-pass filter with cutoff frequency of 150 Hz to remove the wavelength drift of the FBG due to temperature changes. The laser pulse duration (around 15 ns) is large with respect to the time when thermal vaporization arises (10^{-9}-10^{-8} seconds). For that reason thermal and non-thermal effects will generate the plasma plume, and these thermal effects can increase the surrounding temperature for the relatively high pulse frequency and the number of pulses per measurement. FBG transducer has a great sensitivity to temperature and the proximity of sensor to plasma plume induces a temperature increase due to the big amount of pulses. This effect creates a slow increasing on FBG wavelength excursion due to this temperature increase.

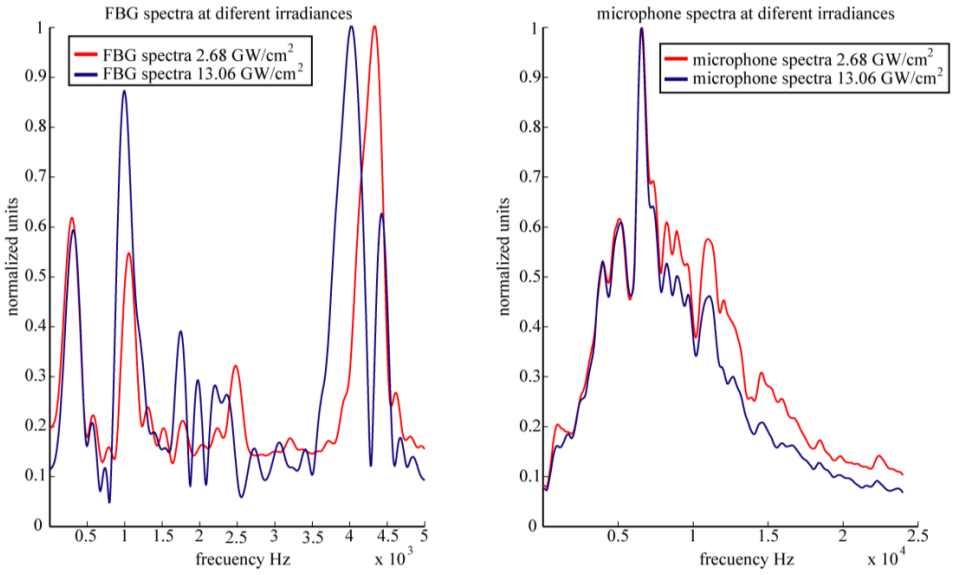

Figure 19: FBG (left) and microphone (right) spectra for lower (red) and higher (blue) irradiance

The complexity of both plasma expansion process and its induced shockwave for this kind of laser pulses cause difficulties to analyze the spectral response of both sensors. The induction of a primary shockwave in the initial stages of plasma life during the first part of the laser pulse, the secondary shockwave due to the last part of laser pulse and the interference of both shockwaves induces the complex spectra shown in Figure 19. FBG transducer spectrum is “clearer” than microphone spectrum, with separated peaks in all the spectral range, from 150 Hz to 5000 Hz limited by the sample rate of interrogation unit (10000 Hz). The increase of laser irradiance increases the number of peaks and induces a displacement of the spectrum to lower frequencies. In contrast the microphone spectrum has a dense spectral content between 4000 Hz and 15000 Hz with peaks without changes due to laser irradiance increases and only small differences induced by laser irradiance changes in the intensity of peaks at the highest frequencies of this spectral range. The larger spectral difference induced by laser irradiance shown by the FBG transducer indicates a better performance of this sensor to measure the laser irradiance using the intensity of the spectral peaks with the highest intensity variation.

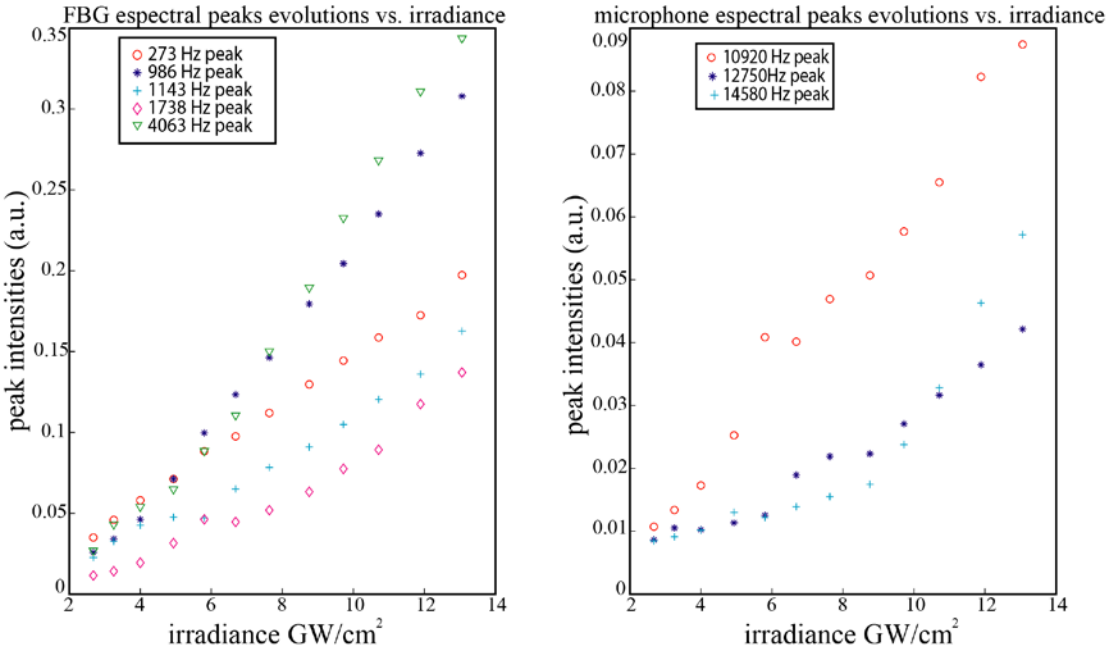

Figure 20: Evolution of different spectral peaks with the increasing of the irradiance for FBG (left) and microphone (right).

Figure 20 shows the behavior of the peaks with the larger excursions for both sensors (FBG on the left and microphone on the right). The microphone has a more irregular behavior, all the peaks rise with the irradiance increase, but there are regions with irregular trends. At the same time, it is difficult to distinguish the region of plasma expansion transition and the spectral behavior is worse than temporal one. Differently, the trend of FBG peaks is more stable and the transition of plasma wave expansion is clearly visible for some peaks as a change in the trend slope. However, other trends have irregular regions, and these troubles can hinder the detection of small changes in laser irradiance. This spectral information can be useful for the measurement of laser irradiance, but these irregular regions can be a problem for the next experiment, which consists on a focal error estimation, as this implies the detection of small changes in the irradiance level. For that reason, the estimation of the focal error has been based on temporal analysis (section 3.3.2).

4. Conclusions

A light collector and acoustic POF sensor device useful in the normalization of LIBS spectra has been proposed and demonstrated in this chapter. The light emitted by the plasma is collected by a POF coil with un-coated cladding and propagated through its core. Its collection efficiency is 6% of the classical solution of volume optics pointed at the plasma plume; however, in contrast, it is able to integrate the optical emission around the plasma and requires no alignment. By the de-centering of POF coil around the plasma emission, more light rays satisfy the total internal reflection condition in the core-cladding interface, and hence the efficiency can be tripled.

The acoustic wave is measured by means of the strain-induced perturbation of the speckle pattern at the fiber's end when light from a He-Ne laser is transmitted through the coil. The speckle images have been captured by a conventional CCD camera. Several processing schemes of the images have been tested in order to obtain an estimation of the acoustic wave that has been compared with a reference conventional microphone. It has been found that the calculation of the intra-image contrast ratio offers the best estimation of the acoustic energy. It has been demonstrated that, using the measured acoustic wave, the optical spectra of the atomic emission from the sample in the LIBS setup can be normalized against unwanted changes in the experimental conditions, such as the laser pulse energy. This normalization can enable a better estimation of the sample's chemical composition.

Besides, other alternative to a standard microphone for the detection of plasma induced shockwave has been demonstrated. This device, a transducer based on an FBG, can detect the transitions between different plasma expansion mechanisms due to the changes induced in shockwave propagation and the laser irradiance level can be estimated using this shockwave signal and a proper processing scheme. Both temporal and spectral comparisons between two different sensors have been made and the performance of FBG transducer shows that this device is a useful tool to acquire the shockwave signal. This laser irradiance estimation can be useful in

order to improve LIBS quantitative analysis, providing another tool for spectral normalization and this should be the next step which will follow this work. Besides, this FBG transducer can detect changes in LTSD allowing the optimization of this parameter and accordingly the ablation process. As the FBG is made of optical fiber, it is possible to measure this shockwave in dangerous or difficult environments where a microphone cannot be used.

Chapter 5

Signal processing: Algorithms for LIBS

LIBS equipment, such as pulsed lasers or spectrometers, has suffered an intense development in the last years. These developments have provided portable LIBS devices, cheaper systems or better detection limits for some chemical elements. As a consequence, LIBS is becoming an interesting choice among spectrochemical techniques in different environments like industrial applications due to these research efforts.

Besides the developments on LIBS hardware, other research lines are opened nowadays. LIBS is being studied from a physical point of view in order to understand the involved processes properly and improve LIBS analysis. Other main goal is to provide an accurate quantitative chemical analysis. The plasma induced by LIBS has some properties and troubles which hinder this kind of analysis and there are research groups which develop new algorithms for quantitative analysis such as the Calibration free algorithm [1]. However, these algorithms have weak points and the improvement of them and the development of new ones can help to increase the relevance of LIBS.

At the same time, there is another interesting point of view. LIBS can provide a spectrum which is a “fingerprint” of the material under analysis. Obviously, this spectrum is different for each sample and this information can be useful to distinguish between different materials without a full analysis of chemical composition. There are a great variety of algorithms which can use this spectrum to separate the different samples under analysis such as Support Vector Machines

(SVM) [2], Principal Component Analysis (PCA) [3] or Artificial Neural Networks (ANN) [4] among others.

In this chapter some approaches for giving new tools for both problems are presented. On the one hand, a new algorithm based on Particle Swarm Optimization (PSO) [5, 6] is presented as a new tool which can be useful for quantitative analysis. On the other hand some classification algorithms such as SVM are proposed as classifiers of different samples, while PCA, an algorithm for feature selection, is applied in the archeological field to date bronze samples.

1. Principal component analysis for metallic archeological samples

In the framework of a collaboration between the Chemical and Industrial Department of the Pisa University and the National Research Council of Pisa it was possible to analyze some archaeological finds. Twelve little bronzes displayed at the National Archaeological Museum in Crotone (Calabria, Italy) were chosen. The research was performed in situ applying the LIBS technique using MODÌ (MObile Dual-pulse Instrument), a mobile instrument for *in situ* analysis. These bronzes were analyzed both qualitatively and quantitatively to obtain the alloy composition. The aim of the analysis was to evidence the presence of some elemental markers that could allow the classification of bronzes according to the composition of the alloy. This is a useful tool for dating the samples due to the different bronze alloys employed in different historical periods. These markers can be obtained from the full chemical composition of the samples, but the use of Principal Component Analysis (PCA) in order to avoid redundant information allows distinguishing the samples using discriminant information only.

1.1 Principal Component analysis (PCA)

Principal Component Analysis (PCA) [3] is an algorithm which uses an orthogonal transformation to convert a set of observations of possibly correlated variables into a set of values of linearly uncorrelated variables called principal components. These uncorrelated variables imply a reduction of redundant information of the dataset

which can improve this dataset in order to obtain a better classification of different kind of data. At the same time, the number of principal components is less or equal than the number of original variables, which can induce a compression of data size. This transformation is defined in such a way that the first principal component has the largest possible variance (that is, it has the highest variability in the data), and each succeeding component in turn has the highest variance possible under the constraint that it be orthogonal to (i.e., uncorrelated with) the preceding components. A procedure to accomplish this analysis is to compute the eigenvectors of the covariance matrix composed by the input data:

$$T = \frac{1}{l}\sum_{j=1}^{l} x_j x_j' \quad (1)$$

Each new vector v that composes the new orthogonal basis should maximize the projected variance $v'Tv$ (cost function) and satisfy $v'v = 1$. That's mean:

$$\lambda v = Tv \quad (2)$$

Where λ represents the eigenvalues. The first vector v corresponds with the maximum value of λ and this is the most representative eigenvector. This procedure allows calculating the new basis of data which avoids the redundant information and it is composed by uncorrelated values which can improve the separation of each kind of data.

1.2 Analyzed materials: Bronze statues

This work was accomplished analyzing a set of 12 bronze statues from National Crotone museum (Calabria, Italy). These statues were donated by marquis Filippo Eugenio Albani in 1933 [7] and the set is composed by 9 statues that represent Hercules, 2 statues classified as offerers and one which represents Hermes. The statues were dated comparing them with statues from other museums and analyzing the techniques employed to make them.

These statues where made during a long period between V century B.C. and I century B.C. The flat and undefined structure of one statue of Hercules suggests that is the oldest [8] (statue C4) together the statue C9, although the date of this sample

is not clear [9]. Samples C2 and C3 which represent Hercules were dated around IV or III century B.C. due to the shape of the muscles which correspond with the typical procedure to make this kind of bronze statues in this period [8, 10, 11]. Samples C1 and C7 were dated more or less in the same period. Sample C1 is an ”Avellino” art style [8] but C7 generated some doubts due to its disrepair [8, 12]. Sample C10 was dated after IV century B.C because the pacific Hercules was represented on this period [13]. Samples C5 and C6 were dated on III century B.C. because the body is proportionate due to the teachings of Lisipo, a Greek artist, in Taranto [11, 14]. The most recently statue of Hercules (sample C8) has been dated in II century B.C. due to its similarities with a Hellenistic clay statue [15]. One of the offerer statues (sample C11) has been dated on II century B.C. because it is similar to a couple of Vetiloniese statues from this period. Finally, it has not been possible to date the sample C12 despite the fact that this sample represents Hermes. Figure 21 shows a temporal line of all the samples in order to allow a fast an easy temporal positioning of the statues.

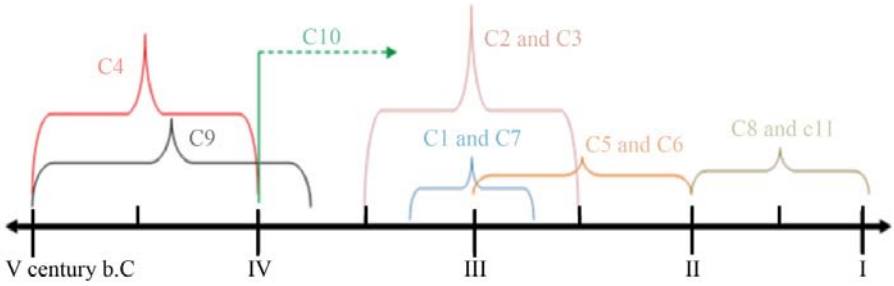

Figure 21: temporal line of samples from stylistic and typological point of view

1.3 Results

The set of statues were analyzed using a mobile LIBS device, called MODI (Mobile Dual-pulse Instrument) [16]. This device was designed and realized by the Applied Laser Spectroscopy group of IPCF-CNR (Istituto per i Procesi Chimico-Fisici, Consiglio Nazionale delle Ricerche) in collaboration with Marwan Technology s.r.l. (Pisa). MODI is a Dual pulse LIBS instrument which emits two Nd-YAG Laser pulses in a collinear configuration with a reciprocal delay variable from 0 to 60 µs at 1064 nm with an energy between 50 mJ and 120 mJ per pulse and 10 ns FWHM. The optical signal is sent through an optical fiber to an Echelle spectrometer

(spectral resolving power $\lambda/\Delta\lambda = 7500$) equipped with an iCCD for time-resolved LIBS measurements in a wavelength range of 200-1000 nm. This device and its internal scheme are shown in Figure 22.

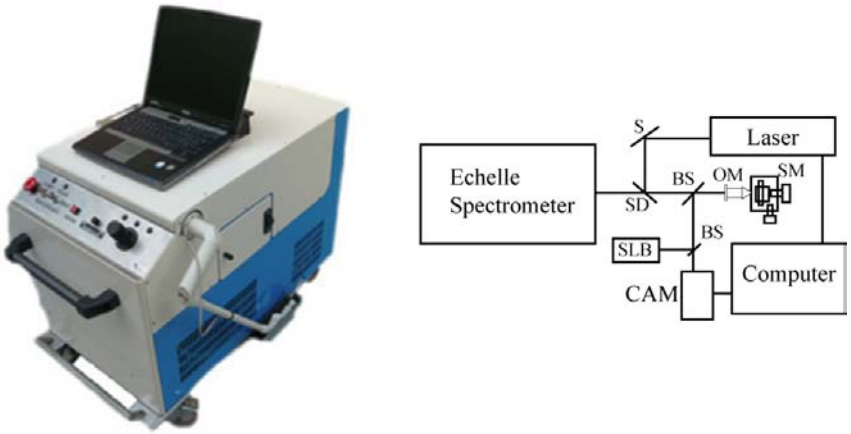

Figure 22: MODI and its internal scheme

LIBS craters were produced 3 to 6 different places of the samples. Each crater was created using 5 laser shots (each shot comprising a double laser pulse using MODI). Each laser shot ablates about 1-2 µm depth and the sequence of laser shots allows the analysis of sample surface and bulk. The detected elements are from the alloy (Cu, Sn, Pb, and Zn), impurities (Fe, Ni, V, Bi, Cr, Ag, Al, Sr) and sample surface (Ca, K, Na, Mn, Si, Mg, Ba, Ti, Li). These elements were detected for the presence of at least one main line of them. The last shot was employed for a quantitative analysis of some reference samples, one of each period (C1, C5, C9, C11), in order to compare the alloys of each group of samples with the results of PCA. This quantitative analysis was carried out analyzing the most important elements in the alloys and the result is shown on Table 1 as a percentage of the total amount of the sample.

	Fe	Sn	Bi	Cu	Ag	Pb	V	Zn
C1	1.5	7	0	63	1.5	27	< 0.1	0.1
C5	3	15	< 0.1	53	0.2	28	0	0.2
C9	5	5	0	54	0.5	20	0	15
C11	3	12	0	66	0.2	17	0	2

Table 1: Quantitative analysis of reference samples

These results were obtained with the CF-LIBS algorithm [1]. The error is around 1% for main components but it can rise to 10% for some trace elements. The presence of Cu and Sn is obvious due to the fact that the alloy of all the samples is bronze. Bronze is an alloy of these elements, but it was common to add Pb in order to reduce the melting point and improve the manufacturing process on the period of the samples. Zn was employed as antirust and the amount of these four elements suggest that they were added voluntarily to the alloy. The presence of other elements, mainly Ag and Fe could be due to impurities in the raw minerals. Other elements like Cr have been detected, but its emission is important on sample surface and disappears in the last laser pulses. Cr oxide was used to polish bronze, and this explains the traces of Cr.

These eight elements have been employed like input dataset to apply PCA. The two most representative components of the eigenvectors (associated with the largest eigenvalues) have been represented on Figure 23.

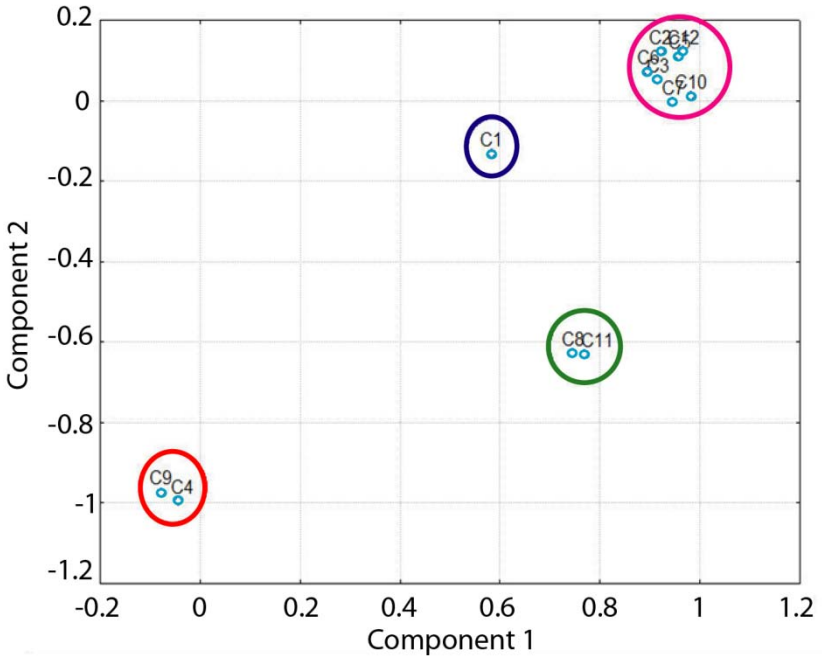

Figure 23: Groups of samples classified using PCA algorithm

The result of PCA algorithm should be compared with the stylistic analysis due to the similarities between both results. Samples C8 and C11 are characterized by a larger

ratio of Cu and a shorter one of Pb. These samples are the newest and both of them have been separated by PCA. Samples C4 and C9 have a larger Zn ratio than in the other statues due to the use of this element like antirust. This group has been perfectly separated with PCA algorithm. The other samples are chronologically mixed in a period between second half of IV century B.C. and III century B.C. Consequently, these samples appear in the same group due to the similar composition (with larger ratio of Sn) induced by the similar manufacture process of this period. Sample C1 has special features with an alloy characterized for a shorter ratio of Fe and a larger ratio of Ag which induces that this sample appears isolated. Figure 24 shows the peak intensity of the eight most important elements which compose the alloy of each sample.

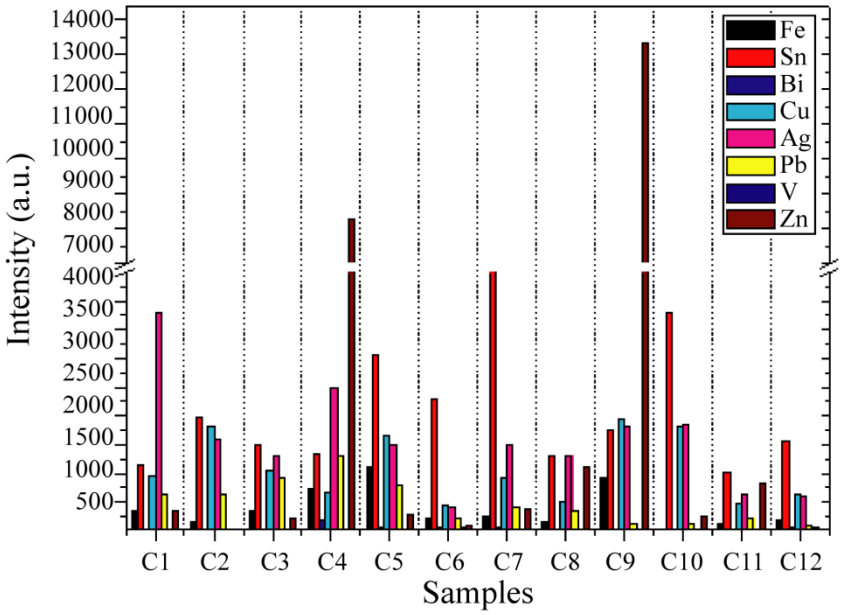

Figure 24: Peak intensity of most important components for each sample

This figure does not show the result of a quantitative analysis, but the peak intensity of each element allows a qualitative analysis and an idea about the different concentration of the same element for all the statues. These differences between the concentrations of the same elements in different statues are due to the different period of each one and the typical alloy employed for this kind of metallic pieces and these results can help to understand the classification result provided by the PCA analysis. Basically, the new space that PCA calculates uses the information provided

for the elements big large variation between the samples and obviates the information from the elements with a similar concentration for all the statues. This process improves the classification results for this elimination of redundant information.

2. Support Vector machines for welding quality.

Welding processes are of great importance in many industrial sectors, and a great deal of research effort has been devoted to the design, monitoring and control of the process, in order to assure the final quality of the weld seam. Many process parameters have influence on the resulting quality: type and composition of materials, joint preparation and cleanness, relative position between the pieces to be joined, the welding technique (laser, arc, friction…), filler material, protection gas, speed, etc [17-20].

One particular problem faced by many industries, in particular, the automotive industry, is the laser welding of boron steel with aluminum-silicon covering, which is a common process for the manufacturing of several automotive components. Laser welding has many advantages in this case, because it is a clean and rapid process, produces narrow welds with a small HAZ (Heat Affected Zone) area, and it is a proven technology [21]. However, boron steel with aluminium-silicon covering are supplied with an antioxidant protective coating usually made of an aluminium and silicon alloy, only some tens microns thick. The presence of residues of aluminium from this coating during welding has been proved to negatively affect the welding quality, resulting in a final joint with a significant reduced strength [19]. For this reason, this protective layer has to be removed from the joint area previously to the welding process. Laser ablation is an effective and rapid process commonly employed to remove the protective coating, but the possibility of remaining traces of the protective material is still not negligible. Thus, a sensor system to detect these residues before the welding process should be desirable.

For this approach, not only the sensitive detection of impurities is an important feature, but also the automatic and real-time identification of the contaminated surface. This could allow preventing potentially defective weldings with a non-

invasive system which could operate after the ablation process or right before the welding process. For this purpose, a fast and efficient processing algorithm of the vast amount of spectral information is needed. Support Vector Machines (SVMs) [22-24] can meet this expectation. There have been many investigations into SVMs applied to spectral data, some specifically regarding to image classification in remote sensing [25], medicine [26] and food industry [27], where they have performed very favorably and demonstrated their ability to classify spectral data.

The aim of this work is to propose and demonstrate an automatic and non-destructive method to detect aluminum impurities from the residual protective coating of boron steel with aluminum-silicon covering. A LIBS set-up has been used to obtain the spectral information of steel sheets with different degrees of protective coating removal, and these spectra have been compressed, discriminated and classified with an optimized SVM algorithm. The following sections deal with the SVM theory and its application to LIBS spectra processing, experimental works performed at the laboratory and a discussion of the results.

2.1 Processing of LIBS spectra: Support Vector Machines

It has been commented above that LIBS can provide Spectral signatures of different materials. The goal of this work is to distinguish between two different materials, specifically steel with and without protective coating. One way could be to accomplish a whole chemical analysis of both of them but this process is not feasible for real time analysis. Other idea is to use an algorithm for working in “blind mode”; LIBS provides spectra of the sample under analysis, and an algorithm can classify the sample using the provided spectral signature on real time. SVM can be used for this purpose allowing a good performance with a short classification time, suitable for real time analysis.

SVM’s are a learning system based on the statistical learning theory [22]. This classification technique aims at finding a separating hyperplane that splits the input data space into two separate regions corresponding to the two classes defined in the discrimination problem, antioxidant layer and steel in this particular case. There are many possible linear classifiers, but there is only one that maximizes the *margin* or

distance between the classification boundary and the nearest data point of each class. Therefore, the larger the separation margin, the better the classification accuracy. The classification problem is defined as follows: x_j is a column vector representing each one of the spectra in the training set, with j = 1,2,...,I (I is the number of training spectra), and $y_j = \{+1, -1\}$, denotes class label for x_j, i.e. target or non-target, respectively. The training data set is said to be linearly separable by a separating hyperplane $w^t x + b = 0$ if there exists a vector w and a scalar b such that:

$$\begin{aligned} w^t x_j + b \geq 1 \;\; if \;\; y_j = +1 \\ w^t x_j + b < 1 \;\; if \;\; y_j = -1 \end{aligned} \tag{3}$$

These can be combined into one set of inequalities:

$$\left[y_j\left(w^t x_j + b\right) - 1\right] \geq 0 \tag{4}$$

The separating margin between the two classes is, therefore $2/\|w\|$. This margin is maximized if the norm $\|w\|$ is minimized with the limitation given in Eq. (4). To represent this optimization problem, a Lagrange function is used:

$$L(w, b, \alpha) = \frac{1}{2}\|w\|^2 - \sum_{j=1}^{l} \alpha_j (y_j\left[\langle w^t, x_j\rangle + b\right] - 1) \tag{5}$$

Where α_j is called a Lagrange multiplier. The so-called support vectors are those spectra of the training set whose associated Lagrange multipliers are non-null. More specifically, the support vectors are the closer data to the hyperplane, and for that reason, they are the most relevant ones in the determination of the separating hyperplane. The optimal case is with two support vectors, one of each class, which means that the data clusters cannot be further separated. Once the criterion function has been solved, the discriminant function, $f(x)$ to classify a new pattern x can be represented by a small subset of support vectors x_j :

$$f(x) = sgn(\textstyle\sum_j y_j \alpha_j \langle x \cdot x_j\rangle + b) \tag{6}$$

As stated in Eq. (6), the decision function depends on the inner product between the patterns. For not linearly separable cases, a nonlinear transform function $\Phi(\cdot)$ is

used to map the input vectors to a higher dimensional feature space, which is more likely linearly separable (Figure 25). Non-linear decision boundaries in the input space will be mapped to linear decision boundaries in the feature space. The classification function is represented by a kernel function $K(x, x_j) = \Phi(x) \cdot \Phi(x_j)$. The non-linear transform function $\phi(x)$ does not need to be specified. Using the kernel function, the discriminant function for a nonlinearly separable problem can be similarly written as:

$$f(x) = sgn(\sum_j y_j \alpha_j K(x, x_j) + b) \tag{7}$$

In this application to material identification a polynomial kernel is chosen because it is a popular method for non-linear modeling, and it is easy to tune.

$$K(x, x_j) = (< x, x_j > +1)^d \tag{8}$$

Where *d* is a parameter that controls the width of the polynomial function.

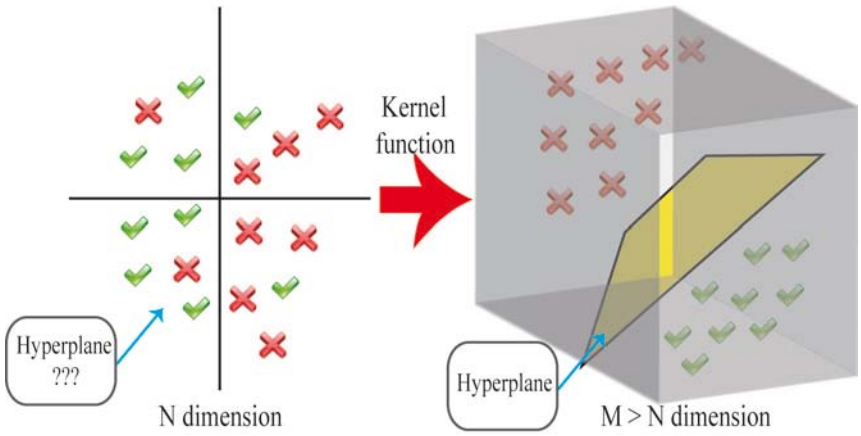

Figure 25: Kernel effect on feature space

There are classification problems with a lot of redundant information that could worsen the classifier performance, for which a more sophisticated treatment, namely the factor analysis in the feature space (*k*-PCA) described in the following lines, is justified. This treatment allows working with less useless information and therefore, the classifier requires less time to process because the two kinds of data clusters are more separated and the classifier has less support vectors. This also yields to an improved classification performance.

By means of the Principal Component Analysis (PCA) [3], data is expressed in such a way that the new basis vectors are those directions of the data which contain the most relevant information. The aim of kernel-PCA is to accomplish a linear PCA in the feature space (*F*). Since the embedding, from input space to feature space is performed with a non-linear relationship, with the polynomial kernel, a non-linear analysis is performed respect to input data. As for classical PCA, the new basis vectors are defined by the successive eigenvalues λ and eigenvectors *V* of the covariance matrix T_F:

$$T_F = \frac{1}{l}\sum_{j=1}^{l} \phi(x_j) \cdot \phi(x_j) \tag{9}$$

Where $\Phi(x)$ is the mapping function to embed the input data into F. The new projection basis vectors are then given by:

$$\lambda V = T_F V \tag{10}$$

Since each vector *V* is a linear grouping of terms $\Phi(x)$ such as $V = \sum_{j=1}^{l} \mu_j \Phi\left(x_j\right)$ and *K* is the dot product matrix with function $K\left(x_i, x_j\right) = \Phi\left(x_i\right) \cdot \Phi(x_j)$, Eq. (10) becomes:

$$l\lambda\mu = K\mu \tag{11}$$

The problem reduces to find l normalized eigenvectors μ^k of *K* (*k* = {1,...,*l*}). All these vectors must be normalized, which leads to:

$$l = \lambda_k(\mu^k \cdot \mu^k) \tag{12}$$

To achieve the *k*-PCA algorithm, the following steps are performed: first, the dot product matrix *K* is computed; then, its eigenvectors μ^k are obtained, and, finally, the eigenvectors are normalized. Data projection onto the n^{th} eigenvector in *F* is computed as

$$\left(V^n \cdot \phi(x)\right) = \sum_{j=1}^{l} \mu_j^n (\phi(x_j) \cdot \phi(x)) \tag{13}$$

That is to say

$$(k - PCA)_n(x) = \sum_{j=1}^{l} \mu_j^n k(x_j, x) \tag{14}$$

2.2 Results: Detection of protective coating remains

The samples analyzed for this work were a set of steel plates (provided by Gestamp Automoción), with a protective layer of an aluminum and silicon alloy. This layer was selectively removed from some parts of the plates using a milling machine in order to ensure the absolute removal of protective coating. The samples were moved under the Nd:YAG pulsed laser beam with a linear stage in order to generate a row of ablation spots, so different spectra were acquired from different places of the samples. Specifically, 100 spectra of each class were acquired (with and without coating), which constitute the training set, and another set of 100 spectra, with a mixture of the two classes, was captured to validate the classifier. Every spectrum was acquired with a compact Czerny-Turner spectrometer coupled to a CCD of 2048 pixels.

An example of one steel plate used for this work is shown on Figure 26. The different rows of ablation spots over zones with and without the antioxidant layer are shown. The depth of these lines is about 300-500 μm enough to remove the layer completely (the layer thickness is about 25 μm). The spots of laser ablation pulses used to train and validate the classifier can be clearly seen. Two spot rows were used to train the SVM algorithm, one on each kind of line (with and without antioxidant layer), and another row in a transversal direction were used to validate the algorithm, in order to test the algorithm with a profile of alternate layers of steel and antioxidant. Figure 27 shows the LIBS spectrum of the plate surface with (up) and without (down) the antioxidant layer. The differences between them are clearly visible; the antioxidant layer has Aluminum emission peaks and the steel spectrum has a lot of emission peaks from the alloy constituents (mainly iron and manganese, chromium and boron in lesser ratio). This difference is clear analyzing the LIBS spectra, but difficult to see with the naked eye. The spectra have been normalized, because SVM algorithm needs normalized input data to work properly, and a background spectrum has been subtracted to avoid interferences from the background noise.

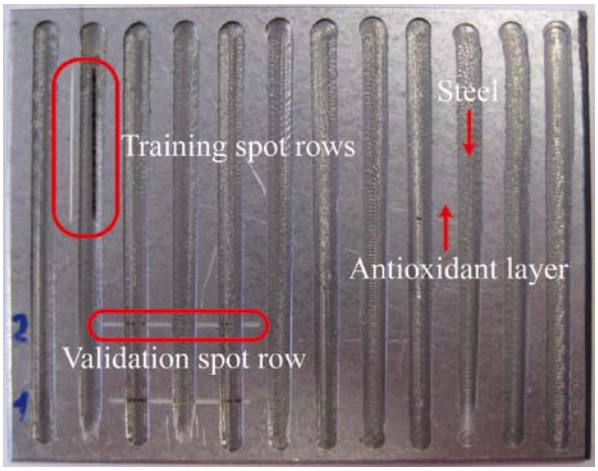

Figure 26: steel sheet used in the experiments

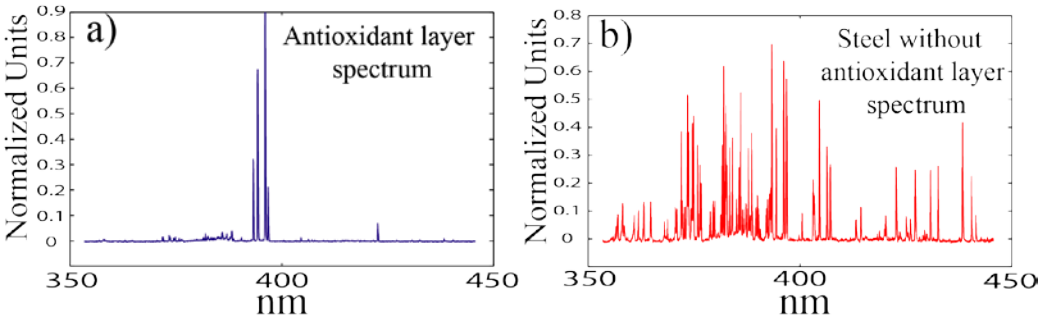

Figure 27: Spectra with (a) and without (b) antioxidant layer

The first part of the processing algorithm is the creation of the dataset, one matrix with all the training spectra and another matrix with the validation spectra, all of them normalized and corrected. Then, the kernel alignment algorithm [28, 29] is used to obtain the optimal value of the kernel parameter *d* in order to avoid several simulations to get this value. Figure 28 shows the result of the kernel alignment process. It is found that the optimal control parameter for the kernel is *d*=2.2, corresponding to the maximum value of the kernel alignment in the curve.

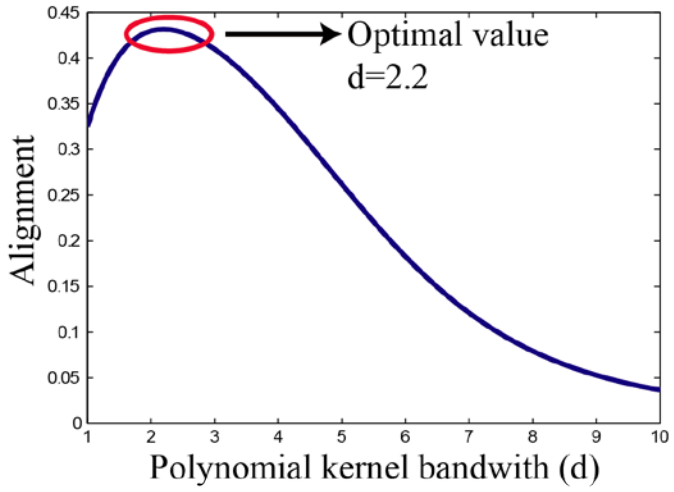

Figure 28 : Kernel alignment result vs. d parameter

The last step is to apply the SVM classifier. The possibility of reducing the amount of data in the SVM classifier is also analyzed by applying the k-PCA spectral compression algorithm to the raw captured spectra. The classification results in both cases (with and without previous treatment based on k-PCA) will be compared.

Figure 29 presents the results of the classification using all the captured spectral information (i.e., without using the k-PCA compression algorithm). A picture of the validation surface is shown at the top of the a) graph. Brighter zones have the protective layer, while darker areas correspond to steel with the coating removed. The a) graph shows the output of the SVM classifier: values above zero mean steel detection and below zero, antioxidant layer detection. Red lines are the mean classification values of each kind of material and the distance between them is 1.92. The graph b) shows the decision space with a blue line which represents the classification threshold. Although the performance of the algorithm seems to be very good, the decision space shows a great scattering of the points, thus resulting in some classification errors (red circles in a) graph).

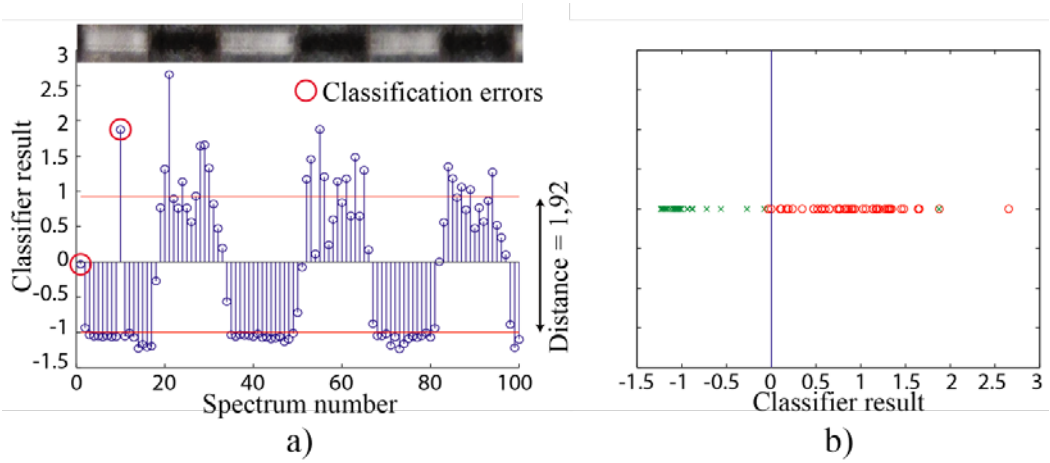

Figure 29: Classifier result (a) and decision space (b) without k-PCA

Figure 30 shows the results when applying k-PCA algorithm. The output of this algorithm is an ordered set of eigenvectors in terms of the discrimination capacity of each one. In this case, the 100 most discriminant eigenvector are passed to the classifier. A lot of redundant information has been removed from the original data thus the distance between the mean classification value of each type (solid red lines) increases. This effect can also be observed in the decision space (graph b), which exhibits two clusters of points farther apart. As a result, some decision errors were corrected and the number of support vectors was reduced achieving less classification time. (4 support vectors without k-PCA and 2 support vectors with k-PCA, the optimal case).

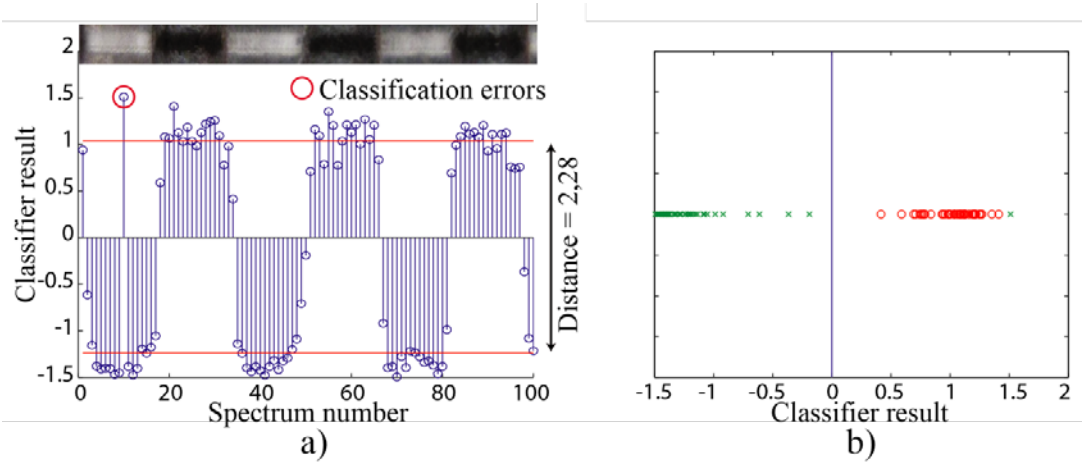

Figure 30: Classifier result (a) and decision space (b) with k-PCA and 100 eigenvectors

Figure 31 and Figure 32 show the evolution of the classifier performance when fewer eigenvectors are considered, i.e. leaving the first, 3 and 1 eigenvectors respectively because in the experiment, the threshold of the value of the valid eigenvectors was changed in order to sweep the behavior of the classifier with different number of them. This sweep allows to select all eigenvectors (all information) with small threshold and only the largest ones (less information but more significant) with a big threshold of the eigenvalues. The result with 3 eigenvectors has been represented because is the shortest number of eigenvectors which ensure a good performance. The distance between clusters increases until there are 3 eigenvectors (Figure 31) but, at the same time, errors begin to rise because the data points are more scattered, leading to a useless classifier with 1 eigenvector (Figure 32). This is the expected behavior because important discriminant information has been removed, and the algorithm does not have enough data to perform the classification. The optimal number of eigenvectors is the one which yields the maximum distance between data clusters and the minimum scatter within the cluster points.

The results indicate that the classifier needs at least 3 eigenvectors to work properly. This represents a huge reduction in the data passed to the SVM classifier, thus allowing a real-time operation without significant loss in its performance to automatically detect residues of the protective layer.

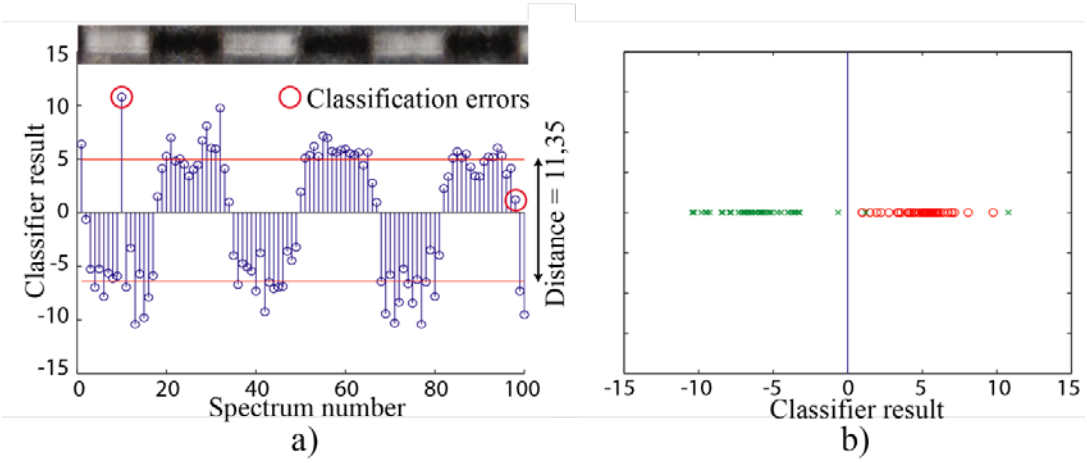

Figure 31: Classifier result (a) and decision space (b) with k-PCA and 3 eigenvectors

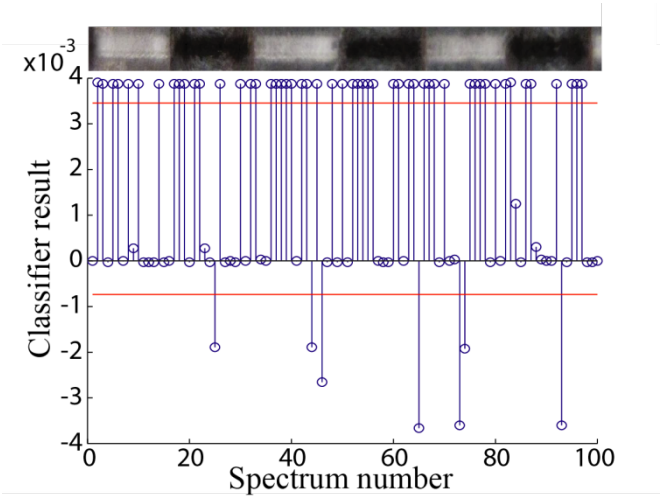

Figure 32: Classifier result with k-PCA and 1 eigenvector

These results demonstrate that SVM's is a feasible technique for the classification of industrial steels allowing the detection of impurities which are not desirable for welding purposes. This is a difficult process without any tool, and SVM's classifier provides an automatic tool which can detect the impurities simultaneously that this layer of impurities is removed.

3. Particle Swarm Optimization: An approach for quantitative LIBS.

LIBS is a useful tool for a fast qualitative chemical analysis. Different research lines have tried to provide an accurate quantitative analysis and these efforts have obtained ways for this analysis such as calibration-free algorithm [1, 30]. Despite this fact, the accuracy of LIBS quantitative analysis is already far from other spectrochemical techniques such as Inductively Coupled Plasma-Atomic Emission Spectrometry (ICP-AES), Electrothermal Atomization-Atomic Absorption Spectrometry (ETA-AAS) and Inductively Coupled Plasma-Mass Spectrometry (ICP-MS). Quantitative analysis for LIBS can provide a relatively good accuracy for the main elements which compose the sample, but the performance is worse for trace elements.

For that reason, it has been exposed in previous chapters that efforts to improve LIBS quantitative analysis should be accomplished. The main advantages of LIBS,

fast analysis, no sample preparation and in situ analysis, together with a quantitative analysis could be the key to an enhancement of LIBS as a whole tool for chemical analysis. This work presents a new approach to achieve a semi-quantitative analysis by means of an autonomous algorithm. The user should introduce the spectra, and the algorithm will detect the peaks and associate them with the corresponding species via the NIST Atomic Spectra Database. A synthetic spectrum will be generated by adding the contributions from the different species and an algorithm based in Particle swarm optimization (PSO) will calculate an approximate ratio of each element present in the sample, without any calibration curve or calculus of temperature and electronic density. This algorithm is a preliminary stage of a more refined algorithm which can achieve a new tool for quantitative analysis.

3.1 PSO algorithm for LIBS quantitative analysis.

The proposed algorithm was initially designed for its use within the framework of welding diagnostics [31], in an attempt, not only to detect defects in real-time, but also to gain a better understanding of the process dynamics, for example on which species are most Discriminant for specific weld flaws [32]. The main idea of the proposed solution can be summarized as follows:

1. The spectra captured during an experiment, initially a welding process, are analyzed and the main species contributing to the plasma (e.g. Ar II, Fe I, Mg I) are identified by the model.

2. A synthetic spectrum (for each sample under analysis) associated with each species is formed by searching in a local database with the required spectroscopic information.

3. The global synthetic spectrum, one for every spectral (i.e. spatial/temporal) sample, is calculated as the sum of all the considered species.

4. Using an optimization algorithm the model tries to determine the participation index for each species, thus generating an output profile based on the evolution of these signal with time, which is expected to show a good correlation to the quality events on the seams, i.e. to be able to detect the

appearance of defect such as porosities, lack of penetration or fusion, contamination of the seam, etc.

The automatic identification of the emission lines is a key stage to perform a suitable analysis of a given sample, being nowadays an active area of research with proposals based on the use of linear correlation methods [33, 34] and inspired by text retrieval techniques [35]. In the proposed model the identification is performed by means of a simple approach: only two spectroscopic parameters, i.e. the emission line central wavelength and its associated relative intensity are employed in this step. If the peak under analysis is close to a given NIST central wavelength, then the probability of an identification associated with that species increases. In the same way, a higher relative intensity implies a higher probability. Both variables are weighted between 0 and 1 depending on aspects such as the spectrometer resolution and spectral range. Although this simple approach could be refined by including for instance a negative exponential weighting factor as the studied and theoretical wavelengths departed, or a correction in terms of the lines to be found in the spectral range under analysis, as suggested in [35]; it offers reasonable results even when the a priori knowledge on the sample composition is not provided to the model. To limit the effect of possible wavelength calibration issues with the CCD-spectrometer, a third parameter, defined as Search Window, allows to control the spectral band around the detected peak where the identification process takes place. Each individual species spectrum is generated by adding those emission lines with relative intensity in the chosen spectroscopic database, i.e. the NIST Atomic Spectra Database [36]. The intensity of each synthetic emission line will be the one offered by the database, which gives rise to some considerations. On the one hand it is known that these relative intensities try to depict the strength of their associated lines as they would appear in an emission spectrum. However, these lines are not normalized, what implies that these values should be taken mainly as qualitative [36]. On the other hand the validity of these intensities, in terms of comparison of the strengths of the spectral lines, decreases as the considered spectral band increases. This difficulty was already noticed in [31], where the Ar II species, the one with higher contribution in the spectral range under analysis, exhibited a poorer performance in terms of welding defect detection than other less significant species.

A possible solution to this lies in the employment of spectral windows that allow reducing the wavelength range for the generation of the synthetic spectra, what will be discussed in the following section.

Once the synthetic spectrum has been created, an optimization stage takes place in order to try to match it with the real spectra acquired during the LIBS experiments. The optimization process is n-dimensional, where n is the number of species contributing to the global synthetic spectrum. The output of this process is the already defined participation, which can be considered as a qualitative estimation of the relative concentration of the species contributing to the plasma. In the original model, a controlled random search implementation, the CRS6, was considered. However, in an attempt to improve the computational performance of the solution, a different alternative based on the PSO (Particle Swarm Optimization) algorithm was chosen. PSO, originally proposed in 1995 [37] and inspired in the social behavior of bird flocking and fish schooling, has been widely used in several applications, from image and video analysis [38-40] to the design of various systems [41, 42].

Basically, PSO is an algorithm that tries to find the optimal solution for a problem by iteratively trying to improve a candidate by following the best candidates within the search space that have to achieve a given optimal solution with a concrete measurement of error. PSO optimizes a problem by having a random population of candidate solutions, called particles, and moving these particles around in the search-space following a movement fixed by a mathematical expression over the particle's position and velocity. Each particle's movement is influenced by its local best known position and is also guided toward the best known positions in the search-space, which are updated as better positions are found by other particles. This is expected to move the swarm toward the best solutions.

For LIBS, PSO works as follows. The first step is to define the search space. This space is a *n*-dimensional space where *n* is defined by the number of species detected during the previous step of the algorithm and the range of each of them is between 0 and 100 where 0 denotes the absence of this specie and 100 implies that all the sample is composed by it. Once the search space is formed, the next step lies in the generation of the particles. These particles are *n*-dimensional and they do not

represent spectra. Each particle is a set of ratios of each species and the number of particles is related to the convergence speed. These particles are placed randomly and they represent a set of multipliers for each species; if the multiplier is 0, the species will not participate in the sample, for this reason these multipliers represent the ratio of each species. The algorithm multiplies each species of the initial synthetic spectra for each particle (the set of multipliers) and compares each result with the real LIBS spectra applying the error metrics. If some particle satisfies this criterion, this result will be valid and the selected particle will represent the ratio of each species. If the particle swarm do not satisfy the established error, the algorithm will apply the movement to the swarm with the new calculated velocities, and it will proceed to move the particles for the next iteration taking into account the historic best result of each particle, as well as the overall best result within the swarm.

3.2 Results for LIBS analysis.

Different kind of materials has been employed to test the feasibility of this algorithm. The first set of samples is composed by four different calibrated brass samples provided by Stanley Michael Angel's Research Group (Department of Chemistry and Biochemistry, University of South Carolina, USA)) and this set has been introduced to the model to analyze the ratios obtained for the two main elements: Cu and Zn. Other set of aluminum-magnesium alloys have been also included in this study to extend the validity of the analysis. In this case the main interest lies in the ability of the model to establish a correct ratio between Al and Mg, the two most significant elements in the considered alloys. To complete this experimental feasibility study, a sample of Nordic Gold was also taken into consideration. Figure 33 shows the composition of the whole sets of alloys employed in this work.

Brass samples	%Zn	%Cu
MB2	32.8	67.17
MB3	26.67	73.26
MB4	21.2	78.77
MB5	15.63	84.25
MB6	9.95	90.07

a)

Other samples	% Cu	% Al	% Zn	% Sn	% Fe	%Pb	% Ni
Nordic gold	89	5	5	1	-	-	-
Sertesa Brass	58.07	0.02	38.63	0.2	0.3	2.67	0.09

b)

Al-Mg samples	% Fe	% Si	% Mn	% Cr	% Ti	% Cu	% Zr	% Mg	% Zn	% Others	% Al
Al 5186	max 0.45	max 0.4	0.2 - 0.5	max 0.15	max 0.15	max 0.25	max 0.05	3.8 - 4.8	max 0.4	total 0.15	Reminder
Al 5182	max 0.35	max 0.20	0.2 - 0.5	max 0.10	max 0.10	max 0.15	-	4.0 - 5.0	max 0.25	total 0.15	Reminder
Al 5754	max 0.40	max 0.40	max 0.50	max 0.30	max 0.15	max 0.10	-	2.6 - 3.6	max 0.20	total 0.15	Reminder

c)

Figure 33: Different groups of samples employed to test the algorithm: a) calibrated brass samples, b) samples of Nordic gold and Brass provided by Sertesa and c) group of aluminum-magnesium alloys

Figure 34 shows the results of the identification stage for spectral samples of these materials. In this figure two different identification analyses have been performed: the so-called guided-identification where the elements to be found are introduced to the model, which tries to match each emission line with one of those species. In the blind-identification mode, all the species considered in the local spectroscopic database can be associated with the considered emission lines. In this regard it is worth noting that the employed database includes information of elements typically found in stainless-steel, aluminum, Inconel, titanium and brass alloys. Once the plasma spectrum species have been correctly identified, those elements with a significant contribution will be considered for the generation of the synthetic spectrum.

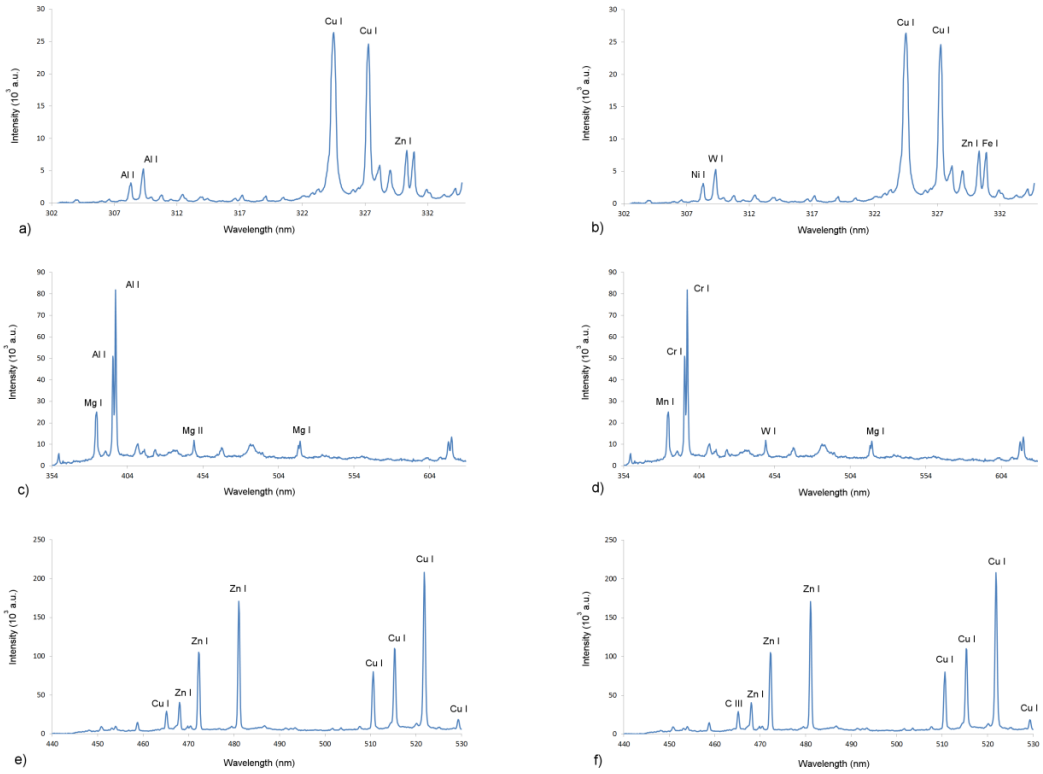

Figure 34: Spectra associated with different materials: a) Nordic Gold sample (guided identification); b) Nordic Gold sample (blind identification); c) aluminium alloy (5186) sample (guided identification); d) aluminium alloy (5186) sample (blind identification); e) Brass sample (guided identification); f) Brass sample (blind identification).

The PSO algorithm is the next step of the process. Once the species are identified for each set of samples, PSO will calculate the ratio of each species for each sample. The results are divided in different groups, one for each set of samples.

3.2.1 Brass alloys

The nominal composition of the samples, expressed in percentage by weight, is shown in Figure 34. As can be observed, the concentrations of both Zn and Cu vary, what can be used for an experimental validation of the proposed model. Figure 35 depicts the spectrum associated with the sample Brass #1, obtained after an averaging of several captures acquired during LIBS tests. Six main emission lines appear in the spectrum, three of them, in lower wavelengths, associated with Zn, and those in the spectral range between 510 and 523 nm with Cu. In addition, the Cu I

line at λ≈465 nm has also been considered in some scenarios. Table 2 includes the spectral information regarding these lines.

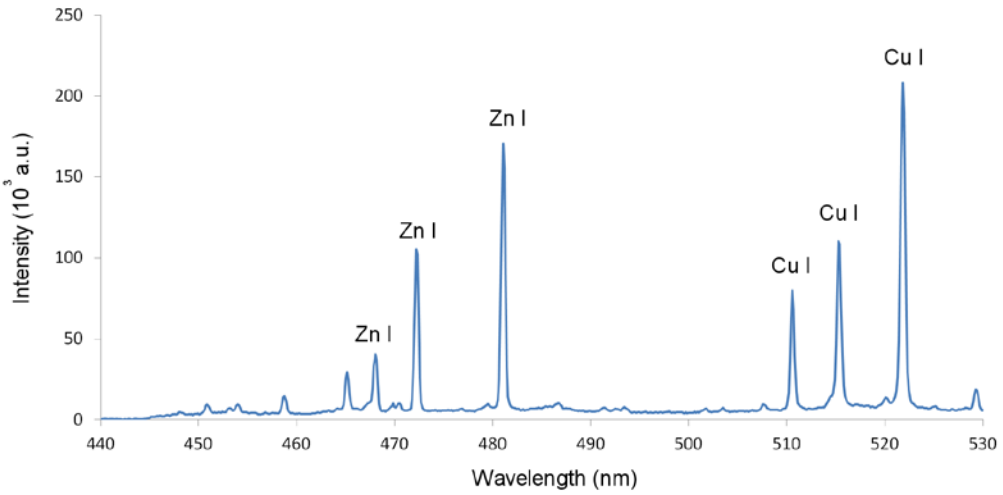

Figure 35: Spectra associated with brass sample #1

Species	λ	Rel. Int.	A
Cu I	465.112	2000	3.8E+07
Zn I	468.014	300	-
Zn I	472.215	400	-
Zn I	481.053	400	-
Cu I	510.554	1500	2.0E+06
Cu I	515.324	2000	6.0E+07
Cu I	521.820	2500	7.5E+07

Table 2: Emission lines of brass alloys

Results obtained with the different samples have been summarized in Table 3, where the participation provided by the model for Zn I and Cu I has been calculated using a spectra formed by 50 captures of each alloy. In this way, the random effect included by PSO can be compensated, and, therefore, participation for each species is determined as the average of the 50 calculated values. To illustrate the performance of the model, it is worth mentioning that the participation standard deviation lies in the range between 2.2 and 1.3 (for participations between 0 and 99%).

Sample	Zn I	Cu I	RC (Zn I (%))	RC (Cu I (%))
Brass #1	11.12	43.27	32.80	67.17
Brass #2	11.35	69.90	26.67	73.26
Brass #3	5.10	43.86	21.20	78.77
Brass #4	4.23	52.87	15.63	84.25
Brass #5	2.96	70.08	9.95	90.07

Table 3: Participation results for brass alloys

On the one hand, it can be observed that the participation results obtained for both species exhibit a certain correlation with the real composition (RC) of the samples. There are some cases, in particular for Zn I and Cu I (Brass #2), where the expected value shows the opposite behavior: for example in Brass #2 the Zn I participation was supposed to be lower than in Brass #2. A detailed study of the plasma spectra was performed to study this effect. On the one hand the ratio of the intensities of two Cu I and Zn I emission lines versus their associated weight in the samples have been depicted in Figure 36, where the experimental values of the intensity ratios are close to the theoretical ones (1.75 for Cu I and 1.5 for Zn I, respectively) [43] . The linear fit for Cu gives rise to a R^2 higher than 0.9, while the one for Zn decreases to R^2 = 0.474 due to the first point of the series, associated with the lowest Zn weight ≈10 %. On the other hand, the evolution of the emission line intensities has been also depicted in Figure 36 c) and d); and in Figure 37, being correlated with the results displayed in Table 3. Although the difficulties inherent to LIBS to obtain accurate quantitative results are different [43], two causes may play a major role in this regard. First, the quantity of mass ablated in each laser shot may vary, thus affecting the stoichiometric composition and even making the plasma optically thick [44]. Secondly, elemental fractionation, i.e. the variation of the composition of the plasma in terms of the original sample, especially affects copper-based alloys [45-47], and it is one of the most likely issues to affect the obtained plasma spectra.

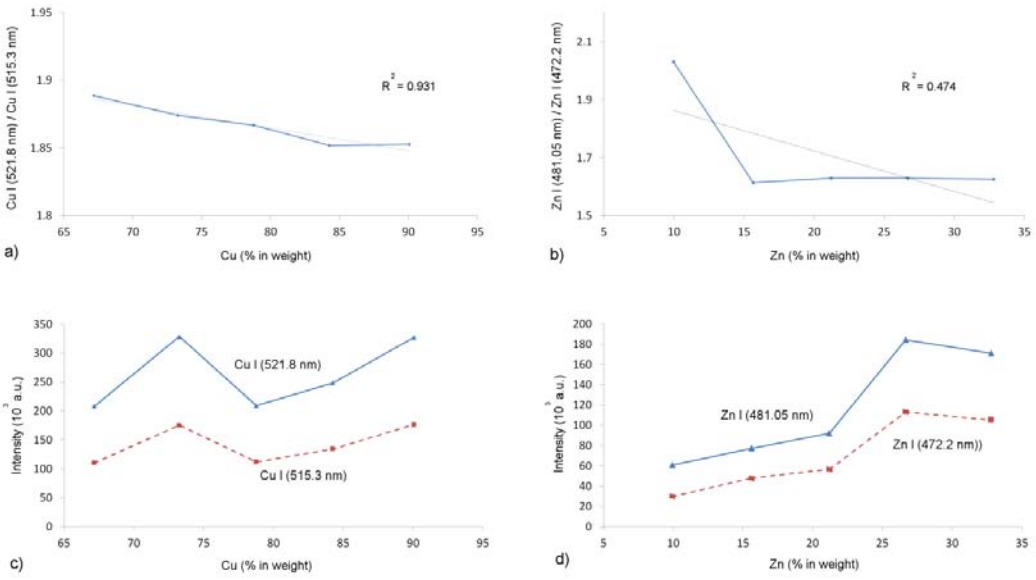

Figure 36: Calibration plot for: a) Cu I (521.8 / 515.3 nm) and b) Zn I (481.05 / 472.2) versus weight (%). Evolution of emission line intensities for: a)Cu I lines and b) Zn I lines

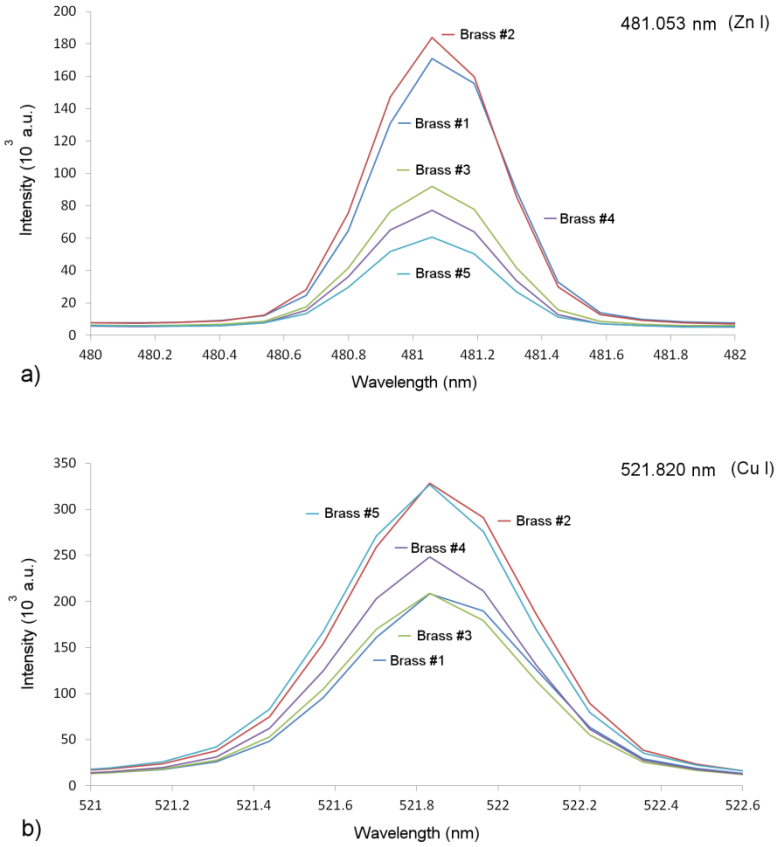

Figure 37: Evolution of: a) 481.053 nm (Zn I) emission line and b) 521.820 nm (Cu I) line associated with Brass alloys #1 to #5

To extend the analysis of brass samples, another brass alloy was studied with a completely different experimental setup. The averaged spectrum used for the concentration estimation is displayed in Figure 38, where it can be appreciated that there are significant differences between this spectrum and the one obtained for the previously discussed Brass alloys. Given that the original composition of this sample was unknown, an initial composition analysis was performed via X-ray fluorescence (XRF) [43, 44] by the Research Scientific-Technical Services of the University of Cantabria. These results, that are quantitative, indicated a 64.27% weight for Cu and a 34.77% for Zn. The estimation obtained with the proposed model is shown in Table 4. In this regard, given the complexity of the associated spectrum in terms of the number of emission lines, a study on the influence of the spectral range considered has been carried out. This parameter determines which wavelengths will be taken into consideration for the optimization process, i.e. will be considered for the estimation of the stopping condition:

$$|f^* - f(\hat{x}^*)| \leq \epsilon \tag{15}$$

Where $f(x)$ is the function to minimize (in this case the difference between the real (experimental) and synthetic spectra), f^* the minimum, x^* the value to be found in the optimization process and $\hat{x}^*$ an approximation to x^*. Four spectral windows were defined, in addition to the whole spectral range under analysis (from 304 to 581 nm). The values displayed in Table 4 show a reasonable good agreement with the real concentration of the sample, especially for Windows #2 and #3, being the Zn I participation slightly lower than the expected (in terms of a semi-quantitative analysis).

Sample	Spectral Range (nm)	Zn I	Cu I
Window #0	304 to 581	24.45	73.16
Window #1	466 to 525.6	24.63	71.41
Window #2	460 to 532	24.90	63.47
Window #3	421 to 532	24.80	64.27
Window #4	316.5 to 336.5 0	3.80	13.12

Table 4: Participation results for unknown Brass alloy

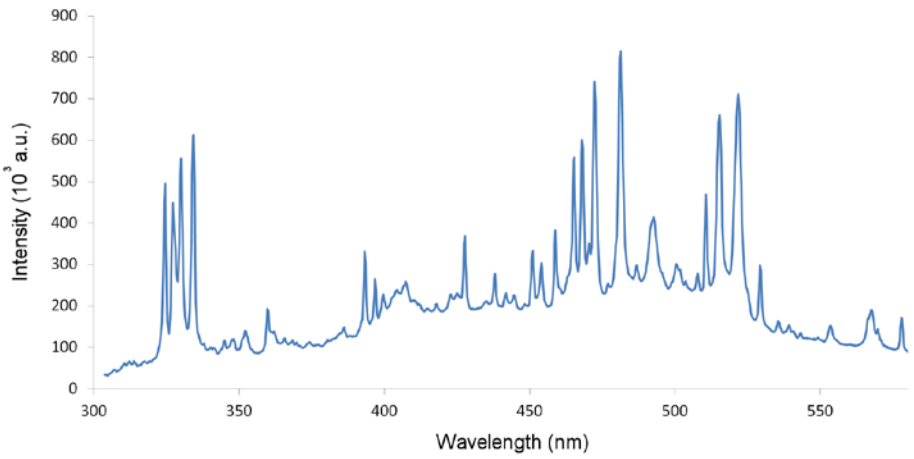

Figure 38: Averaged spectrum associated with the Brass sample

3.2.2 Aluminum alloys

Aluminum-magnesium alloys have been also included in this study to extend the validity of the analysis. In this case the main interest lies in the ability of the model to establish a correct ratio between Al and Mg, the two most significant elements in the considered alloys: Al5754, Al5186 and Al5182. The chemical composition of the former indicates a contribution of Mg between 2.6 and 3.2, in comparison to 4.7 and from 4 to 5 of the two latter, respectively. In this case it is also interesting to test if the model is able to correctly discriminate among subtle variations in composition, in the range of 1 and 2%. The spectra captured for the different Al samples are quite similar to the one presented in Figure 34, given their similar composition. Four different craters have been analyzed for each sample, being calculated as the average of 10 spectra (generated as the accumulation of 20 spectra), and two different spectral windows have also been considered, from 354.5 to 631 nm (Window #0, equal to the whole spectral range of the spectrometer) and from 368 to 409 nm (Window #1, covering the two Al I emission lines at 394.40 and 396.15 nm and one Mg I line at 383.23 nm). Table 5 contains the data provided by the algorithm. On the one hand, it can be observed that the ratio between the concentrations of Al and Mg are very close to the expected results, although the participation of Al slightly exceeds its real value. On the other hand, the relation between the weight of Mg in the three different Al alloys is correctly offered by the model when the Window #1 is used, as the averaged values of Mg participation for craters #1 to #4 are 3.65 for Al5754, 4.375 for Al5186 and 4.103 for 5182, which are

in a reasonably good agreement with their chemical compositions. It should be mentioned that the previously discussed results were obtained without taking into consideration the spectral response of the experimental system, i.e. the spectrometer+ICCD+optics. In this regard new data were gathered to analyze the effect of the acquisition system response on the overall performance of the model. Participation values for Al and Mg on the previously analyzed samples are again presented in Table 6. It can be observed that a subtle variation in comparison to data displayed in Table 5 can be appreciated, in particular the participation values obtained in this case are slightly higher than those calculated without correcting the intensity of the spectral lines under analysis.

	Al5754				Al5186				Al5182			
	Window #0		Window #1		Window #0		Window #1		Window #0		Window #1	
Crater #	Al	Mg	Al	Mg	Al	Mg	Al	Mg	Al	Mg	Al	Mg
Crater #1	99.00	4.02	99.00	3.88	98.86	2.71	99.00	3.61	99.00	4.00	99.00	3.92
Crater #2	99.00	2.94	99.00	2.96	97.26	2.16	99.00	4.40	98.83	2.20	99.00	4.61
Crater #3	98.98	3.84	99.00	3.80	97.26	2.90	99.00	5.41	99.00	2.39	98.98	3.06
Crater #4	98.96	3.96	99.00	3.96	98.98	1.98	99.00	4.08	98.41	2.80	99.00	4.82

Table 5: Participation results for Mg-based Al alloys

	Al5754				Al5186				Al5182			
	Window #0		Window #1		Window #0		Window #1		Window #0		Window #1	
Crater #	Al	Mg	Al	Mg	Al	Mg	Al	Mg	Al	Mg	Al	Mg
Crater #1	98.98	4.82	99.00	5.00	98.84	2.37	98.96	4.80	98.96	2.86	99.00	5.82
Crater #2	99.00	3.24	99.00	4.00	98.86	2.31	98.98	4.59	97.67	2.98	99.00	6.49

Table 6: Participation results for Mg-based Al alloys: considering the acquisition system response

3.2.3 Nordic gold

To complete this experimental feasibility study, a sample of Nordic Gold was also taken into consideration. Its chemical composition is composed of Cu (89%), Al (5%), Zn (5%) and Pb (1%), and the spectra acquired were already presented in Figure 34. Again, the study was carried out using a spectrum generated by an average of 10 spectral captures, formed as the accumulation of 20 spectra. The results in this case show a very good agreement for Cu and Zn, as the participation results indicate a weight for Cu of 96.94 and 6.1 for Zn (97.84 and 6.86) if a spectral

window from 308.43 to 330.39 nm is employed (the total spectral range goes from 302 to 334 nm). In this case the algorithm does not detect de Al lines, as their signal to noise ratio (i.e., the relation between their intensity and their associated continuum radiation) is too low. If the associated parameter is modified to allow these lines to be considered, the results for Al in this case are higher than expected: 61.53 (total spectral range) and 42.94. A possibility to solve this problem could lie in the internal normalization of each individual species spectrum, as suggested by Amato et al. [35].

4. Conclusions

The post-processing of raw LIBS spectra is of paramount importance to obtain significant and reliable results on each specific LIBS application. These spectra can be employed in a “blind” mode, without any qualitative or quantitative analysis. The spectral signature can be used to distinguish between different materials using a suitable algorithm. Furthermore, these algorithms can be employed as an extra tool in order to complete a whole chemical analysis obtaining new information about the samples under study. Besides, a new approach to quantitative analysis based on LIBS has been exposed in order to extend the number of tools for this purpose.

The two first applications shown in this chapter are examples of this point of view. A PCA algorithm has been employed in order to complement a stylistic and chemical analysis, giving useful information that can help to date a set of bronze statues. This dating is obtained easier using PCA than with a quantitative or qualitative analysis, and PCA allows working directly and automatically with the raw LIBS spectra without any difficult process. Secondly, a whole classification algorithm based on SVM’s has been used in a real industrial application. This algorithm allows the detection of impurities on steels in real time and with the raw LIBS spectra. The use of this algorithm with an appropriate set of internal parameters achieves an accurate detection without any information of quantitative analysis working in a real “blind mode”.

Finally, a new approach for semi-quantitative analysis via LIBS has been proposed in the last part of this chapter. It is based on the generation of synthetic spectra and

optimization algorithms to generate the so-called participation index that can be directly related to the weight of the different elements in the samples. Different samples (Brass, aluminum-magnesium alloys and Nordic gold) have been analyzed providing results in reasonable good agreement with the known concentrations, always in terms of a semi-quantitative analysis. In particular, the estimated ratios between the main elements exhibit a good correlation, although in some cases some issues inherent to LIBS have prevented the model to provide the expected results. On the other hand, a method totally independent of the relative intensities might be investigated, using an initial estimation of the electronic temperature to establish the ratios between different pairs of lines of various species, thus being able to build the synthetic spectra by using those known ratios. It is worth mentioning that the proposed solution does not need the use of calibration curves or any previous spectroscopic parameter estimation, for example the plasma electronic temperature or density, as it occurs with other methods. In addition, it may work in a completely autonomous mode, although some aspects regarding the emission lines identification should be revised. It has been discussed above the importance of an accurate quantitative chemical analysis based on LIBS, and new improvements can achieve a new tool for quantitative analysis.

Chapter 6

Experimental contributions: LIBS for real applications

Different LIBS works have been shown in previous chapters. These works are related to the induced shockwave detection, different algorithms for sample classification or quantitative analysis based on LIBS measurements.

This chapter is devoted to LIBS applications for two different fields. The first of them is the industrial environment, specifically LIBS will be used to detect precious metal alloys on the control of recovery and recycling procedure of scraps and wastes of industrial processes. In particular, the possibility of obtaining sensitivity and trueness comparable to the current systems used in industrial environment will be explored. This kind of industrial waste can be recycled and the detection of these metals can increase the performance of this process due to the increase of waste value.

Secondly, the other part of this chapter will show some applications of LIBS for archaeological purposes. LIBS provides a fast and in situ chemical analysis without sample preparation and with a minimum damage in the sample. These features are interesting for archaeological applications due to the nature of archaeological sites and samples.

The first work related with archaeology uses LIBS as a tool for a whole chemical analysis of a vase attributed to the I century C.E. The joint use of infrared spectroscopic analysis and laser techniques, as well as pyrolysis-gas chromatography coupled with mass spectrometry and thermoluminescence, allowed a characterization of the vase material and its content. The chemical data were

combined with morphological and stylistic examinations of the object and helped in defining its actual geographical and chronological pertinence.

The second work is another example of a complementary chemical analysis using different spectrochemical techniques. The set of samples is composed by a large collection of silver roman republican denarii, encompassing about two centuries of history. The joint use of Laser-Induced Breakdown Spectroscopy (LIBS) and X-Ray Fluorescence (XRF) spectroscopy allowed an accurate determination of the coins' elemental composition; the measurements, performed mostly in situ at the 'Monetiere' in Florence, revealed a striking connection between the 'quality' of the silver alloy and some crucial contemporary events. This finding was used to classify a group of denarii whose dating was otherwise impossible.

The last part of this chapter shows another point of view of LIBS as an archaeological tool. Paleonutritional analysis is a powerful tool for the investigation of the habits and economy of ancient civilizations. This kind of analysis is usually performed searching for trace elements in archaeological bones relying on the fact that their relative abundance is related to the diet followed by people, especially in the last years of their lives. LIBS allows the detection of chemical elements in a wide range of samples, thus encouraging the study of its feasibility for this challenge. Thirteen human bones coming from a XVI Century plague mass grave found in an island near Venice, in Northern Italy, have been analyzed. Analysis has been performed both with (LIBS) and Inductively-Coupled Plasma - Optical Emission Spectroscopy (ICP-OES), in order to compare the results of both of them and test the feasibility of LIBS as a tool for paleonutritional analysis.

1. LIBS for archaeological samples: single and Multi-technique studies

It has been explained above that LIBS is a feasible technique for archaeological fields. But a whole study for an archaeological sample needs more information than LIBS can provide. For instance some kind of organic samples are not adequate for

LIBS analysis because LIBS provides elemental information and the molecular information could be essential to identify them.

For that reason LIBS can be one analysis of a whole set of measurements for an archaeological analysis. There are better techniques for different purposes, for instance Thermoluminescence analysis [1] can be very useful for the authentication of a sample but this is a micro destructive technique as LIBS and there are samples where this kind of analysis is not possible due to the induced damage on the sample. For this kind of samples there are techniques such as X-ray fluorescence [2] that does not damage the sample and can provide a more accurate quantitative analysis than LIBS. If the molecular information is necessary, techniques as Fourier transform infrared (FTIR) spectroscopy [3] can provide this kind of information about the kind of molecules which compose the sample. For that reasons, this part shows multi-technique studies which have been carried out with different samples in order to obtain a whole spectrochemical study. Specifically, a ceramic archaeological artifact and a set of roman denarii have been analyzed using different spectrochemical techniques.

1.1 Spectrochemical techniques employed for these works

Different spectrochemical techniques have been employed for the analysis of the samples. Obviously one of them is LIBS, whose main features have been already exposed. Despite this fact, a set of measurements have been carried out with other techniques and, a small overview of all of them will be explained here.

1.1.1 Thermoluminescence spectroscopy

The best technique to date ceramic samples is thermoluminescence analysis (TL) [1]. Its principles are based on the fact that some of the components of clays (quartz and feldspars) are thermoluminescent, i.e., they emit light under the effect of high temperature (hundreds of degrees Celsius). These materials in fact are able to accumulate in stable traps the electrons produced by the environmental natural radioactivity. All this energy is emitted when the material is heated at high temperatures. At the moment of firing of the clay, the thermoluminescence

accumulated during the geological existence is ‘zeroed’. Since that time, it starts to rebuild steadily (depending on the environment and on the characteristics of the material itself). Therefore, the measurement of the residual thermoluminescence is also a measurement of the time elapsed since the last high temperature event in the history of the object due to the fact that all the amount of energy is emitted in each heating process. The determination of the age of the object can be rather precise (±5%) provided both the internal and environmental radiation levels are known. This technique needs only a small amount of clay from the sample. For that reason, Thermoluminescence is a micro-destructive analysis

1.1.2 Pyrolysis gas chromatography mass spectrometry (Py-GC/MS) spectroscopy

Py-GC/MS is a spectrochemical method that enables a reproducible characterization of the complex and non-volatile molecules found in virtually all materials in the natural environment [4, 5]. The sample is rapidly heated in a range of 600-1000 ºC or even higher in an inert atmosphere or vacuum to decomposition in order to produce smaller molecules that are separated by gas chromatography [6, 7] and detected using mass spectrometry [8, 9].

Samples such as carbohydrates belong to this group of complex molecules. One of the samples under analysis is a ceramic vase, and an analysis of its content has been carried out. The compounds which were probably inside include vine or beer, and these liquids content a big amount of different kind of carbohydrates. For that reason Py/GC/MS could be adequate for this analysis.

1.1.3 Fourier Transform Infrared (FTIR) spectroscopy

Infrared spectroscopy [10, 11] exploits the fact that when a sample is irradiated with an infrared light, the molecules absorb specific frequencies that are characteristic of their structure. These absorptions are resonant frequencies and induce vibrations on the molecules or groups, i.e. the frequency of the absorbed radiation matches the frequency of the bond or group that vibrates. The energies are determined by the shape of the molecular potential energy surfaces, the masses of the atoms, and the associated vibronic coupling.

Fourier transform infrared (FTIR) spectroscopy is a spectrochemical technique used initially for qualitative and quantitative analysis of organic compounds, providing specific information on molecular structure, chemical bonding and molecular environment [12]. FTIR uses a spectrometer which allows obtaining the spectra of the acquired light calculating its Fourier transform. This is a non-destructive technique, and for that reason is suitable for archaeological samples whose structure should be preserved.

1.1.4 X-Ray Fluorescence (XRF) spectroscopy

X-ray fluorescence (XRF) [13] is the emission of characteristic fluorescent light from a material that has been excited with high-energy X-rays or gamma rays. Theoretically, the lightest element that can be analyzed is beryllium (Z = 4), but due to instrumental limitations and low X-ray emission performance for the light elements, it is often difficult to quantify elements lighter than sodium (Z = 11), unless background corrections and very comprehensive inter-element corrections are made. For that reason, XRF is suitable for the analysis of heavy elements or compounds such as metals, glass, ceramics and building materials, and for research in geochemistry, forensic science and archaeology due to the fact that XRF is a non-destructive technique.

The feasibility of XRF for metal analysis and archaeological samples has been exploited for the analysis of a set of samples which satisfy these requirements. A set of Roman denarii has been analyzed with both LIBS and XRF in order to obtain a whole chemical analysis of these samples.

1.1.5 Inductively Coupled Plasma Optical Emission Spectrometry

Inductively Coupled Plasma Optical Emission Spectrometry (ICP-OES), is an analytical technique used for the detection of a big amount of different trace elements in a wide range of samples which include gases, liquids and solids (solid samples require a complex sample preparation) [14, 15]. It is a type of emission spectroscopy that uses the inductively coupled plasma to produce excited atoms and ions that emit electromagnetic radiation at wavelengths characteristic of a particular

element. The emission intensity indicates the concentration of the element in the sample composition.

The plasma is induced into a chamber by a RF discharge which ionizes a support gas, usually argon, in order to induce and stabilize the plasma. When the plasma is created, the sample is introduced into the chamber as a gas or a nebulization. The sample elements are excited and emit photons with different energies which depend of the emitter element.

Within the optical chamber(s), the light is separated in different wavelengths with a diffraction grating and then is detected using different devices such as photomultipliers or CCD's for simultaneous detection of many elements. The intensity of each line is then compared with previously measured intensities of known concentrations of the elements, and their concentrations are then computed by interpolation along the calibration lines providing an accurate quantitative analysis.

1.2 Multi-technique analysis of a ceramic artifact.

A multi-technique study of a ceramic vase has been carried out in this work. The goal of this work has been to authenticate the vase but its content during its use has also been tried to analyze. Figure 39 shows the vase that has been analyzed; it was manufactured in black ceramics. It is 192 mm high with an annular foot, with rounded external profile (diameter 76 mm, height 8.5 mm), ovoid body (diameter 119 mm) and a cylindrical neck 64 mm high with a diameter of 56 mm. The lip is trilobate, the frontal lobe is 86 × 33 mm, while the two lateral lobes are 82 × 41 mm both, pointing down towards the outside. The handle is rather thick (15 mm), 20 mm wide and is attached to the main body of the vase 96 mm from the foot and in correspondence of the upper extremity of the neck. Moreover, a handwritten piece of paper is glued to the body, carrying some information about the alleged provenience of the vase as a gift from the excavations of Herculaneum, destroyed by the Mount Vesuvius eruption in 79 C.E.

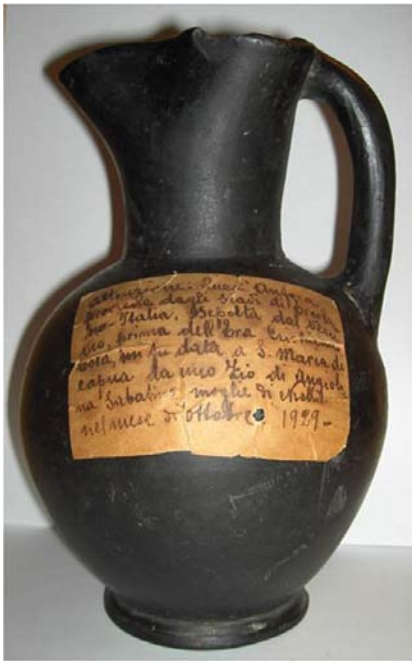

Figure 39: The Vase under study

1.2.1 Results of LIBS and FTIR

The main feature of the vase is its solid black color, typical of the Bucchero ceramics [16]. It has been studied that in the antiquity this color was obtained through firing of the clay in reducing atmosphere. These techniques have been used in order to detect black pigments (e.g. manganese oxide) in the vase. LIBS can carry out a quantitative elemental analysis of the vase clay, and FTIR can provide a molecular analysis of it. Both techniques together can demonstrate the absence or presence of pigments and this is a preliminary evidence of the authenticity of the vase due to the fact that these pigments suggest a manufacturing process dated in other period [17].

The FTIR analysis of the clay has been carried out with three micro-samples from three points on the foot (1 mg in KBr pellet). The analysis detected the presence of silicates, quartz, iron oxides (Fe–O stretching bands at 463 cm^{-1}) and aluminum oxides as expected in natural clays [18, 19]. The FTIR spectrum is shown on Figure 40 .

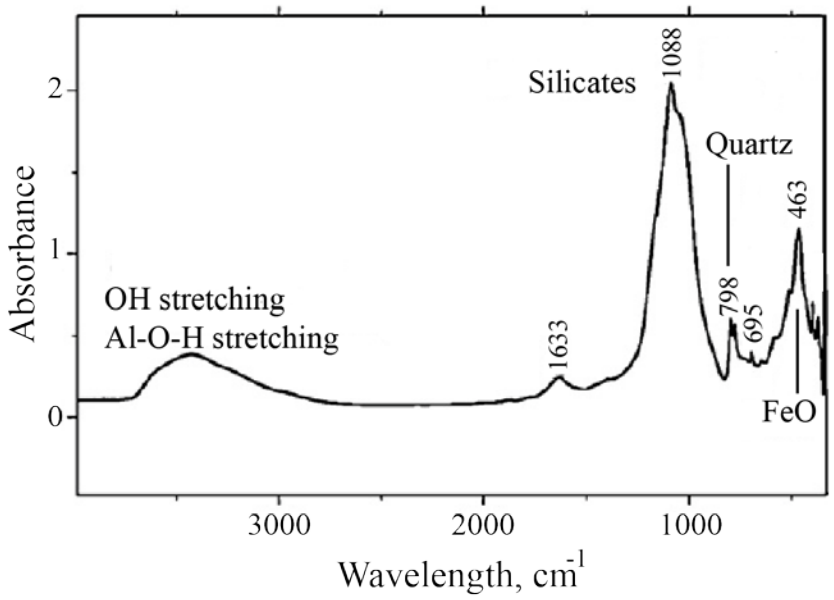

Figure 40: FTIR spectrum of vase clay

LIBS has been used for the determination of the elemental composition of the vase material. Figure 41 shows the LIBS spectrum of the vase clay.

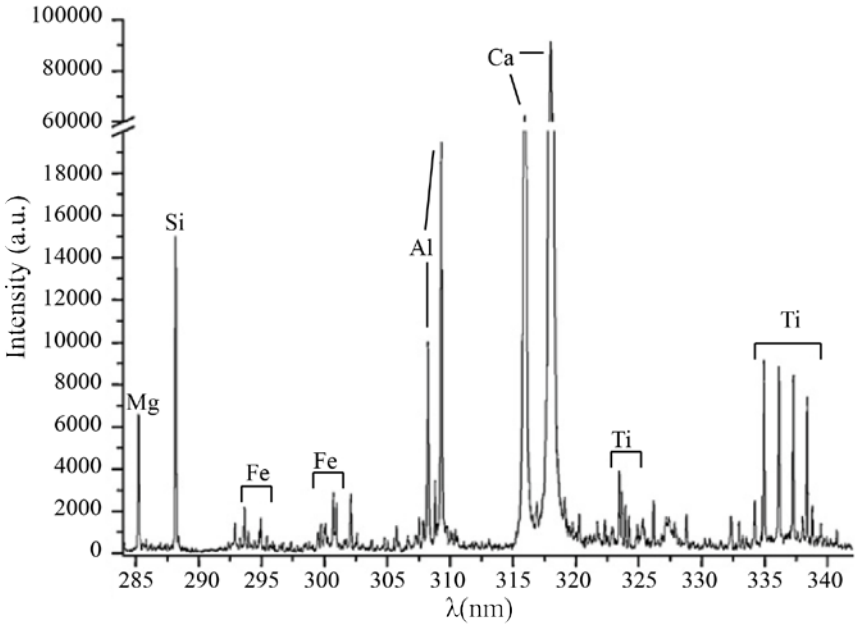

Figure 41: LIBS spectrum of vase clay

The qualitative analysis of the spectrum by means the identification of the main emission peaks, excludes that natural or artificial black pigments were added to the clay in order to obtain the black color. Instead, all the expected elements of natural

clay (iron, magnesium, silicon, aluminum, calcium, titanium) are clearly present in the sample. Therefore, the absence of pigments demonstrated by LIBS results does not disprove the authenticity of the vase.

To summarize, the black color of the vase is due to the presence of FeO stretching bands at 463 cm^{-1} in the FTIR spectrum, confirmed by the evidence of intense Fe lines in LIBS spectrum. For that reason, it is reasonable to conclude that the clay composition is coherent with the manufacture of an original Bucchero.

1.2.2 Thermoluminescence analysis: age of the vase

The identification of the vase as a Bucchero could imply a doubt about the authenticity and the date of the vase. This kind of black terracotta is well documented in the Campania region, near Herculaneum, from the beginning of VI century BCE to the end of V century CE. However, in 79 CE, at the time of the Mount Vesuvius eruption which destroyed Pompeii and Herculaneum, this kind of vase was not used anymore [20, 21]. In order to obtain a definite answer on the authenticity of the vase, a thermoluminescence study was performed. There is no precise information about the placement of the object and this fact implies that the radioactivity parameters cannot be determined. For that reason, thermoluminescence analysis cannot provide a precise estimation of the age of the object, but the date is enough for checking its authenticity.

The thermoluminescence analysis was carried out by means of the fine-grain technique [21]. It was determined that the natural thermoluminiscence (TL) signal was quite high, with a broad peak around 300 ◦C. A linear growth as a function of the calibration dose was observed, and a total absorbed dose of 16.8 ± 0.7 Gy was measured. Assuming the typical radioactivity parameters from the place where bucchero was produced and taking into account their possible natural variations (3–6 ppm 238U; 10–25 ppm 232 Th, 1.0–2.0% K2O), the manufacture of the vase can be date between VII century BCE and I century CE. Thus, It demonstrates the authenticity of the vase and, although the dating obtained by thermoluminescence is marginally compatible with the I century CE, the typological and stylistic analysis suggests that the vase is much older.

The shape and the fabrication technique define the vase under study as an Oinochoe (vase for serving wine) in heavy bucchero. Oinochoai were present in the Campania region since the first quarter of VI century BCE. In particular, the Oinochoe under study corresponds to type 13b1 in the Pontecagnano classification [22] and is very similar to other vases conserved in the Museo Campano in Capua and to other material from Campania necropolis. Thus, on the basis of these associations, the present Oinochoe can be likely attributed to the phase IVc of Capua, in the first quarter of VI century BCE, probably manufactured by local handicrafts.

1.2.3 Analysis of vase content: FTIR and Py-GC/MS

Before the authentication of the vase and its identification as an Oinochoe, the possibility of the identification of the vase content arose. FTIR can provide molecular information and Py-GC/MS is suitable for the analysis of complex molecules. The use of an Oinochoe as an alcoholic drink container suggests that these techniques can help to discover the kind of drink, due to fact that these drinks have a presence of complex molecules such as carbohydrates.

The most common drinks for this kind of vases in that period are wine and beer. Moreover, it is known that in the Mediterranean and Central Europe area a honey fermented beverage called hydromel (mead or honey wine) was also consumed [23]. This is a drink currently non-existent, thus the hydromel has been fermented in the laboratory. FTIR spectrum of the rinsing solution of the content of the vase and the spectra of these three drinks are shown on Figure 42.

The comparison of the FTIR spectra with the vase rinsing solution shows that the content of the vase is an alcoholic substance obtained from fermentation. However, the results does not allow a clear discrimination between the three drinks, since the characteristic peeks of the FTIR spectrum are present in all the samples and their relative intensity is not useful for discrimination, due to the probable degradation of the vase content.

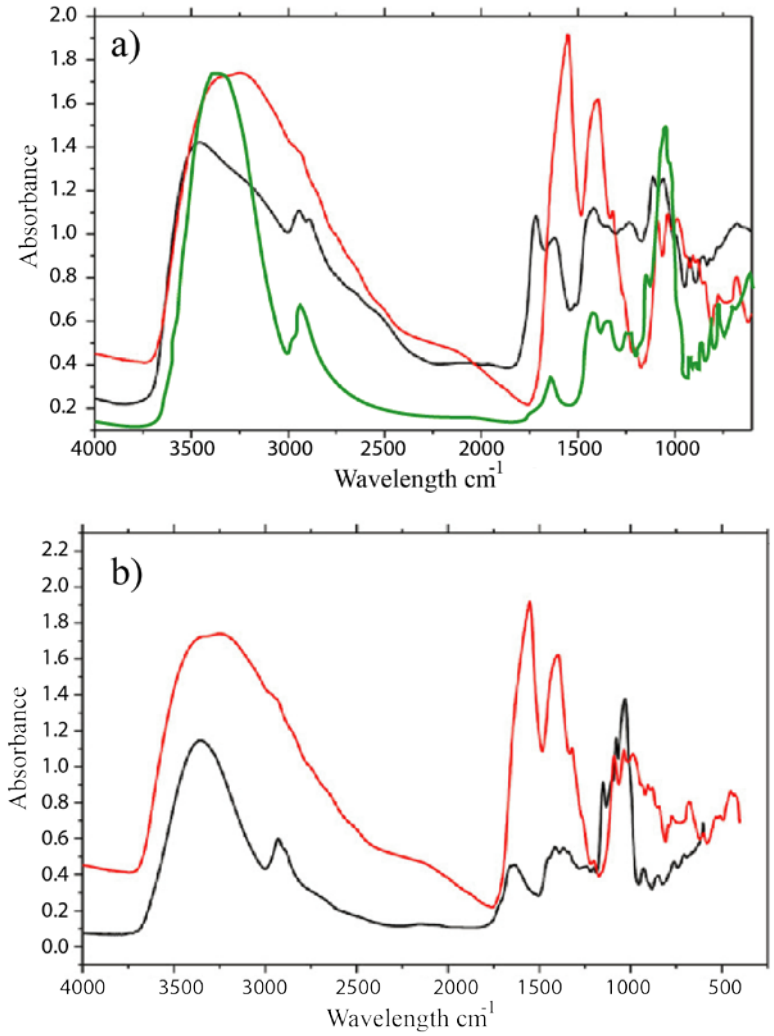

Figure 42: a) FTIR spectrum of wine (black) and hydromel (green) (in red, the FTIR spectrum of the vase rinsing solution). b) FTIR spectrum of beer (in red, the FTIR spectrum of the vase rinsing solution).

On the other hand, the analysis of particles micro-sampled inside the vase by pyrolysis coupled to GC–MS (Figure 43) evidenced the pyrolysis products characteristic of polysaccharide materials [24, 25] derived from fruit or vegetables fermentation.

It is known from the Homeric poems that around the VI century BCE the word ‘wine’ is related with a wide range of fermented products from grape to fruits [26]. The Py-GC/MS pattern observed is coherent with the presence of fruit or vegetable matter in the alcoholic beverage contained in the vase. It should be noted that, although the presence of alcoholic residuals in archaeological vases has been scientifically

confirmed in many circumstances [27, 28] (the earliest chemically confirmed archaeological beer dates ca. 3400–3000 B.C., while the earliest wine remains date back to ca. 5400 B.C. (Early Neolithic Period)), there is no way of knowing, at least with the techniques used in this paper, at what time in its long life the beverage was actually contained in the vase [28].

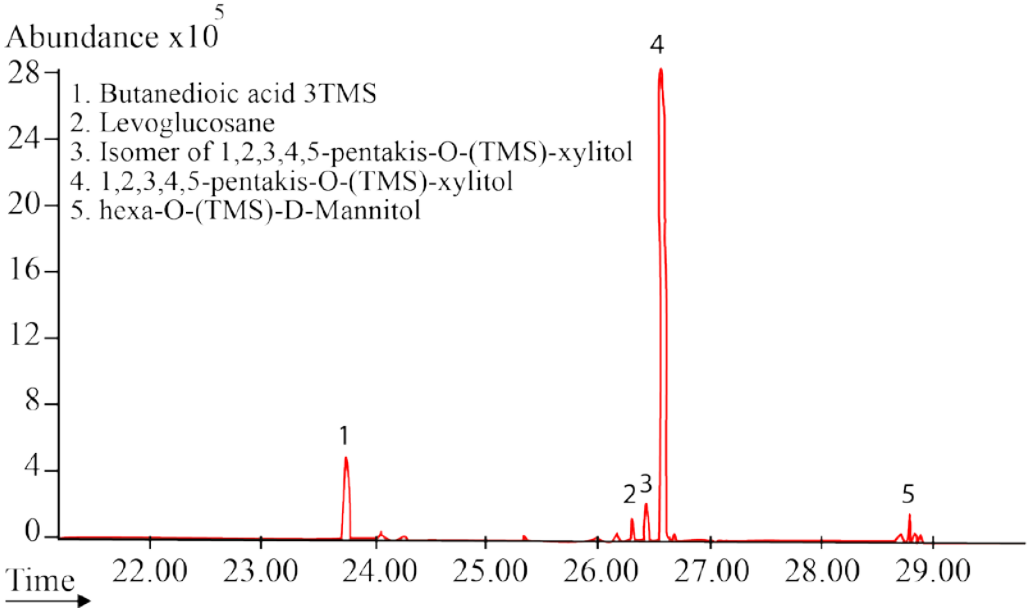

Figure 43: Pyrogram of the base rising solution

1.3 Multi-Analysis of Roman silver Denarii

Numismatics includes a large number of fields such as Economy, History, Archaeology, Art and, last but not least, Metallurgy. The analysis of the metal alloy of the coin can be invaluable for understanding the techniques used for its realization, as well as the effect that time and the environment produced on it. Furthermore, a date of the sample and its origin and location can be achieved indirectly analyzing the bulk and surface of the sample.

A metallurgic analysis of ancient coins could be important for historic and numismatic purposes. Nowadays, a non-destructive analysis on coin patina and bulk is a great challenge. Different kinds of well assessed non-destructive techniques, such as XRF [29, 30] can be used to characterize the surface of the coin, while in depth analysis can be carried out using other techniques, such as LIBS [31], despite the fact that

LIBS is micro-destructive. The great majority of studies published up to now, however, are based on destructive methods that are obviously unacceptable for the analysis of numismatics valuable coins.

A large amount of spectrochemical techniques need the transportation of the sample to the lab due to the fact that the equipment is big, heavy or it can suffer decalibration due to movements. Moreover, some of these techniques can provide an accurate quantitative analysis, but a complex sampling and sample preparation are required. A large amount of archaeological samples are subjected to hard requirements of conservation, and movement or sampling is not recommended. For that reasons, the portable solutions are desirable for some archaeological or artistic applications, and XRF and LIBS set-ups satisfy this requirement [32]. In fact, it is well known that the presence of surface deterioration layers affects XRF measurements and prevents a reliable achievement of the bulk composition [33]. Although LIBS measurements of the bulk composition are possible, deeply corroded objects may require protract ablation to reach the bulk, which would result in greater damage to the piece. Thus it is important to devise a method that would be benefitted by both the intrinsic non-destructivity of the XRF technique, and by the capability of LIBS to perform true bulk composition measurements even in the presence of heavy surface deterioration. This work demonstrates that a proper use of these techniques together can achieve valuable information of the sample about aspects as fabrication context and technology, and deterioration mechanisms of archaeological and historical metals, preserving the state of the samples.

1.3.1 Material under analysis: Roman Denarii

The measurements were performed on more than 100 republican denarii, issued in a period of two centuries of Roman history. There is still a controversy about the date of the first issuing of Roman Denarii [34-36]; accordingly to several authors, the issuing of Denarius was introduced in the year 211 B.C., after the sack of Syracuse which made a large amount of silver available to the Roman republic. The republican denarius was issued from that date to the end of the republic, which is conventionally related to the battle of Actium (31 B.C.), which brought the defeat of Mark Antony and Cleopatra and the beginning of the Principate of Octavian Augustus. During

these years, the weight and value of the republican denarius changed several times; however, it is widely accepted that the ratio of silver of Denarius was maintained on 95% in weight or more, with the exception of the late Mark Antony 'legionary' denarii which were coined on debased silver flans during the civil war against Octavian. No systematic metallurgic studies were performed on a statistically significant number of republican denarii for assessing their 'quality' in the course of those years. The use of portable instrumentation for in situ micro-analysis, in conjunction with the availability of a large number of republican coins at the Monetiere in Florence, allowed testing a statistically significant sample of coins, determining precisely their elemental composition and, for the first time, correlating the silver content of the coins with important historical events. The relationship between wars and the issuing of Denarius with a lower ratio of silver has allowed dating indirectly some coins whose features did not allow their classification with other proceedings. Such an example can be given in the case of the Mark Antony 'legionary' denarius (Figure 44).

Figure 44: The Mark Antony 'legionary' denarius (Legio V), an example of analyzed coins

1.3.2 Results of multi-analysis: LIBS as a checker

The first step for the analysis of Roman Denarii is to cross-validate the measurements of LIBS and XRF, following a process described in previous works [32]. However, the corrosion suffered by metallic archaeological samples can modify the composition of sample surface, changing it with respect the bulk. In the case of silver coins, the use of surface information for deducing bulk composition has led in

the past to incorrect deductions, as in the case of roman 'Antoniniani' (a special kind of coin with an enriched surface of silver and a poorer bulk composition). For that reason, the first analysis with roman coins based on XRF surface analysis [37] in the seventies, are now being challenged by new, in depth analysis [38].

A limited –although significant – set of coins has been selected to carry out the LIBS analysis in order to validate the results of XRF for the analysis of bulk composition. The coins were selected to be representative of the different conservation status and colors of the patina of the whole set of denarii. The LIBS experimental parameters have been selected to assure a readable LIBS spectrum with the minimum crater to avoid large damages in the surface of the coins. It turned out that three double pulses with an energy of 50 mJ each were able to pass through the surface patina with very limited damage to the surface of the coin. The diameter of the laser-induced microcrater on the coin surface was around 200 µm and the depth, estimated from optical microscopy, was around 4 µm. A typical spectrum of a republican denarius is shown on Figure 45

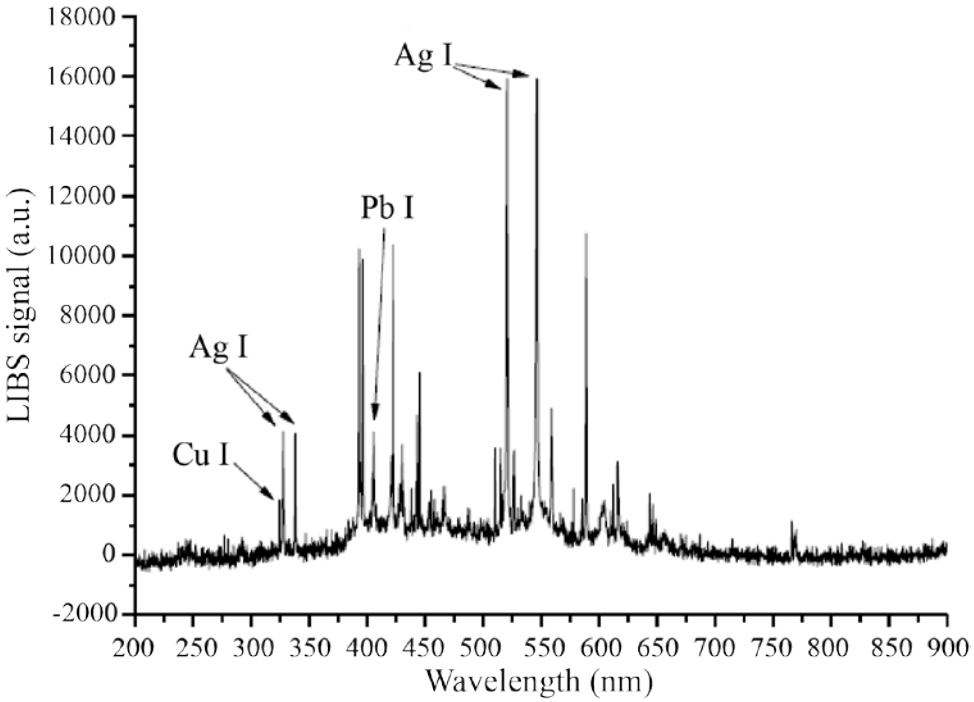

Figure 45: LIBS spectrum of a republican denarius

Figure 46 shows the comparison of the line intensities of the main elements of the alloy (normalized to the background) measured by XRF with those obtained with LIBS for the same elements. In order to minimize enrichment, patina and geometry effects, XRF data were obtained by averaging two measurements obtained on the most worn out areas of each side of the coin.

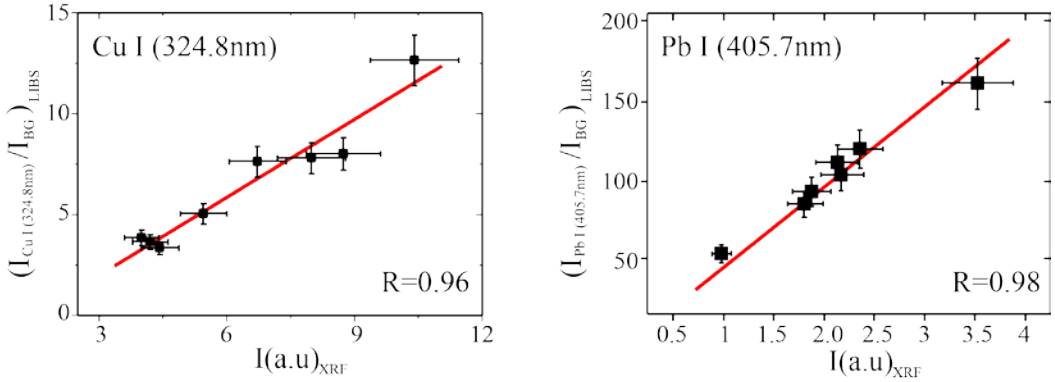

Figure 46: Correlation between XRF and LIBS measurements floor copper (left) and lead (right)

A high correlation has been founded between the XRF and LIBS results (R=0.96 for Cu and R=0.98 for Pb), obtained despite of the different spot sizes (200 µm for LIBS vs. 2 mm for XRF) and penetration lengths (the LIBS analysis is performed between 3 and 4 µm under the surface, while the maximum XRF signal comes from the sample surface, down to about 10 µm under it) and not considering possible self-absorption effects in LIBS analysis. This correlation suggests the feasibility of an XRF set-up for the analysis of the bulk composition, avoiding the damage induced by a LIBS measurement. Roman denarii are valuable samples and even the small damage induced by LIBS can be a problem for the sample quality. Even for this kind of analysis, LIBS is useful. A LIBS analysis can be carried out in a reduced set of samples as a checker tool, in order to assure the feasibility of other non-destructive techniques without deep analysis capability.

Once the feasibility of XRF analysis has been tested with LIBS, the whole set of samples was analyzed with XRF. The silver content of the coins can be determined by difference (%Ag ≈ 100% - %Cu, due to the fact that silver and copper are the main components of the republican denarii (with lead as a trace); this determination

is more precise than the direct measurement of the silver content, since the silver concentration is always larger than 90% in weight and the experimental error in the silver determination (around 10%) is of the same order than the variations to be measured. The results are shown on Figure 47.

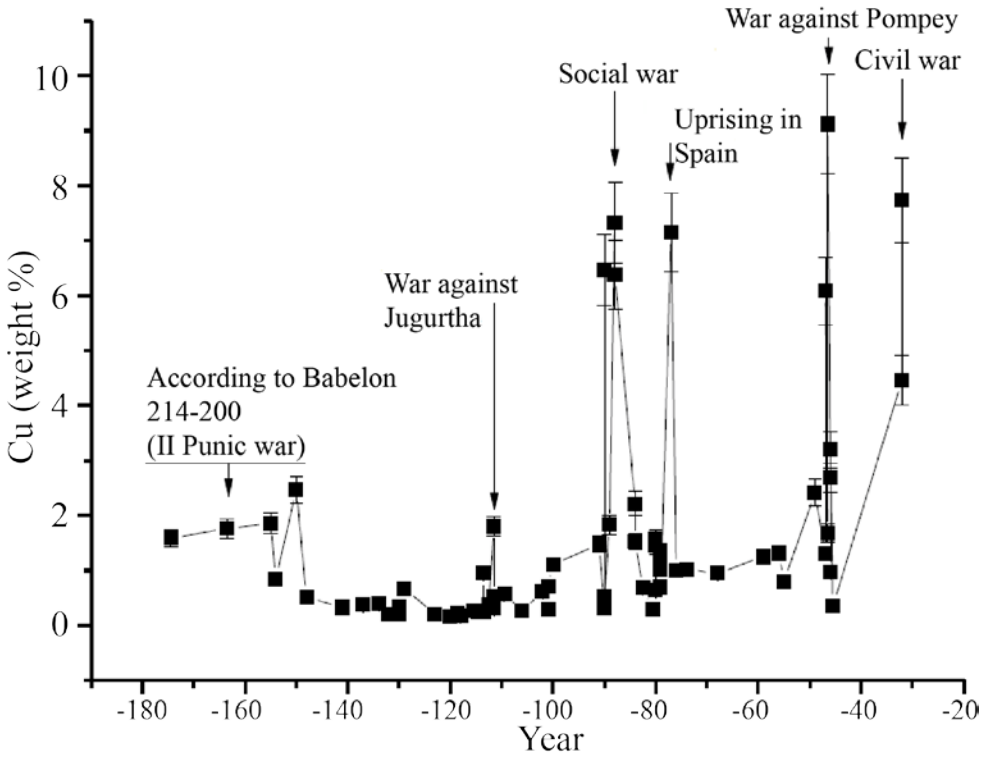

Figure 47: Time evolution of copper content on denarii

XRF analysis of copper-silver ratio on coins can provide interesting information about the date of samples and interesting events related with coins composition. A high correlation can be noticed between the copper increase (and, thus, the reduction of the silver) in the coins with the most critical events in the Roman history of this period (the war against Jugurtha, the Social War, the Uprising in Spain with the associated problems of silver supply, the War against Pompey and, finally, the Civil War between Octavian and Mark Anthony). Moreover, the first 5 denarii considered, issued between 180 and 150 B.C. according to Crawford [34] should be placed around the year 200 B.C. according to other scholars, at the time of the Second Punic War [33]. This dating can be reinforced for the fact that silver content of the coins of this period is lower than the average.

The results described could sustain the hypothesis that in time of crisis, the silver content of the denarii would be reduced in order to save on the coin value that, at the time, coincided with the value of the precious metal in the alloy.

1.4 LIBS: a feasible tool for paleonutritional analysis

The goal of the paleonutritional analysis [39-41] is to derive information about the dietary habits of people lived in the past. Some trace elements which are present on bone composition can provide information about these dietary habits. Bones, in fact, act a sort of reservoir for the mineral's ions taken with food, therefore a trace of people's diet is imprinted in their composition and it can be retrieved back with a compositional analysis, even hundreds of years after the death of the person.

The most important requirement that must be satisfied is that the concentrations of analyzed elements are the same as ante mortem. In fact, some elements which compose the bone can suffer variations in its concentration due to the elemental interchange between the surrounding media and the bone. These post-mortem alterations of chemical constituents are usually known as diagenetic effects [42, 43] and they represent a serious drawback in the case that the absolute concentration of the elements is the main goal of the research. This effect induces changes in bone composition due to the grave ground composition for people with the same dietary habits in different places. Concerning this latter point, it has been demonstrated that bones originating from different places can be safely compared with each other by taking into account the ratio of the elements' concentration with the one of calcium. Element/calcium ratio, in fact, implies that calcium increasing or decreasing reflects in a similar increasing/decreasing in the other elements. However, this ratio can be distorted due to the fact that calcium is a diagenetic elements and some of the elements employed for paleonutritional analysis are non-diagenetic.

The main feature of analyzed elements for paleonutritional analysis is that the concentration of the element has to be related with only one kind of food. The trace elements that are mainly studied for a paleonutritional analysis are strontium, barium and magnesium, as indicators of a vegetarian diet [44], and zinc as marker of a diet rich of proteins [38]. Strontium and barium are particularly abundant in vegetables,

which absorb them from the ground by the roots. Moreover, strontium is present with high concentrations in small fishes and in shellfishes too [39]. Magnesium also is related to a high consumption of vegetables and cereals; in particular, it is quite abundant in bran, millet, soy, walnuts and nuts. On the other hand, high concentration of zinc can be found in red meat, milk, cheese and legumes, thus indicating a different dietary habit, with a higher contribution of proteins.

There are a large amount of parameters which should be taken into account in order to obtain a useful paleonutritional analysis. That is the reason why most of the works devoted to this kind of analysis use laboratory techniques, such as Atomic Absorption Spectrometry (AAS) [45, 46] or ICP-OES, whose sensibility is very high, up to parts per billion (ppb) and the uncertainty very low. The problems associated with these techniques are the sample preparation, the non-availability of in-situ analysis and the price of equipment. In addition, these techniques need a big amount of material to carry out the analysis and sometimes the value of the samples forbids this kind of damages on them. For these reasons, a technique like LIBS that preserves the integrity of the sample and is fast and relatively not expensive would be very welcome in this field.

The main goal of this work is to compare LIBS with ICP-OES in the analysis of archaeological bones. LIBS, in fact, has some advantages with respect to ICP-OES; LIBS allows the possibility to operate directly in situ, the relatively low cost of the instrumentation, fastness of the analysis, etc... For this reason, the use of LIBS in paleonutritional analysis could be a viable alternative to the aforementioned techniques, especially in those cases where the fastness of the analysis is of paramount importance.

1.4.1 Bones under analysis

Thirteen samples from the thick bones of people found in a XVI century plague mass grave have been analyzed. Actually, in order to perform a correct and meaningful paleonutritional analysis, it is necessary to have a sampling of the place surrounding the grave, just to evaluate the possible contaminations from the environment. Unfortunately, these samples have not been supplied and a meaningful quantitative analysis is not possible. For that reason, this work intends to compare the trend of

the ratios for the paleonutritional elements of all the bones with both techniques, LIBS and ICP-OES in order to test the feasibility of a paleonutritional analysis using LIBS.

The set of spectra from bones alloys was acquired with the same device described in Chapter 5, The MODÌ [47], coupled to a compact Czerny-Turner CCD spectrometer. The problem with bones is related to their inhomogeneity so, in order to overcome this drawback, 4 different points have been sampled; in every spot, 5 cleaning shots and 150 spectra were acquired. The average of 100 spectra for each bone was then analyzed, i.e., and only 25 spectra were considered as 'good' from every spot, from 6th to 30th. All the other acquired spectra have been exploited for the stratigraphic analysis that will be discussed in section 1.4.3. In all the cases, the errors reported for LIBS results were calculated as the half-difference between the higher and lower value of the four points. The usual approach of the standard deviation has not been used because of the reduced number of variables.

Determination of the concentrations was performed with *Varian 720 ES* for ICP_OES analysis. About 0.5 g from every sample were weighted and placed in PTFE holder, where 8ml of HNO3 69 and 2 ml of H2O2 were added. Samples were let to react at ambient temperature for around 40 hours. Then, they were treated in a microwave digester (*Start D*, Milestone Italy) with thermal cycle up to 200 degrees. Once cooled down, the solutions were moved to 50 ml flasks and adjusted in volume with ultrapure H_2O_2. The detected elements were Ba, Mg, Sr and Zn.

1.4.2 Results: ICP-OES vs. LIBS for bones

The composition of the bones was measured with ICP-OES. On the other hand, the amount of spectra obtained with LIBS analysis was huge and only the peak intensities of the interesting elements were analyzed instead the whole spectrum in order to reduce the flow of information. For this reason, a quantitative analysis based on LIBS information was not calculated. Instead of this analysis, the peak intensity for each element was compared for both techniques due to the fact that the concentration of the element is proportional to its peak intensity. This comparison can demonstrate the feasibility of LIBS for paleonutritional analysis because a high correlation between both techniques validates the results obtained with LIBS.

Five elements have been analyzed for paleonutritional analysis, strontium (Sr II @ 407.771 nm), barium (Ba II @ 455.403 nm), magnesium (Mg I @ 280.970 nm), zinc (Zn I @ 636.234 nm) and calcium (Ca I @ 634.907 nm and Ca II @ 370.706 nm). As explained in the introduction, Sr, Ba and Mg are indicators of a vegetarian diet, so their behavior is expected to be, more or less, the same. Contrarily, Zn is an indicator of a proteic diet, and its ratio with Sr can provide information about the amount of proteic food in the dietary habits of each person [48].

In Figure 48, the trend of the zinc over strontium ratio is reported for ICP-OES (black squares), and for LIBS (open squares). As it can be seen, LIBS results are in quite good agreement with ICP-OES, at least within the LIBS error bar. The inhomogeneity of bone 5 can induce the difference between both results for this sample.

The comparison between LIBS and ICP-OES for the trend of barium and magnesium is reported in Figure 49 and Figure 50, respectively. The results are even closer for these elements than the previous one.

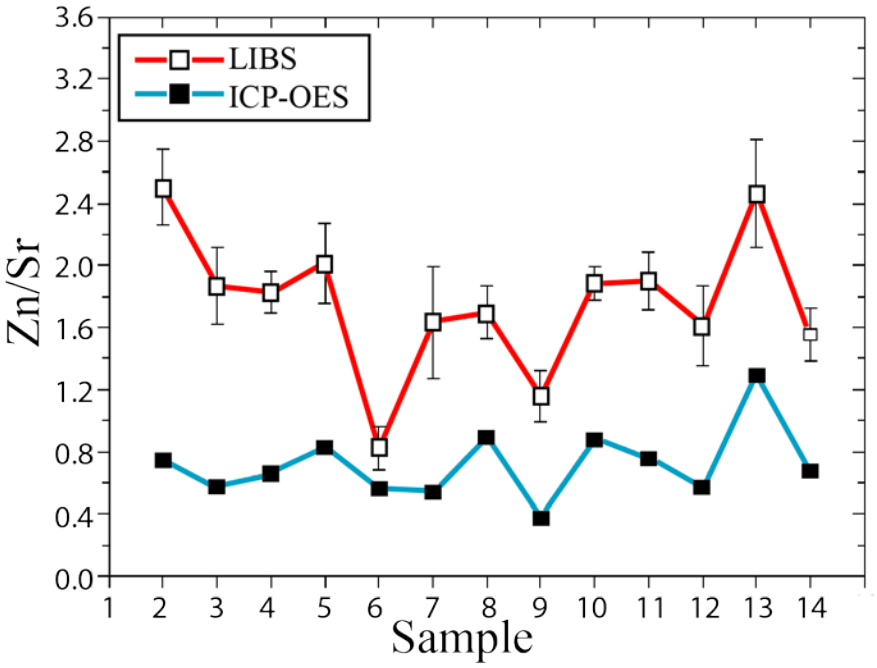

Figure 48: ratio between Zn and Sr for all bones

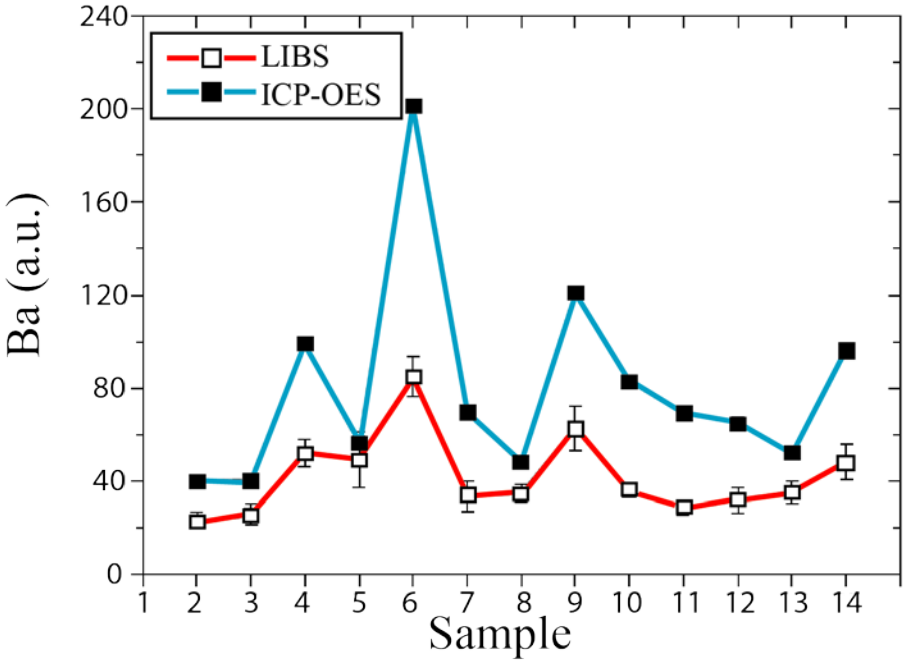

Figure 49: Emission intensity for Ba

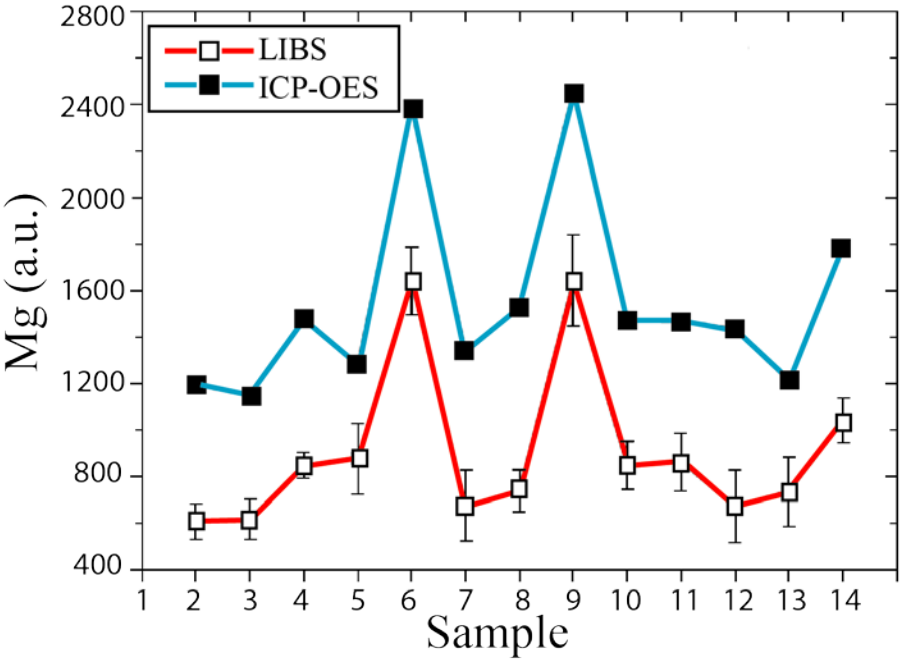

Figure 50: Emission intensity for Mg

In Figure 51, the ratios of both strontium and barium related with calcium are shown. The reason is that barium is an indicator of a vegetarian diet, so its behavior is expected to be very similar to strontium, being their nature very similar from the point of view of the biological purification of calcium. This premise is demonstrated on Figure 51, where the trends of Sr and Ba related with Ca are similar. This is a very

good point for LIBS measurements, because it means that they are perfectly consistent among themselves.

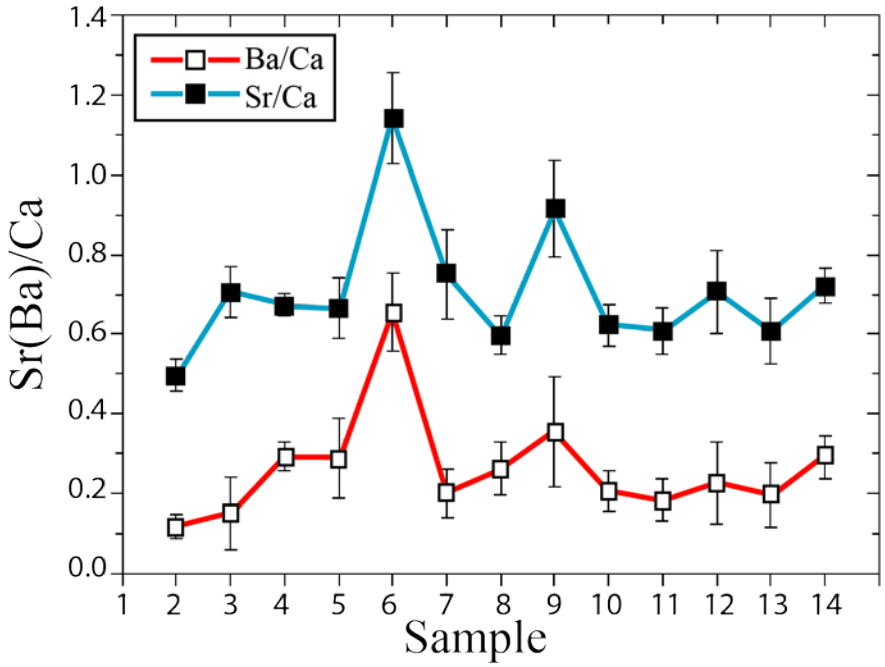

Figure 51: Ratios between Sr and Ba with Ca

From the figures above, we can infer some information about the diet of those people. In fact, from Figure 48, both LIBS and ICP-OES results seem to agree that sample 12 has a high zinc over strontium ratio. This result implies that this person followed a proteic diet and indicates that he belonged to a high social class considering that at that time the consumption of meat was mainly prerogative of high social classes. On the other hand, samples 5 and 8 show the lower values of the ratio, thus indicating the possibility of a vegetarian diet and, as a consequence, their belonging to a lower social class. The other figures confirm these results. In Figure 49 and Figure 50, in fact, the higher values of barium and magnesium are relative to sample 5 and 8, i.e., they show a similar behavior as the zinc over strontium ratio in Figure 48. The differences between barium and magnesium are due to the fact that the concentration of barium and strontium are strictly related with a vegetarian diet, whereas the concentration of magnesium is determined by other kind of diets, such as the presence of crustaceans and fishes. For this reason, their trends are expected not to be exactly the same.

1.4.3 Stratigraphic analysis of bones

As explained in the previous sections, bones are expected to be contaminated by the surrounding environment where they have been lying for 400 years; contamination that can result in the leaking out of some elements, such as calcium or strontium, from the bone's surface or vice versa (the so called diagenetic effect). LIBS can provide an in-depth analysis (stratigraphic analysis) unlike other techniques. With ICP-OES, instead, that is not possible, because a big amount of sample has to be dissolved to obtain the composition and it is difficult to separate the bulk and the surface of the bone. ICP-OES provides an average of bones composition in all the depth and surface analyzed but LIBS can analyze different parts of them.

In order to evaluate the changing in concentration of some elements due to the diagenetic effects, a LIBS in-depth analysis has been carried out. The evolution of peak intensity for the elements explained above has been analyzed for the whole sequence of pulses of each crater as I(element)-I(Background)]/I(element), where I(Background) was the intensity of the background measured in a point close to the line under study. Results of this calculation for one of the bones using strontium as test-case are shown in Figure 52.

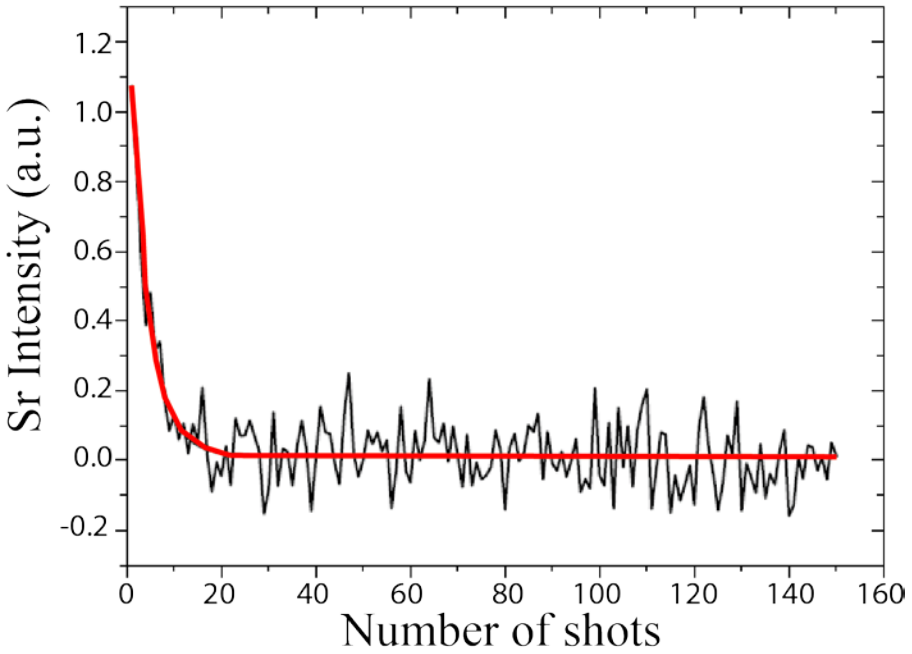

Figure 52: Evolution of Sr intensity with number of pulses

The real measurements are represented in black, and the interpolated trend in red. The figure shows that strontium signal decreases as the laser pulses ablate the sample and penetrate into it. However, this can be due to two different effects; for the change in element concentration for diagenetic effect or problems associated with laser focalization in the induced crater at different depths. The answer to this question could be found by analyzing the bulk directly. A small piece of each bone was removed in order to analyze different points of bone bulk. In this way, the first laser shot was already measuring the bulk. 100 spectra from 3 different points from every bone were acquired for this second campaign of measurements. In this case also, a decreasing of the signal whose limiting value was zero was found and the initial intensity in all points of the bulk was the same. Therefore this is a clear demonstration that the observed decreasing shown in Figure 52 is not related to the decreasing of the concentration, but rather to laser defocusing caused by the soft bone's matrix that creates a deep hole in which the laser ablation efficiency get worse and worse as the deepness increases. In order to assure this theory, the trend of the temperature has been calculated. Actually the "true" temperature has not been obtained with the Saha-Boltzmann plot, but the ratio of a ionized and a neutral peak of calcium, times the electron density (calculated from Balmer H line of hydrogen) has been plotted. The trend of these ratios is shown on Figure 53.

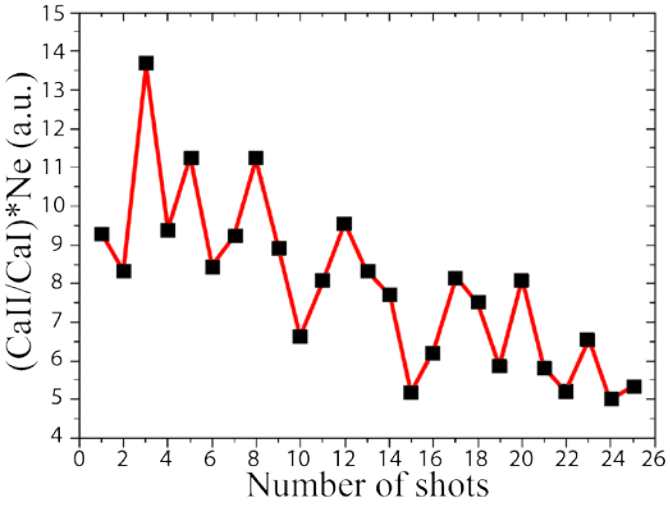

Figure 53: trends of Ca II and Ca I intensities multiplied by electron density. This measurement is directly related to plasma temperature

This trend is due to the slightly decreasing of the Ca II intensity, whereas the Ca I one is more or less constant. These trends are shown on Figure 54:

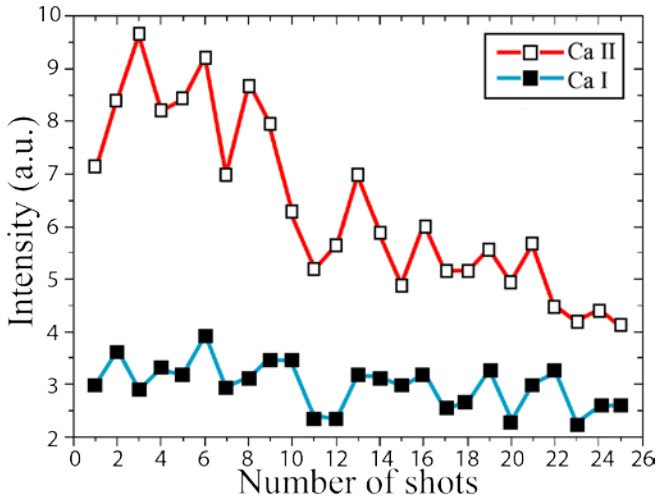

Figure 54: trends of Ca I and CaII

The above results are from the measurements on just one bone (Bone 4), using Ca I @ 643.907 nm and Ca II @ 370.706 nm. This analysis suggests that the decreasing of the signal is not due to a lower concentration, but rather to a worsening of the laser efficiency (that reflects in a colder plasma).

These results suggest two different explanations. The first one is an absence of diagenetic effect. This alternative is not enough plausible because this process is demonstrated in archeological environments of buried samples and it supposes the natural evolution of this kind of samples. The second one is a diagenetic evolution of the whole bulk of the sample. This option implies that the pollutants within the surrounding soil have been leaked out to the whole bone. If this alternative is correct it is not possible to carry out an accurate paleonutritional analysis due to the variation of the ratios of the diagenetic elements and the induced changes of ratios between diagenetic and non-diagenetic elements which are analyzed for these measurements without the correction provided by a surrounding soil sample.

2. LIBS for precious metal recovery

The recovering of precious metals from industrial waste is raising due to the increase of precious metals prices [49]. The quantity of gold, silver, palladium, platinum, rhodium and ruthenium [50] that different recycling process can recover is minimal, but the huge amount of waste products such as batteries or circuit boards with precious metals inside allows recovering a large amount of precious materials [51].

The complexity of the study of waste material is high due to the huge amount of industrial waste materials. Most of the instruments used for waste recovering are based on Atomic Absorption and/or Inductively Coupled Plasma (ICP) techniques. The gold and silver content in the recovered alloy could be also measured using the traditional (and complex) method of 'fire assay', technically called cupellation [52]. The use of these techniques has the definite advantage of requiring relatively low-cost equipment; on the other hand, the measurement process is long and requires, in case of ICP, a sample preparation before the analysis [53] through a process of dilution that may introduce errors in the determination of the precious metal content in the recovered alloys.

More recently, several companies have tried to use instrumentation based on X-Ray Fluorescence (XRF) technique [2, 13]. The XRF technique has adequate features for metal recovering. The concentrations of the elements of interest are typically well within the sensitivity of the technique, and the possibility of working without sample preparation greatly improves the accuracy of the analytical results. Moreover, the time needed for a single analysis is much less than cupellation, Atomic Absorption or ICP techniques. On the other hand, the laboratory XRF systems used for the analysis of precious alloys are much more expensive than the instrumentation for other techniques. Moreover, the prolonged use of X-Rays could be dangerous for the operators and this issue might not be neglected [54].

The problems of other techniques for metal recovering suggest the use of LIBS instrument in substitution of XRF. LIBS should have, for the specific application to precious alloys, all the characteristics of the XRF technique (ease of use, operability on untreated samples, multi elemental detection, and quickness of the analysis) [55].

The effectiveness of LIBS for the analysis of precious alloys has been already demonstrated [56-59] and, in particular, of double-pulse LIBS [60]. However, most of the previous studies on the application of LIBS to the analysis of precious metals were devoted to the determination of gold purity or, more generally, to the measurement of the concentration of main elements in the alloy. In contrast, metal recovery industry needs the detection of trace elements. Thus, the capability of LIBS to fulfill the needs of metal recovery industry should be demonstrated.

2.1 Materials under study

The set of spectra from waste materials and precious alloys was acquired with the same device described in Chapter 5, The MODI [47], but with an important modification. The standard configuration of MODÌ includes an Echelle spectrometer coupled to an intensified CCD. The Echelle/iCCD configuration ensures excellent performance in terms of sensitivity and signal to noise ratio; however, the cost of the spectrometer is comparably high in comparison with XRF equipment. For that reason, the couple Echelle spectrometer-iCCD has been replaced for a cheaper equipment composed by a compact Czerny-Turner spectrometer coupled to a linear CCD. The feasibility of this equipment for metal alloys analysis has been demonstrated by Sorrentino et.al. [61]. This spectrometer has both a fixed grating and CCD which offer a high reproducibility for LIBS spectra, a desirable feature for this application.

The measurements have been performed adopting the same strategy used by the analytical chemists for a typical XRF analysis. A small sample of the recovered precious alloy was mixed with copper (in fixed proportions) in order to matrix-matching the calibration samples of the XRF instrument. This dilution of the sample can be harmful for the LIBS measurements due to the fact that LIBS has problems to detect some elements even using Dual Pulse configuration [62]. On the other hand, it is interesting to test LIBS performance in the same conditions than XRF in order to test the real feasibility of LIBS for metal recovering. The set of samples is composed by 8 samples, already characterized by XRF, with the following composition (Table 7). The trueness of the XRF analysis is of the order of +/- 0.1 % in weight.

	Au g/kg	Ag g/kg	Pt g/kg	Pd g/kg	Rh g/kg
Q0	0	0	0	0	0
Q1	8.7	9.0	0.3	13.7	0.5
Q2	13.0	4.5	0.5	9.2	1.3
Q3	17.4	2.3	1	6.7	2.5
Q4	22.6	0.5	2.2	4.4	4.8
Q5	3.7	0.8	8.8	0	0.6
Q6	6.2	1.0	0	4.2	0
Q7	2.3	30.1	1.2	0.9	0.1

Table 7: Composition of the precious alloys standards.

2.2 Results

The first goal of this work is to determine, with reasonable certainty, the possibility of detecting all the elements of interest in a complex sample. This is a difficult task due to both the high intensity of copper lines related to the interesting elements lines (see Figure 55) and the absence of studies about some interesting elements for precious metals recovering for LIBS.

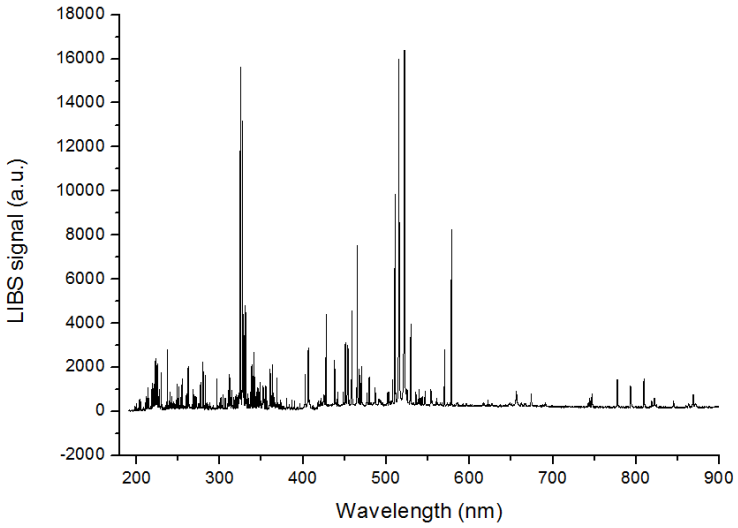

Figure 55: LIBS spectrum of a precious alloy

It is desirable an objective method in order to determine with certainty the possibility of detection of the precious elements of the sample. For this purpose, a method described in ref. [63] has been applied. This technique, based on algorithms for text retrieval, gives to each element eventually detected in the LIBS spectrum a 'score' which is related to the probability of actually having the same element in the spectrum. The higher the score, the higher the probability of having correctly detected the corresponding element in the LIBS spectrum. The sample with the spectrum shown on Figure 55 was analyzed with the retrieval algorithm [63] and the obtained scores are shown on Table 8.

#	Element	Ionization	Score
1	Cu	1	2.702411
2	Cu	2	2.529916
3	Pd	1	1.915787
4	Ag	1	1.407494
5	Pb	1	1.168331
6	Au	1	1.108252
7	Pb	2	0.976548
8	Rh	1	0.865978
9	Mg	2	0.845286
10	Au	2	0.823994
11	Ru	1	0.814889
12	Pt	1	0.759302

Table 8: Element scores from the retrieval algorithm

All the elements of interest (including Cu from the matrix and Pb, present as an impurity in the alloy) are detected in the first positions in the element ranking. These results suggest that the detection of precious metals on waste material is possible even with the interference of main materials (copper in this case)

The next step is to carry out a quantitative analysis. Calibration-Free LIBS (CF-LIBS) has been demonstrated to be a promising approach to the quantitative analysis of precious alloys [56, 64]. However, the detection of precious metal on waste materials requires the detection of traces materials, and this is the worst condition for CF-LIBS [65] because the normalization condition induces that small errors in the concentrations of main elements can provoke large errors of the concentration of traces elements. Moreover, the application of CF-LIBS method requires the knowledge of the spectroscopic parameters of the emission lines considered, and

the uncertainty in these parameters could be quite high, especially for the minor elements in the precious alloy. For that reasons a standard quantitative analysis based on calibration curves has been carried out for this work. The lines considered for building the calibration curves are shown in Table 9.

Au I	267.6 nm	
Ag I	338.3 nm	
Pt I	306.5 nm	
Pd I	355.3 nm	
Rh I	343.5 nm	385.7 nm

Table 9: Emission lines considered for building the calibration curves. The calibration curve of Rh is built taking the sum of the intensities of the two lines indicated.

The next five figures show the calibration curves obtained for the five precious elements under study: gold, silver, palladium, platinum and rhodium.

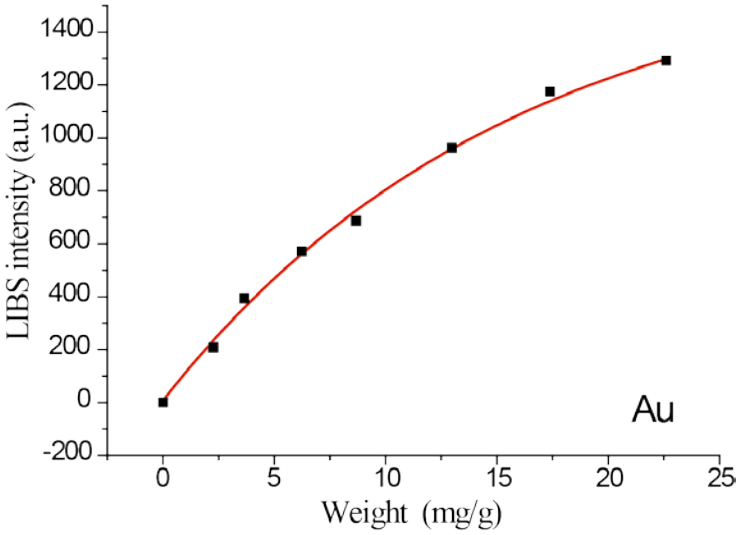

Figure 56: Calibration curve for gold

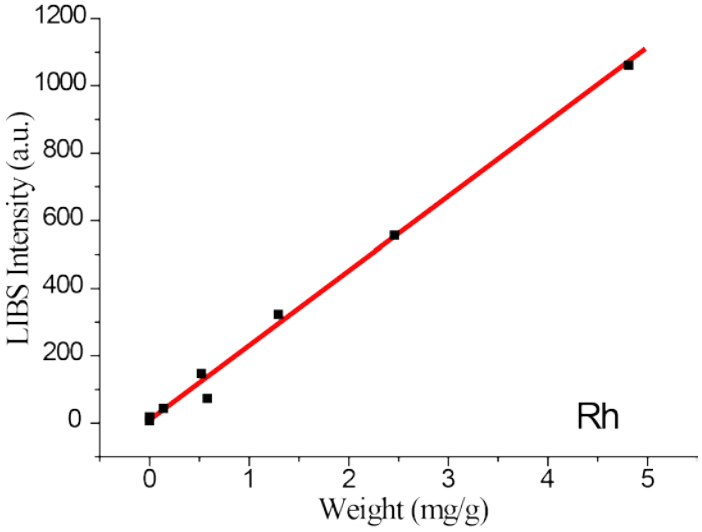

Figure 57: Calibration curve for rhodium

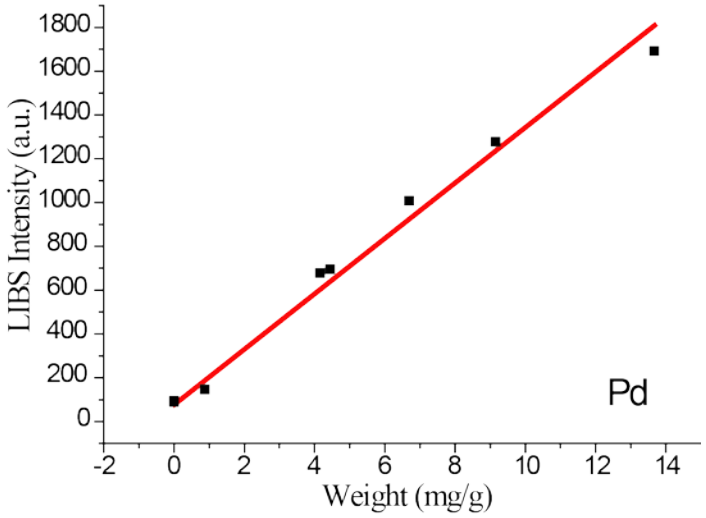

Figure 58: Calibration curve for paladium

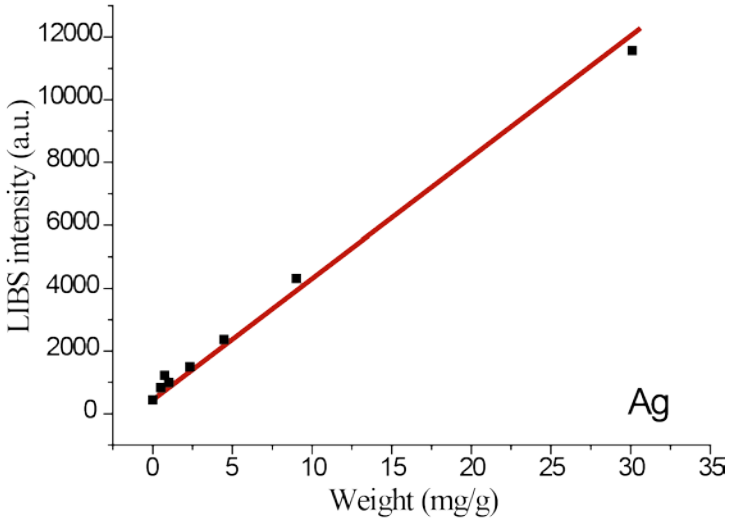

Figure 59: Calibration curve for silver

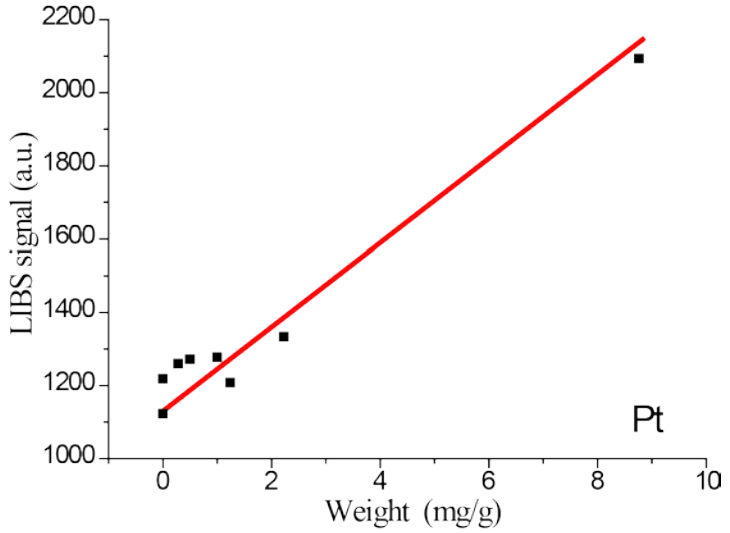

Figure 60: Calibration curve for platinum

Some considerations should be noticed about the figures. Firstly, the LIBS calibration curve for Gold is clearly non-linear. However, one has to consider that the LIBS signal should be proportional to the number of emitting atoms, which is not immediately proportional to the weight % concentration of the corresponding elements. Moreover, the other calibration curves can be relatively well approximated with a linear function (except one point for silver, all the concentrations of these

elements are well below 1.5% of the total weight). The Limits of Detection are of the order of 0.2% for all the elements. These results would definitely improve using a lower dilution factor in the matrix-matched samples. The calibration curves should be, in that case, corrected for the nonlinear dependence of the number of emitters (to whom the LIBS signal should be proportional) and the weight percent concentration of the element.

These results suggest that LIBS can be a feasible technique for precious metal recovering. The LIBS instrumentation would be cheaper, more suitable and safety than XRF for routine laboratory analysis; nevertheless, the trueness of the LIBS results should be improved in order to obtain a dependable tool for industrial environments. This goal could be achieved by modifying the sampling strategy, through the realization of matrix-matched test samples with higher weight concentration of the elements of interest.

3. Conclusions

This chapter demonstrates the versatility of LIBS for different kinds of environments. LIBS is a useful tool for applications related with fields absolutely different such as industry or archaeology. Moreover it has been demonstrated that a whole set of techniques can analyze a sample from different points of view providing information about sample composition, dating or even about the life of the object under analysis.

LIBS is helpful for archaeology. The first part of this chapter analyzes a vase using different spectrochemical techniques to provide different information about it. The multi-technique analysis performed in this part, together with the stylistic and typological study of the vase, has allowed the authentication of the vase and an analysis about its content. The complete analysis provided for the techniques employed demonstrates that the vase studied, originally attributed to the I century C.E. on the basis only of its label, is authentic but much older (VI century B.C.). The reference to the Herculaneum excavations was probably given at the time of the ‘gift’ (October 1929, according to the paper label glued on the vase body) to increase its value, considering that just a couple of years before the Italian king Vittorio

Emanuele III inaugurated the new excavations in Herculaneum, thus bringing the site to the popular attention.

The second work related with archaeology is a different point of view for the use of LIBS in this field. The value and the size of the samples, Roman Denarii, do not recommend a LIBS chemical analysis due to the induced crater on coin surface. For that reason LIBS has been employed as a validation tool for the feasibility of a XRF surface study. These kind of metallic samples suffer oxidation and the surface composition can change with respect the bulk of the coin. LIBS provides a stratigraphic analysis in a small set of coins and the result can be compared with XRF composition. This comparison allows the validation of XRF measurements, and LIBS has been employed in this way.

The last work in archaeological fields tries to demonstrate the feasibility of LIBS for paleonutritional analysis. This work demonstrates that LIBS can be used as a meaningful tool for this kind of purpose. The analysis is fast and clean with LIBS and the researcher does not need a sample preparation to carry out the experiment. These features are interesting by themselves, but the results are very close to the obtained measurements using ICP-OES, a technique which provides an accurate quantitative composition of sample but with a difficult and slow sample preparation. The ratios between different elements which act as a diet marker or the amount of them separately are similar for LIBS and ICP-OES which allows supposing the feasibility of LIBS for this kind of analysis. Moreover, LIBS can provide a stratigraphic analysis of the bone, providing useful information for the analysis of diagenetic processes. These results could be improved with the correction of elements concentrations with samples of surrounding soil, avoiding the problems of diagenetic effects.

The last work of this chapter is related with industrial environment. The results of this last study demonstrate that LIBS is a feasible technique for the analysis of alloys obtained from the recovery of precious metals from industrial wastes. LIBS instrumentation is cheaper than XRF systems, and the analysis is safer for a continuous laboratory analysis; However the accuracy and reliability of the LIBS results should be improved. This goal could be achieved by modifying the sampling

strategy, through the realization of matrix-matched test samples with higher weight concentration of the elements of interest.

Part III

Conclusions and open future lines

This part is devoted to summarize the conclusions of this thesis work and to show the open research lines.

Chapter 7

Summary & Conclusions

The previous chapters of this work have described the works carried out during this PhD, reviewing the obtained results and discussing them. Present chapter is devoted to summarize the results obtained and to emphasize the main conclusions.

It must be noticed that after the review of the state of the art, three main objectives were formulated:

1. To design and develop new sensors based on Optical Fiber. These sensors measure the shockwave induced by the plasma plume using different approaches, like Fiber Bragg Gratings or speckle analysis at the end of the optical fiber.

2. To apply different algorithms for LIBS spectra processing and analysis. A first group of algorithms use the raw spectra obtained with LIBS set-ups in order to distinguish between different materials, while a second group of algorithms represents a new approach to quantitative analysis, and are based on synthetic spectra generation and optimization algorithms to obtain quantitative values for the chemical composition.

3. To apply LIBS to real applications in different fields in order to demonstrate the versatility of LIBS for a wide range of fields both in research lines and in commercial applications.

New optical fiber sensors have been designed and demonstrated. The first of them has employed FBG for shockwave detection. FBG's allow the detection and quantification of different effects which induce strain, deformation or temperature

changes on their structure. The induced shockwave is a pressure wave, and this wave can hit the FBG and induce this deformation. The works associated with this line demonstrate the feasibility of this kind of sensor. The FBG transducer can detect and quantify the intensity of the shockwave and its features are close to a standard microphone, a device widely employed for shockwave detection. Even its performance is surpassed in terms of linearity for the estimation of laser energy. The capability of FBG transducer for the detection of small changes in the laser irradiance has been employed for the detection of errors in laser focalization with a satisfactory result. This kind of transducer can open a new approach for shockwave detection, allowing the stand-off measurement of plasma shockwave with a device immune to electromagnetic fields. Moreover, this measurement of shockwave energy could be employed for spectral normalization, and the measurement carried out for FBG transducer can be useful for this purpose in order to improve a quantitative chemical analysis.

The second proposed Optical fiber sensor is based on optical fiber speckle transducers. Speckle interferometry allows the detection of vibrations, strains and deformations on the optical fiber, and this feature has been employed in the same way than the FBG transducer for shockwave detection. The speckle transducer has been developed using a plastic optical fiber, and the works associated to this research line demonstrate the feasibility of this kind of transducer for shockwave detection or quantification and even for optical emission normalization. Moreover, a new and interesting device has been developed related with this line. A speckle transducer based on coiled plastic optical fiber allows the simultaneous detection of both the shockwave and the optical emission. This device allows a complete stand-off detection system, allowing the detection of the spectrum and the measurement of the shockwave intensity, an interesting parameter for the normalization of the optical emission for improving a quantitative analysis.

There are open research lines which try to design and develop new hardware for LIBS devices to improve the sensibility or accuracy of LIBS analysis. However, this thesis works are focused to improve the software to process the big amount of information that is provided by a LIBS spectrum. Three groups of algorithms have been checked.

The first group works with the raw spectra obtained with a LIBS set-up. The goal of these algorithms is to classify different samples with different criteria without a complex quantitative or qualitative chemical analysis. These algorithms work with all the information that a LIBS spectra provide, but an identification of the elements which compose the sample is not necessary to use them. The first group of works related to this line is based on SVM's classifiers with the goal of the detection of an aluminum-silicon coating on industrial steels. One approach to this problem could be to carry out a qualitative analysis in order to detect the aluminum or silicon lines on LIBS spectra, but this approach needs a calibration of the set-up or a filtering of the spectra for the detection of the part of spectra with the interesting lines. The approach proposed in this work uses a classifier to detect these impurities on real time when the steel is being treated to remove the coating. This algorithm is feeded with the raw spectra and in a short period of time is able to detect the impurities. This algorithm based on SVM's needs to be trained, but a quantitative analysis or even the spectral range of the spectra is not necessary. For that reason a complex calibration is not necessary. This classifier has been tested with industrial steels, but a wide range of applications could be solved using the classification of different kind of materials based on these algorithms. Only a spectral range with changes between the different materials is necessary for the classification.

The other work included in this group of algorithms in based on PCA. This algorithm allows projecting a group of correlated spectra (with a big amount of redundant or common information for all the spectra of the different kind of samples) in a new uncorrelated basis. This new space has not redundant or common information and only the discriminating information is maintained, allowing an easier and faster classification. This algorithm has been employed with archaeological samples, specifically a set of bronze statues. The application of the PCA algorithm to the LIBS spectrum of each sample allowed a dating which is consistent with the dating provided by the stylistic and typological analysis. A complex quantitative or qualitative chemical analysis was not necessary for this dating, and the algorithm shown its capability to work in a "blind" mode with the raw spectra, avoiding consumption of time and resources to the researchers.

The second algorithm for LIBS spectra processing is a new approach to quantitative analysis. It is based on the automatic generation of synthetic spectra and PSO, an optimization algorithm, to calculate the so-called participation index that can be directly related to the weight of the different elements in the samples. A wide set of samples has been analyzed to test the capability of the algorithm, including calibrated brass samples, aluminum samples or Nordic gold. The results have a good correlation with the real concentrations, although in some cases some issues inherent to LIBS have prevented the model to provide the expected results. This algorithm should be improved with new approaches based on a model independent of relative line intensities but it is an interesting option for a semi quantitative analysis. These new approaches should provide a new tool for a real quantitative analysis.

The feasibility for using LIBS for chemical analysis in different fields was also investigated. Specifically, LIBS has been used in two different areas. In archaeology, it has been used in combination with other spectrochemical techniques to provide a complete chemical analysis of different archaeological samples. In industrial environment, it has been investigated for recovering precious metals from industrial waste.

The first couple of works on archaeology are an example of multi-technique analysis. The first work analyzes a vase using different spectrochemical techniques to provide, together with the stylistic and typological study of the vase, the authentication of the vase and an analysis about its content. This work demonstrates that a complete set of spectrochemical techniques can supply valuable information about archaeological samples. The second work of this research line analyzed a set of Roman Denarii, coins of high value. The LIBS analysis induces a small crater on sample surface, and this damage is not allowed for this kind of coins. However, these kind of metallic samples suffer oxidation and the surface composition can change with respect the bulk of the coin. For that reason LIBS has been employed as a validation tool for the feasibility of a XRF surface study. LIBS provides a stratigraphic analysis in a small set of coins and the result can be compared with XRF result. This comparison allows the validation of XRF measurements, and LIBS has been employed in this way.

The last work in the archaeological field tries to demonstrate the feasibility of LIBS for paleonutritional analysis. LIBS can be used as a useful tool for this kind of analysis. Unlike other spectrochemical techniques, LIBS analysis is fast and clean and the researcher does not need a sample preparation to carry out the experiment. These features are interesting by themselves, but the results for paleonutritional analysis are in the order of the obtained measurements using ICP-OES, a technique which provides an accurate quantitative composition of sample but with a difficult and slow sample preparation. The ratios between different elements which act as a diet marker or the amount of them separately are similar for LIBS and ICP-OES which suggests that LIBS is a feasible technique for paleonutritional analysis. Moreover, LIBS can provide an in-depth analysis of the sample and this analysis has been carried out, providing useful information for the analysis of the diagenetic process. To obtain an accurate quantitative analysis of bone composition, a correction of diagenetic effect with samples of surrounding soil has proved to be necessary.

In the industrial manufacturing environment, the obtained results demonstrate that LIBS is a feasible technique for the recovery of precious metals from industrial wastes. LIBS has been compared with XRF, probably the most common technique for this purpose and the results demonstrate the viability of LIBS as a tool for this purpose. LIBS can detect all the precious elements which are present in these wastes and the instrumentation is cheaper and less dangerous for a continuous laboratory analysis than XRF. However, the accuracy and reliability of the LIBS results should be improved. This goal could be achieved by modifying the sampling strategy, through the realization of matrix-matched test samples with higher weight concentration of the elements of interest.

To summarize, this Thesis work demonstrates that LIBS is a spectrochemical technique with a promising future in a wide range of fields. Topics as different as algorithms development, optical fiber sensors for plasma shockwave detection or spectrochemical analysis of different kinds of samples using LIBS have been carried out in this work. This demonstrates that there are a huge amount of things to do about LIBS.

Chapter 8

Open future lines

This thesis work is the first step of a open research line in the Photonic Engineering Group. However, several aspects that should be improved and developed in order to apply LIBS in real applications have been identified.

The first one, and probably the most important, is related to quantitative chemical analysis based on LIBS. An accurate quantitative analysis is one of the most important goals of LIBS, and the achievement of this objective could multiply exponentially the applications based on LIBS. This work has shown a new approach to quantitative analysis and different techniques for spectral normalization has been tested in order to improve the accuracy of a quantitative analysis of chemical composition. Accordingly, new efforts in this line should be accomplished in the future, developing new sensors and devices for shockwave detection or new algorithms for quantitative analysis.

Other interesting line researched in this period is related to algorithms for processing the LIBS spectra. LIBS cannot still provide an accurate quantitative analysis, but there are fields where this is not necessary. This work has shown algorithms based on PCA or SVM's to classify different kind of samples, but there are a huge amount of algorithms which can provide new tools for material classification and this is an interesting application for the future.

New developments related to archaeological fields have been carried out during the last part of PhD period. LIBS has ideal features for this field, and there are a huge variety of archaeological samples which can be analyzed with LIBS. Moreover, these

works demonstrate that a multi-technique analysis is a powerful tool for archaeology. For that reason, new samples should be analyzed with different techniques, LIBS set-ups or algorithms in order to improve and intensify the relationship between LIBS and artistic and archaeological fields [1].

Part IV

References

This part includes all the references cited in the document, separated by chapters and also ordered alphabetically. Finally, the list of publications obtained during the PhD period is shown, classified both as the ones close related with the PhD work and the obtained ones as a consequence of collaborations with members of Photonic Engineering Group.

References by chapter

References chapter 2

[1] B. Kearton, Y. Mattley, Laser-induced breakdown spectroscopy: Sparking new applications, Nature Photonics, 2 (2008) 537-540.

[2] D.A. Cremers, L.J. Radziemski, J. Wiley, Handbook of laser-induced breakdown spectroscopy, John Wiley & Sons Ltd., 2006.

[3] A.W. Miziolek, V. Palleschi, I. Schechter, Laser-induced breakdown spectroscopy (LIBS): fundamentals and applications, Cambridge Univ Pr, 2006.

[4] W.B. Lee, J. Wu, Y.I. Lee, J. Sneddon, Recent applications of laser-induced breakdown spectrometry: A review of material approaches, Applied Spectroscopy Reviews, 39 (2004) 27-97.

[5] J.D. Winefordner, I.B. Gornushkin, T. Correll, E. Gibb, B.W. Smith, N. Omenetto, Comparing several atomic spectrometric methods to the super stars: special emphasis on laser induced breakdown spectrometry, LIBS, a future super star, J. Anal. At. Spectrom., 19 (2004) 1061-1083.

[6] B. Cagnac, J.C. Pebay-Peyroula, Modern atomic physics: fundamental principles, (1975).

[7] J.P. Singh, Laser-induced breakdown spectroscopy, Elsevier Science, 2007.

[8] D. Bulajic, M. Corsi, G. Cristoforetti, S. Legnaioli, V. Palleschi, A. Salvetti, E. Tognoni, A procedure for correcting self-absorption in calibration free-laser induced breakdown spectroscopy, Spectrochimica Acta Part B: Atomic Spectroscopy, 57 (2002) 339-353.

[9] M. Corsi, G. Cristoforetti, M. Hidalgo, S. Legnaioli, V. Palleschi, A. Salvetti, E. Tognoni, C. Vallebona, Double pulse, calibration-free laser-induced breakdown spectroscopy: A new technique for in situ standard-less analysis of polluted soils, Applied geochemistry, 21 (2006) 748-755.

[10] H.R. Griem, Spectral line broadening by plasmas, New York, Academic Press, Inc.(Pure and Applied Physics. Volume 39), 1974. 421 p., 1 (1974).

[11] G. Cristoforetti, A. De Giacomo, M. Dell'Aglio, S. Legnaioli, E. Tognoni, V. Palleschi, N. Omenetto, Local thermodynamic equilibrium in laser-induced breakdown spectroscopy: beyond the McWhirter criterion, Spectrochimica Acta Part B: Atomic Spectroscopy, 65 (2010) 86-95.

[12] J. Vadillo, J. Fernandez Romero, C. Rodriguez, J. Laserna, Effect of plasma shielding on laser ablation rate of pure metals at reduced pressure, Surface and interface analysis, 27 (1999) 1009-1015.

[13] J. Aguilera, C. Aragon, F. Penalba, Plasma shielding effect in laser ablation of metallic samples and its influence on LIBS analysis, Applied surface science, 127 (1998) 309-314.

[14] S.M. Angel, D.N. Stratis, K.L. Eland, T. Lai, M.A. Berg, D.M. Gold, LIBS using dual-and ultra-short laser pulses, Fresenius' journal of analytical chemistry, 369 (2001) 320-327.

[15] Y.B. Zel'Dovich, Y.P. Raizer, Physics of shock waves and high-temperature hydrodynamic phenomena, Dover Pubns, 2002.

[16] L. Sedov, Similarity methods and dimensional analysis in mechanics, Moscow Izdatel Nauka, 1 (1977).

[17] B. Le Drogoff, J. Margot, M. Chaker, M. Sabsabi, O. Barthelemy, T. Johnston, S. Laville, F. Vidal, Y. Von Kaenel, Temporal characterization of femtosecond laser pulses induced plasma for spectrochemical analysis of aluminum alloys, Spectrochimica Acta Part B: Atomic Spectroscopy, 56 (2001) 987-1002.

[18] X. Zeng, X. Mao, R. Greif, R. Russo, Experimental investigation of ablation efficiency and plasma expansion during femtosecond and nanosecond laser ablation of silicon, Applied Physics A: Materials Science & Processing, 80 (2005) 237-241.

[19] A. Semerok, C. Dutouquet, Ultrashort double pulse laser ablation of metals, Thin Solid Films, 453 (2004) 501-505.

[20] B. Castle, K. Talabardon, B. Smith, J. Winefordner, Variables influencing the precision of laser-induced breakdown spectroscopy measurements, Applied Spectroscopy, 52 (1998) 649-657.

[21] Y. Iida, Effects of atmosphere on laser vaporization and excitation processes of solid samples, Spectrochimica Acta Part B: Atomic Spectroscopy, 45 (1990) 1353-1367.

[22] W. Sdorra, K. Niemax, Basic investigations for laser microanalysis: III. Application of different buffer gases for laser-produced sample plumes, Microchimica Acta, 107 (1992) 319-327.

[23] R. Wisbrun, I. Schechter, R. Niessner, H. Schroeder, K.L. Kompa, Detector for trace elemental analysis of solid environmental samples by laser plasma spectroscopy, Analytical Chemistry, 66 (1994) 2964-2975.

[24] L. St-Onge, M. Sabsabi, P. Cielo, Analysis of solids using laser-induced plasma spectroscopy in double-pulse mode, Spectrochimica Acta Part B: Atomic Spectroscopy, 53 (1998) 407-415.

[25] G. Abdellatif, H. Imam, A study of the laser plasma parameters at different laser wavelengths, Spectrochimica Acta Part B: Atomic Spectroscopy, 57 (2002) 1155-1165.

[26] L. Cabalin, J. Laserna, Experimental determination of laser induced breakdown thresholds of metals under nanosecond Q-switched laser operation, Spectrochimica Acta Part B: Atomic Spectroscopy, 53 (1998) 723-730.

[27] R. Russo, X. Mao, O. Borisov, H. Liu, Influence of wavelength on fractionation in laser ablation ICP-MS, J. Anal. At. Spectrom., 15 (2000) 1115-1120.

[28] X. Mao, W.T. Chan, M. Caetano, M.A. Shannon, R.E. Russo, Preferential vaporization and plasma shielding during nano-second laser ablation, Applied surface science, 96 (1996) 126-130.

[29] W. Koechner, Solid-state laser engineering, Springer Verlag, 2006.

[30] X. Mao, A. Ciocan, O. Borisov, R. Russo, Laser ablation processes investigated using inductively coupled plasma-atomic emission spectroscopy (ICP-AES), Applied surface science, 127 (1998) 262-268.

[31] A. Ciucci, V. Palleschi, S. Rastelli, R. Barbini, F. Colao, R. Fantoni, A. Palucci, S. Ribezzo, H. Van Der Steen, Trace pollutants analysis in soil by a time-resolved laser-induced breakdown spectroscopy technique, Applied Physics B: Lasers and Optics, 63 (1996) 185-190.

[32] D.A. Cremers, L.J. Radziemski, T.R. Loree, Spectrochemical analysis of liquids using the laser spark, Applied Spectroscopy, 38 (1984) 721-729.

[33] J. Uebbing, J. Brust, W. Sdorra, F. Leis, K. Niemax, Reheating of a laser-produced plasma by a second pulse laser, Applied Spectroscopy, 45 (1991) 1419-1423.

[34] R. Sattmann, V. Sturm, R. Noll, Laser-induced breakdown spectroscopy of steel samples using multiple Q-switch Nd: YAG laser pulses, Journal of Physics D: Applied Physics, 28 (1995) 2181.

[35] V. Sturm, L. Peter, R. Noll, Steel analysis with laser-induced breakdown spectrometry in the vacuum ultraviolet, Applied Spectroscopy, 54 (2000) 1275-1278.

[36] L. St-Onge, V. Detalle, M. Sabsabi, Enhanced laser-induced breakdown spectroscopy using the combination of fourth-harmonic and fundamental Nd: YAG laser pulses, Spectrochimica Acta Part B: Atomic Spectroscopy, 57 (2002) 121-135.

[37] D.N. Stratis, K.L. Eland, S.M. Angel, Enhancement of aluminum, titanium, and iron in glass using pre-ablation spark dual-pulse LIBS, Applied Spectroscopy, 54 (2000) 1719-1726.

[38] D.N. Stratis, K.L. Eland, S.M. Angel, Dual-pulse LIBS using a pre-ablation spark for enhanced ablation and emission, Applied Spectroscopy, 54 (2000) 1270-1274.

[39] D.N. Stratis, K.L. Eland, S.M. Angel, Effect of pulse delay time on a pre-ablation dual-pulse LIBS plasma, Applied Spectroscopy, 55 (2001) 1297-1303.

[40] J. Scaffidi, W. Pearman, J.C. Carter, B.W. Colston, S.M. Angel, Temporal dependence of the enhancement of material removal in femtosecond-nanosecond dual-pulse laser-induced breakdown spectroscopy, Applied optics, 43 (2004) 6492-6499.

[41] K.L. Eland, D.N. Stratis, D.M. Gold, S.R. Goode, S.M. Angel, Energy dependence of emission intensity and temperature in a LIBS plasma using femtosecond excitation, Applied Spectroscopy, 55 (2001) 286-291.

[42] J.F. James, R. Sternberg, The design of optical spectrometers, London: Chapman and Hall, 1969, 1 (1969).

[43] H. Bauer, F. Leis, K. Niemax, Laser induced breakdown spectrometry with an echelle spectrometer and intensified charge coupled device detection, Spectrochimica Acta Part B: Atomic Spectroscopy, 53 (1998) 1815-1825.

[44] J.E. Carranza, E. Gibb, B.W. Smith, D.W. Hahn, J.D. Winefordner, Comparison of nonintensified and intensified CCD detectors for laser-induced breakdown spectroscopy, Applied optics, 42 (2003) 6016-6021.

[45] A.S. Eppler, D.A. Cremers, D.D. Hickmott, M.J. Ferris, A.C. Koskelo, Matrix effects in the detection of Pb and Ba in soils using laser-induced breakdown spectroscopy, Applied Spectroscopy, 50 (1996) 1175-1181.

[46] C. Aragon, J.A. Aguilera, F. Penalba, Improvements in quantitative analysis of steel composition by laser-induced breakdown spectroscopy at atmospheric pressure using an infrared Nd: YAG laser, Applied Spectroscopy, 53 (1999) 1259-1267.

[47] P. Fichet, P. Mauchien, J.F. Wagner, C. Moulin, Quantitative elemental determination in water and oil by laser induced breakdown spectroscopy, Analytica chimica acta, 429 (2001) 269-278.

[48] Y.I. Lee, S.P. Sawan, T.L. Thiem, Y.Y. Teng, J. Sneddon, Interaction of a laser beam with metals. Part II: Space-resolved studies of laser-ablated plasma emission, Applied Spectroscopy, 46 (1992) 436-441.

[49] C. Chaleard, P. Mauchien, N. Andre, J. Uebbing, J. Lacour, C. Geertsen, Correction of Matrix Effects in Quantitative Elemental AnalysisWith Laser Ablation Optical Emission Spectrometry, J. Anal. At. Spectrom., 12 (1997) 183-188.

[50] G.A. Theriault, S. Bodensteiner, S.H. Lieberman, A real-time fiber-optic LIBS probe for the in situ delineation of metals in soils, Field Analytical Chemistry & Technology, 2 (1998) 117-125.

[51] B.J. Marquardt, S.R. Goode, S.M. Angel, In situ determination of lead in paint by laser-induced breakdown spectroscopy using a fiber-optic probe, Analytical Chemistry, 68 (1996) 977-981.

[52] A.K. Rai, H. Zhang, F.Y. Yueh, J.P. Singh, A. Weisburg, Parametric study of a fiber-optic laser-induced breakdown spectroscopy probe for analysis of aluminum alloys, Spectrochimica Acta Part B: Atomic Spectroscopy, 56 (2001) 2371-2383.

[53] D. Cremers, J. Barefield, A. Koskelo, Remote elemental analysis by laser-induced breakdown spectroscopy using a fiber-optic cable, Applied Spectroscopy, 49 (1995) 857-860.

[54] S. Konorov, A. Fedotov, O. Kolevatova, V. Beloglazov, N. Skibina, A. Shcherbakov, E. Wintner, A. Zheltikov, Laser breakdown with millijoule trains of picosecond pulses transmitted through a hollow-core photonic-crystal fibre, Journal of Physics D: Applied Physics, 36 (2003) 1375.

[55] M. Losada, I. Garcés, J. Mateo, I. Salinas, J. Lou, J. Zubia, Mode coupling contribution to radiation losses in curvatures for high and low numerical aperture plastic optical fibers, Lightwave Technology, Journal of, 20 (2002) 1160-1164.

[56] R. Krasniker, V. Bulatov, I. Schechter, Study of matrix effects in laser plasma spectroscopy by shock wave propagation, Spectrochimica Acta Part B: Atomic Spectroscopy, 56 (2001) 609-618.

[57] A. Whitehouse, J. Young, I. Botheroyd, S. Lawson, C. Evans, J. Wright, Remote material analysis of nuclear power station steam generator tubes by laser-induced breakdown spectroscopy, Spectrochimica Acta Part B: Atomic Spectroscopy, 56 (2001) 821-830.

[58] J. Laserna, S. Palanco, Spectral analysis of the acoustic emission of laser-produced plasmas, Optical Society of America, 2002.

[59] A. Hrdlicka, L. Zaorálková, M. Galiová, T. Ctvrtnícková, V. Kanický, V. Otruba, K. Novotný, P. Krásenský, J. Kaiser, R. Malina, Correlation of acoustic and optical emission signals produced at 1064 and 532 nm laser-induced breakdown spectroscopy (LIBS) of glazed wall tiles, Spectrochimica Acta Part B: Atomic Spectroscopy, 64 (2009) 74-78.

[60] K.O. Hill, G. Meltz, Fiber Bragg grating technology fundamentals and overview, Lightwave Technology, Journal of, 15 (1997) 1263-1276.

[61] J.M. López-Higuera, L. Rodriguez Cobo, A. Quintela Incera, A. Cobo, Fiber Optic Sensors in Structural Health Monitoring, Journal of Lightwave Technology, 29 (2011) 587-608.

[62] C. Lopez-Moreno, S. Palanco, J.J. Laserna, F. DeLucia Jr, A.W. Miziolek, J. Rose, R.A. Walters, A.I. Whitehouse, Test of a stand-off laser-induced breakdown spectroscopy sensor for the detection of explosive residues on solid surfaces, J. Anal. At. Spectrom., 21 (2005) 55-60.

[63] J.L. Gottfried, F.C. De Lucia, C.A. Munson, A.W. Miziolek, Double-pulse standoff laser-induced breakdown spectroscopy for versatile hazardous materials detection, Spectrochimica Acta Part B: Atomic Spectroscopy, 62 (2007) 1405-1411.

[64] Y. Ralchenko, NIST atomic spectra database, Memorie della Societa Astronomica Italiana Supplementi, 8 (2005) 96.

[65] I. Bassiotis, A. Diamantopoulou, A. Giannoudakos, F. Roubani-Kalantzopoulou, M. Kompitsas, Effects of experimental parameters in quantitative analysis of steel alloy by laser-induced breakdown spectroscopy, Spectrochimica Acta Part B: Atomic Spectroscopy, 56 (2001) 671-683.

[66] R.A. Multari, L.E. Foster, D.A. Cremers, M.J. Ferris, Effect of sampling geometry on elemental emissions in laser-induced breakdown spectroscopy, Applied Spectroscopy, 50 (1996) 1483-1499.

[67] B. Sallé, D.A. Cremers, S. Maurice, R.C. Wiens, Laser-induced breakdown spectroscopy for space exploration applications: Influence of the ambient pressure on the calibration curves prepared from soil and clay samples, Spectrochimica Acta Part B: Atomic Spectroscopy, 60 (2005) 479-490.

[68] L. St-Onge, E. Kwong, M. Sabsabi, E. Vadas, Quantitative analysis of pharmaceutical products by laser-induced breakdown spectroscopy, Spectrochimica Acta Part B: Atomic Spectroscopy, 57 (2002) 1131-1140.

[69] A. Ciucci, M. Corsi, V. Palleschi, S. Rastelli, A. Salvetti, E. Tognoni, New procedure for quantitative elemental analysis by laser-induced plasma spectroscopy, Applied Spectroscopy, 53 (1999) 960-964.

[70] B. Yegnanarayana, Artificial neural networks, PHI Learning Pvt. Ltd., 2004.

[71] V.N. Vapnik, The nature of statistical learning theory, Springer Verlag, 2000.

[72] C. Cortes, V. Vapnik, Support-vector networks, Machine learning, 20 (1995) 273-297.

[73] N. Roussopoulos, S. Kelley, F. Vincent, Nearest neighbor queries, ACM, 1995, pp. 71-79.

[74] J.M. Keller, M.R. Gray, J.A.J. Givens, A Fuzzy k-Nearest Neighbor Algorithm IEEE Transactions on Systems, Man, and Cybernetics, 15 (1985) 581.

[75] P. Pudil, J. Novovicová, J. Kittler, Floating search methods in feature selection, Pattern recognition letters, 15 (1994) 1119-1125.

[76] H. Yu, J. Yang, A direct LDA algorithm for high-dimensional data-with application to face recognition, Pattern recognition, 34 (2001) 2067.

[77] S. Wold, K. Esbensen, P. Geladi, Principal component analysis, Chemometrics and intelligent laboratory systems, 2 (1987) 37-52.

[78] J.B. Sirven, B. Bousquet, L. Canioni, L. Sarger, S. Tellier, M. Potin-Gautier, I.L. Hecho, Qualitative and quantitative investigation of chromium-polluted soils by laser-induced breakdown spectroscopy combined with neural networks analysis, Analytical and Bioanalytical Chemistry, 385 (2006) 256-262.

[79] Q. Godoi, F.O. Leme, L.C. Trevizan, I.A. Rufini, D. Santos Jr, F.J. Krug, Laser-induced breakdown spectroscopy and chemometrics for classification of toys relying on toxic elements, Spectrochimica Acta Part B: Atomic Spectroscopy, (2011).

[80] L. Fornarini, F. Colao, R. Fantoni, V. Lazic, V. Spizzicchino, Calibration analysis of bronze samples by nanosecond laser induced breakdown spectroscopy: A theoretical and experimental approach, Spectrochimica Acta Part B: Atomic Spectroscopy, 60 (2005) 1186-1201.

[81] M.A. Kasem, R.E. Russo, M.A. Harith, Influence of biological degradation and environmental effects on the interpretation of archeological bone samples with laser-induced breakdown spectroscopy, J. Anal. At. Spectrom., 26 (2011) 1733-1739.

[82] K. Melessanaki, M. Mateo, S.C. Ferrence, P.P. Betancourt, D. Anglos, The application of LIBS for the analysis of archaeological ceramic and metal artifacts, Applied surface science, 197 (2002) 156-163.

[83] P. Maravelaki, V. Zafiropulos, V. Kilikoglou, M. Kalaitzaki, C. Fotakis, Laser-induced breakdown spectroscopy as a diagnostic technique for the laser cleaning of marble, Spectrochimica Acta Part B: Atomic Spectroscopy, 52 (1997) 41-53.

[84] L. Torrisi, F. Caridi, L. Giuffrida, A. Torrisi, G. Mondio, T. Serafino, M. Caltabiano, E. Castrizio, E. Paniz, A. Salici, LAMQS analysis applied to ancient Egyptian bronze coins, Nuclear Instruments and Methods in Physics Research Section B: Beam Interactions with Materials and Atoms, 268 (2010) 1657-1664.

[85] V. Lazic, F. Colao, R. Fantoni, V. Spizzicchino, Recognition of archeological materials underwater by laser induced breakdown spectroscopy, Spectrochimica Acta Part B: Atomic Spectroscopy, 60 (2005) 1014-1024.

[86] L. Caneve, A. Diamanti, F. Grimaldi, G. Palleschi, V. Spizzichino, F. Valentini, Analysis of fresco by laser induced breakdown spectroscopy, Spectrochimica Acta Part B: Atomic Spectroscopy, 65 (2010) 702-706.

[87] I. Osticioli, N.F.C. Mendes, S. Porcinai, A. Cagnini, E. Castellucci, Spectroscopic analysis of works of art using a single LIBS and pulsed Raman setup, Analytical and Bioanalytical Chemistry, 394 (2009) 1033-1041.

[88] M. Alberghina, R. Barraco, M. Brai, T. Schillaci, L. Tranchina, Comparison of LIBS and μ-XRF measurements on bronze alloys for monitoring plasma effects, IOP Publishing, 2011, pp. 012017.

[89] X.Y. Liu, W.J. Zhang, Recent developments in biomedicine fields for laser induced breakdown spectroscopy, Journal of Biomedical Science, 1 (2008).

[90] S. Hamzaoui, R. Khleifia, N. Jaïdane, Z. Ben Lakhdar, Quantitative analysis of pathological nails using laser-induced breakdown spectroscopy (LIBS) technique, Lasers in Medical Science, (2011) 1-5.

[91] C. Tameze, R. Vincelette, N. Melikechi, V. Zeljkovic, E. Izquierdo, Empirical analysis of LIBS images for ovarian cancer detection, IEEE, 2007, pp. 76-76.

[92] S.J. Rehse, Q. Mohaidat, S. Palchaudhuri, Laser-Induced Breakdown Spectroscopy (LIBS) for the Rapid Field Identification and Classification of Pathogenic Bacteria, Optical Society of America, 2010.

[93] R.A. Multari, D.A. Cremers, M.L. Bostian, Use of laser-induced breakdown spectroscopy for the differentiation of pathogens and viruses on substrates, Applied optics, 51 (2012) B57-B64.

[94] L.C. Trevizan, D. Santos, R.E. Samad, N.D. Vieira, L.C. Nunes, I.A. Rufini, F.J. Krug, Evaluation of laser induced breakdown spectroscopy for the determination of micronutrients in plant materials, Spectrochimica Acta Part B: Atomic Spectroscopy, 64 (2009) 369-377.

[95] R. González, P. Lucena, L. Tobaria, J. Laserna, Standoff LIBS detection of explosive residues behind a barrier, J. Anal. At. Spectrom., 24 (2009) 1123-1126.

[96] V. Lazic, A. Palucci, S. Jovicevic, M. Carapanese, C. Poggi, E. Buono, Detection of explosives at trace levels by laser-induced breakdown spectroscopy (LIBS), Anal. And Bioanal. Chem, 2010, pp. 76650V.

[97] A. Sarkar, V.M. Telmore, D. Alamelu, S.K. Aggarwal, Laser induced breakdown spectroscopic quantification of platinum group metals in simulated high level nuclear waste, J. Anal. At. Spectrom., 24 (2009) 1545-1550.

[98] Q. Guo, H. Yu, Y. Xin, X. Li, X. Li, Experimental study on high alloy steel sample by laser-induced breakdown spectroscopy], Guang pu xue yu guang pu fen xi= Guang pu, 30 (2010) 783.

[99] C. Aragon, J. Aguilera, J. Campos, Determination of carbon content in molten steel using laser-induced breakdown spectroscopy, Applied Spectroscopy, 47 (1993) 606-608.

[100] A. Rai, F. Yueh, J. Singh, Laser-induced breakdown spectroscopy of molten aluminum alloy, Applied optics, 42 (2003) 2078-2084.

[101] N.K. Rai, A. Rai, LIBS--an efficient approach for the determination of Cr in industrial wastewater, Journal of hazardous materials, 150 (2008) 835-838.

[102] J.M.D. Kowalczyk, J. Perkins, J. Kaneshiro, N. Gaillard, Y. Chang, A. DeAngelis, S.A. Mallory, D. Bates, E. Miller, Measurement of the sodium concentration in CIGS solar cells via laser induced breakdown spectroscopy, IEEE, 2010, pp. 001742-001744.

[103] J. Cuñat, S. Palanco, F. Carrasco, M. Simon, J. Laserna, Portable instrument and analytical method using laser-induced breakdown spectrometry for in situ characterization of speleothems in karstic caves, J. Anal. At. Spectrom., 20 (2005) 295-300.

[104] J.M. Anzano, M.A. Villoria, A. Ruíz-Medina, R.J. Lasheras, Laser-induced breakdown spectroscopy for quantitative spectrochemical analysis of geological materials: Effects of the matrix and simultaneous determination, Analytica chimica acta, 575 (2006) 230-235.

[105] B. Salle, D.A. Cremers, S. Maurice, R.C. Wiens, P. Fichet, Evaluation of a compact spectrograph for in-situ and stand-off laser-induced breakdown spectroscopy analyses of geological samples on Mars missions, Spectrochimica Acta Part B: Atomic Spectroscopy, 60 (2005) 805-815.

[106] D.W. Hahn, N. Omenetto, Laser-Induced Breakdown Spectroscopy (LIBS), Part II: Review of Instrumental and Methodological Approaches to Material Analysis and Applications to Different Fields, Applied Spectroscopy, 66 (2012) 347-419.

[107] G. Amato, S. Legnaioli, G. Lorenzetti, V. Palleschi, L. Pardini, F. Rabitti, Element detection relying on information retrieval techniques applied to laser spectroscopy, ACM, 2011, pp. 89-95.

[108] F. Fortes, J. Laserna, Characteristics of solid aerosols produced by optical catapulting studied by laser-induced breakdown spectroscopy, Applied surface science, 256 (2010) 5924-5928.

[109] M. Abdelhamid, F. Fortes, J. Laserna, M. Harith, Optical Catapulting Laser Induced Breakdown Spectroscopy (OC-LIBS) And Conventional LIBS: A comparative Study, ICLA, 2011, pp. 55.

[110] S. Rai, A.K. Rai, Characterization of organic materials by LIBS for exploration of correlation between molecular and elemental LIBS signals, AIP Advances, 1 (2011) 042103-042103-042111.

References chapter 4

[1] C. Chaleard, P. Mauchien, N. Andre, J. Uebbing, J. Lacour, C. Geertsen, Correction of Matrix Effects in Quantitative Elemental AnalysisWith Laser Ablation Optical Emission Spectrometry, J. Anal. At. Spectrom., 12 (1997) 183-188.

[2] B. Castle, K. Talabardon, B. Smith, J. Winefordner, Variables influencing the precision of laser-induced breakdown spectroscopy measurements, Applied Spectroscopy, 52 (1998) 649-657.

[3] H. Lindner, K.H. Loper, D.W. Hahn, K. Niemax, The influence of laser-particle interaction in laser induced breakdown spectroscopy and laser ablation inductively coupled plasma spectrometry, Spectrochimica Acta Part B: Atomic Spectroscopy, (2011).

[4] E. Tognoni, G. Cristoforetti, S. Legnaioli, V. Palleschi, A. Salvetti, M. Mueller, U. Panne, I. Gornushkin, A numerical study of expected accuracy and precision in Calibration-Free Laser-Induced Breakdown Spectroscopy in the assumption of ideal analytical plasma, Spectrochimica Acta Part B: Atomic Spectroscopy, 62 (2007) 1287-1302.

[5] N.B. Zorov, A.A. Gorbatenko, T.A. Labutin, A.M. Popov, A review of normalization techniques in analytical atomic spectrometry with laser sampling: From single to multivariate correction, Spectrochimica Acta Part B: Atomic Spectroscopy, 65 (2010) 642-657.

[6] E. Runge, Spectrochemical analysis using a pulsed laser source, Spectrochimica Acta, 20 (1964) 733-736.

[7] K. Watkins, C. Curran, J.M. Lee, Two new mechanisms for laser cleaning using Nd: YAG sources, Journal of cultural Heritage, 4 (2003) 59-64.

[8] G. Drach, S. Dretler, W. Fair, B. Finlayson, J. Gillenwater, D. Griffith, J. Lingeman, D. Newman, Report of the United States cooperative study of extracorporeal shock wave lithotripsy, The Journal of urology, 135 (1986) 1127.

[9] T.W. Murray, J.W. Wagner, Laser generation of acoustic waves in the ablative regime, Journal of applied physics, 85 (1999) 2031.

[10] Z. Rui, L. Zhong-Cheng, H. Bing, Z. Hong-Chao, X. Rong-Qing, L. Jian, N. Xiao-Wu, Mechanism of laser-induced plasma shock wave evolution in air, Chinese Physics B, 18 (2009) 1877.

[11] J. Diaci, J. Možina, A study of blast waveforms detected simultaneously by a microphone and a laser probe during laser ablation, Applied Physics A: Materials Science & Processing, 55 (1992) 352-358.

[12] C. Stauter, P. Gerard, J. Fontaine, T. Engel, Laser ablation acoustical monitoring, Applied surface science, 109 (1997) 174-178.

[13] S. Palanco, J. Laserna, Spectral analysis of the acoustic emission of laser-produced plasmas, Applied optics, 42 (2003) 6078-6084.

[14] S. Conesa, S. Palanco, J. Laserna, Acoustic and optical emission during laser-induced plasma formation, Spectrochimica Acta Part B: Atomic Spectroscopy, 59 (2004) 1395-1401.

[15] W. Spillman Jr, B. Kline, L. Maurice, P. Fuhr, Statistical-mode sensor for fiber optic vibration sensing uses, Applied optics, 28 (1989) 3166-3176.

[16] A. Hrdlička, L. Prokeš, A. Staňková, K. Novotný, A. Vitešníková, V. Kanický, V. Otruba, J. Kaiser, J. Novotný, R. Malina, Development of a remote laser-induced breakdown spectroscopy system for investigation of calcified tissue samples, Applied optics, 49 (2010) C16-C20.

[17] C. Bohling, D. Scheel, K. Hohmann, W. Schade, M. Reuter, G. Holl, Fiber-optic laser sensor for mine detection and verification, Applied optics, 45 (2006) 3817-3825.

[18] M. Corsi, G. Cristoforetti, M. Giuffrida, M. Hidalgo, S. Legnaioli, V. Palleschi, A. Salvetti, E. Tognoni, C. Vallebona, Three-dimensional analysis of laser induced plasmas in single and double pulse configuration, Spectrochimica Acta Part B: Atomic Spectroscopy, 59 (2004) 723-735.

[19] F. Anabitarte, L. Rodriguez-Cobo, M. Lomer, J. Mirapeix, J.M. Lopez-Higuera, A. Cobo, Laser Induced Breakdown Spectroscopy light collector based on coiled plastic optical fiber, in: International conference on Plastic Optical fibers POF, Bilbao, 2011, pp. 315-319.

[20] B.J. Marquardt, S.R. Goode, S.M. Angel, In situ determination of lead in paint by laser-induced breakdown spectroscopy using a fiber-optic probe, Analytical Chemistry, 68 (1996) 977-981.

[21] R.E. Russo, X. Mao, H. Liu, J. Gonzalez, S.S. Mao, Laser ablation in analytical chemistry-a review, Talanta, 57 (2002) 425-451.

[22] J.P. Singh, Laser-induced breakdown spectroscopy, Elsevier Science, 2007.

[23] X. Zeng, X. Mao, R. Greif, R. Russo, Experimental investigation of ablation efficiency and plasma expansion during femtosecond and nanosecond laser ablation of silicon, Applied Physics A: Materials Science & Processing, 80 (2005) 237-241.

[24] G. Aldabaldetreku, I. Bikandi, M.Ý.A. Illarramendi, G. Durana, J. Zubia, A comprehensive analysis of scattering in polymer optical fibers, Optics Express, 18 (2010) 24536-24555.

[25] G. Hernán Sendra, Activity analysis on dynamic speckle patterns (Análisis de actividad en patrones de speckle dinámico), (2009).

[26] R. Arizaga, M. Trivi, H. Rabal, Speckle time evolution characterization by the co-occurrence matrix analysis, Optics & Laser Technology, 31 (1999) 163-169.

[27] R. Kashyap, Fiber bragg gratings, Academic Pr, 1999.

[28] A. Othonos, Fiber bragg gratings, Review of Scientific Instruments, 68 (1997) 4309.

[29] J. Leng, A. Asundi, Structural health monitoring of smart composite materials by using EFPI and FBG sensors, Sensors and Actuators A: Physical, 103 (2003) 330-340.

[30] J.M. López-Higuera, L. Rodriguez Cobo, A. Quintela Incera, A. Cobo, Fiber Optic Sensors in Structural Health Monitoring, Journal of Lightwave Technology, 29 (2011) 587-608.

[31] A.S. Eppler, D.A. Cremers, D.D. Hickmott, M.J. Ferris, A.C. Koskelo, Matrix effects in the detection of Pb and Ba in soils using laser-induced breakdown spectroscopy, Applied Spectroscopy, 50 (1996) 1175-1181.

[32] J. Aguilera, C. Aragon, F. Penalba, Plasma shielding effect in laser ablation of metallic samples and its influence on LIBS analysis, Applied surface science, 127 (1998) 309-314.

[33] C. Lopez-Moreno, S. Palanco, J.J. Laserna, F. DeLucia Jr, A.W. Miziolek, J. Rose, R.A. Walters, A.I. Whitehouse, Test of a stand-off laser-induced breakdown spectroscopy sensor for the detection of explosive residues on solid surfaces, J. Anal. At. Spectrom., 21 (2005) 55-60.

[34] R. Srinivasan, B. Braren, R. Dreyfus, L. Hadel, D. Seeger, Mechanism of the ultraviolet laser ablation of polymethyl methacrylate at 193 and 248 nm: laser-induced fluorescence analysis, chemical analysis, and doping studies, JOSA B, 3 (1986) 785-791.

[35] R. Srinivasan, B. Braren, Ultraviolet laser ablation of organic polymers, Chemical Reviews, 89 (1989) 1303-1316.

References chapter 5

[1] A. Ciucci, M. Corsi, V. Palleschi, S. Rastelli, A. Salvetti, E. Tognoni, New procedure for quantitative elemental analysis by laser-induced plasma spectroscopy, Applied Spectroscopy, 53 (1999) 960-964.

[2] V.N. Vapnik, The nature of statistical learning theory, Springer Verlag, 2000.

[3] I.T. Jolliffe, MyiLibrary, Principal component analysis, Wiley Online Library, 2002.

[4] B. Yegnanarayana, Artificial neural networks, PHI Learning Pvt. Ltd., 2004.

[5] Y. Shi, R.C. Eberhart, Empirical study of particle swarm optimization, IEEE, 1999.

[6] A.P. Engelbrecht, Fundamentals of computational swarm intelligence, Recherche, 67 (2005) 02.

[7] V.G. Galati, Gli scrittori delle Calabrie:(dizionario bio-bibliografico), Vallecchi, 1928.

[8] G. Colonna, Bronzi votivi umbro-sabellici a figura umana: Periodo" arcaico", Sansoni, 1970.

[9] M. Cristofani, I bronzetti italici del museo di Crotone, Klearkos, 1968.

[10] G. Maetzke, La collezione del Museo Archeologico Nazionale di Chiusi', Studi Etruschi, 25 (1957) 489-523.

[11] E.W. Psenner, G. Ciurletti, I bronzetti figurati antichi del Trentino, Provincia Autonoma, Assessorato alle attività culturali, 1983.

[12] H. Rolland, Bronzes antiques de Haute Provence, Recherche, 67 (1965) 02.

[13] M. provinciale sannitico di Campobasso, A. Di Niro, Piccoli bronzi figurati nel museo di Campobasso, P. Laveglia, 1978.

[14] P.C. Guida, Bronzetti a figura umana: dalle collezioni dei Civici musei di storia ed arte de Trieste, Electa, 1979.

[15] S. Besques, Catalogue raisonne des figurines et reliefs en terre-cuite grecs et romains, Editions des Musées nationaux, 1963.

[16] A. Bertolini, G. Carelli, F. Francesconi, M. Francesconi, L. Marchesini, P. Marsili, F. Sorrentino, G. Cristoforetti, S. Legnaioli, V. Palleschi, Modì: a new mobile instrument for in situ double-pulse LIBS analysis, Analytical and Bioanalytical Chemistry, 385 (2006) 240-247.

[17] P. García-Allende, J. Mirapeix, O. Conde, A. Cobo, J. López-Higuera, Spectral processing technique based on feature selection and artificial neural networks for arc-welding quality monitoring, NDT & E International, 42 (2009) 56-63.

[18] S. Nakamura, Y. Ito, T. Nakabayashi, M. Watanabe, T. Inoue, A. Matsunawa, Analysis of optical and acoustic emissions during CO 2 laser welding of a stainless steel, ICALEO'97: Laser Materials Processing., 83 (1997).

[19] J. Lee, J. Kim, J. Oh, S. Park, Effect of Al coating conditions on laser weldability of Al coated steel sheet, Transactions of Nonferrous Metals Society of China, 19 (2009) 946-951.

[20] J. Lancaster, The physics of welding, Physics in Technology, 15 (1984) 73-79.

[21] R. Martukanitz, A critical review of laser beam welding, Proc. SPIE, 2005, pp. 11.

[22] S. Gunn, Support vector machines for classification and regression, ISIS technical report, 14 (1998).

[23] N. Cristianini, J. Shawe-Taylor, An introduction to support Vector Machines: and other kernel-based learning methods, Cambridge Univ Pr, 2000.

[24] J.A.K. Suykens, J. Vandewalle, Least squares support vector machine classifiers, Neural processing letters, 9 (1999) 293-300.

[25] R. Zhang, J. Ma, An improved SVM method P-SVM for classification of remotely sensed data, International Journal of Remote Sensing, 29 (2008) 6029-6036.

[26] T. Mu, A. Nandi, Breast cancer detection from FNA using SVM with different parameter tuning systems and SOM–RBF classifier, Journal of the Franklin Institute, 344 (2007) 285-311.

[27] G. ElMasry, N. Wang, A. ElSayed, M. Ngadi, Hyperspectral imaging for nondestructive determination of some quality attributes for strawberry, Journal of Food Engineering, 81 (2007) 98-107.

[28] Y. Langeron, M. Doussot, D. Hewson, J. Duchêne, Classifying NIR spectra of textile products with kernel methods, Engineering Applications of Artificial Intelligence, 20 (2007) 415-427.

[29] P.B. Garcia-Allende, F. Anabitarte, O.M. Conde, J. Mirapeix, F.J. Madruga, J.M. Lopez-Higuera, Support vector machines in hyperspectral imaging spectroscopy with application to material identification, Proc. SPIE, 2008, pp. 69661V.

[30] M. Corsi, G. Cristoforetti, M. Hidalgo, S. Legnaioli, V. Palleschi, A. Salvetti, E. Tognoni, C. Vallebona, Double pulse, calibration-free laser-induced breakdown spectroscopy: A new technique for in situ standard-less analysis of polluted soils, Applied geochemistry, 21 (2006) 748-755.

[31] J. Mirapeix, A. Cobo, D. González, J. López-Higuera, Plasma spectroscopy analysis technique based on optimization algorithms and spectral synthesis for arc-welding quality assurance, Optics Express, 15 (2007) 1884-1897.

[32] A. Ancona, V. Spagnolo, P.M. Lugara, M. Ferrara, Optical Sensor for real-time Monitoring of CO2 Laser Welding Process, Applied optics, 40 (2001) 6019-6025.

[33] I. Gornushkin, M. Mueller, U. Panne, J. Winefordner, Insights into linear and rank correlation for material identification in laser-induced breakdown spectroscopy and other spectral techniques, Applied Spectroscopy, 62 (2008) 542-553.

[34] I. Gornushkin, U. Panne, J. Winefordner, Linear correlation for identification of materials by laser induced breakdown spectroscopy: Improvement via spectral filtering and masking, Spectrochimica Acta Part B: Atomic Spectroscopy, 64 (2009) 1040-1047.

[35] G. Amato, G. Cristoforetti, S. Legnaioli, G. Lorenzetti, V. Palleschi, F. Sorrentino, E. Tognoni, Progress towards an unassisted element identification from Laser Induced Breakdown Spectra with automatic ranking techniques inspired by text retrieval, Spectrochimica Acta Part B: Atomic Spectroscopy, 65 (2010) 664-670.

[36] Y. Ralchenko, NIST atomic spectra database, Memorie della Societa Astronomica Italiana Supplementi, 8 (2005) 96.

[37] J. Kennedy, R. Eberhart, Particle swarm optimization, IEEE, 1995, pp. 1942-1948 vol. 1944.

[38] S. Zhen-gang, L. Qin-zi, Edge detection for Medical Image based on PSO Algorithm, IEEE, 2010, pp. 84-87.

[39] W. Ding, A New Method for Image Noise Removal using Chaos-PSO and Nonlinear ICA, Procedia Engineering, 24 (2011) 111-115.

[40] R.H. Wang, B. Fang, Emotion Fusion Recognition for Intelligent Surveillance with PSO-CSVM, Advanced Materials Research, 225 (2011) 51-56.

[41] J. Izquierdo, I. Montalvo, R. Pérez, V.S. Fuertes, Design optimization of wastewater collection networks by PSO, Computers & Mathematics with Applications, 56 (2008) 777-784.

[42] G. Zhitao, Y. Jinli, G. Junhua, Design and research of RFID microstrip antenna based on improved PSO neural networks, IEEE, 2010, pp. 251-254.

[43] M. Alberghina, R. Barraco, M. Brai, T. Schillaci, L. Tranchina, Comparison of LIBS and μ-XRF measurements on bronze alloys for monitoring plasma effects, IOP Publishing, 2011, pp. 012017.

[44] M. Brai, G. Gennaro, T. Schillaci, L. Tranchina, Double pulse laser induced breakdown spectroscopy applied to natural and artificial materials from cultural heritages: A comparison with micro-X-ray fluorescence analysis, Spectrochimica Acta Part B: Atomic Spectroscopy, 64 (2009) 1119-1127.

[45] O. Borisov, X. Mao, A. Fernandez, M. Caetano, R. Russo, Inductively coupled plasma mass spectrometric study of non-linear calibration behavior during laser ablation of binary Cu-Zn Alloys, Spectrochimica Acta Part B: Atomic Spectroscopy, 54 (1999) 1351-1365.

[46] M. Gagean, J. Mermet, Study of laser ablation of brass materials using inductively coupled plasma atomic emission spectrometric detection, Spectrochimica Acta Part B: Atomic Spectroscopy, 53 (1998) 581-591.

[47] L. Fornarini, F. Colao, R. Fantoni, V. Lazic, V. Spizzicchino, Calibration analysis of bronze samples by nanosecond laser induced breakdown spectroscopy: A theoretical and experimental approach, Spectrochimica Acta Part B: Atomic Spectroscopy, 60 (2005) 1186-1201.

References chapter 6

[1] L. Campanella, G. Favero, P. Flamini, M. Tomassetti, Prehistoric terracottas from the libyan tadrart acacus, Journal of thermal analysis and calorimetry, 73 (2003) 127-142.

[2] K. Norrish, B. Chappell, X-ray fluorescence spectrometry, Physical methods in determinative mineralogy, (1977) 201-272.

[3] P.R. Griffiths, J.A. De Haseth, Fourier transform infrared spectrometry, John Wiley & Sons, 2007.

[4]E.R. Kaal, M. Kurano, H.G. Janssen, Hyphenation of aqueous liquid chromatography to pyrolysis-gas chromatography and mass spectrometry for the comprehensive characterization of water-soluble polymers, Journal of Chromatography A, 1186 (2008) 222-227.

[5] D. Van de Meent, S.C. Brown, R.P. Philp, B.R.T. Simoneit, Pyrolysis-high resolution gas chromatography and pyrolysis gas chromatography-mass spectrometry of kerogens and kerogen precursors, Geochimica et Cosmochimica Acta, 44 (1980) 999-1013.

[6] R.L. Grob, E.F. Barry, J. Wiley, Modern practice of gas chromatography, Wiley Online Library, 1985.

[7] C.F. Poole, S.K. Poole, Chromatography today, Elsevier Science Publishers, 1991.

[8] J.B. Fenn, M. Mann, C.K. Meng, S.F. Wong, C.M. Whitehouse, Electrospray ionization for mass spectrometry of large biomolecules, Science, 246 (1989) 64-71.

[9] R. Aebersold, M. Mann, Mass spectrometry-based proteomics, Nature, 422 (2003) 198-207.

[10] B. Stuart, Infrared spectroscopy, Wiley Online Library, 2004.

[11] D.A. Burns, E.W. Ciurczak, Handbook of near-infrared analysis, CRC, 2008.

[12] J.R. Ferraro, L.J. Basile, Fourier transform infrared spectroscopy, (1985).

[13] B. Beckhoff, N. Langhoff, B. Kanngiefer, R. Wedell, H. Wolff, Handbook of practical X-ray fluorescence analysis, Springer Verlag, 2006.

[14] A. Montaser, D. Golightly, Inductively coupled plasmas in analytical atomic spectrometry, (1987).

[15] R.H. Scott, V.A. Fassel, R.N. Kniseley, D.E. Nixon, Inductively coupled plasma-optical emission analytical spectrometry, Analytical Chemistry, 46 (1974) 75-80.

[16] G. Pianu, Il bucchero, Edipuglia srl, 2000.

[17] L. Angeli, C. Arias, G. Cristoforetti, C. Fabbri, S. Legnaioli, V. Palleschi, G. Radi, A. Salvetti, E. Tognoni, Spectroscopic Techniques Applied to the Study of Italian Painted Neolithic Potteries, Laser Chemistry, 2006 (2006) 1-7.

[18] J. Madejova, FTIR techniques in clay mineral studies, Vibrational Spectroscopy, 31 (2003) 1-10.

[19] P.S. Nayak, B. Singh, Instrumental characterization of clay by XRF, XRD and FTIR, Bulletin of Materials Science, 30 (2007) 235-238.

[20] W. Johannowsky, M. Merolla, Materiali di età arcaica dalla Campania, G. Macchiaroli, 1983.

[21] M.J. Aitken, Thermoluminescence dating, Academic Press London, 1985.

[22] M. Minoja, Il Museo Archeologico dell'Antica Capua, Napoli, 1995, pp. 27-29.

[23] I.S. Hornsey, A history of beer and brewing, Royal Society of Chemistry, 2003.

[24] C. Riedo, D. Scalarone, O. Chiantore, Advances in identification of plant gums in cultural heritage by thermally assisted hydrolysis and methylation, Analytical and Bioanalytical Chemistry, 396 (2010) 1559-1569.

[25] A. Andreotti, I. Bonaduce, M.P. Colombini, F. Modugno, E. Ribechini, A diagnosis of the yellowing of the marble high reliefs and the black decorations in the chapel of the tomb of Saint Anthony (Padua, Italy), International Journal of Mass Spectrometry, 284 (2009) 123-130.

[26] F. Fedele, O. Longo, P. Scarpi, Storie del vino. Homo Edens. Ragioni, miti e pratiche dell'alimentazione nella civiltà del Mediterraneo II, Diapress, Milano, 1991, pp. 35-68.

[27] P.E. McGovern, D.L. Glusker, L.J. Exner, M.M. Voigt, Neolithic resinated wine, Nature, 381 (1996) 480-481.

[28] A. Prieto, M. Avella, M. González, J. Jiménez, F. Romero, R. De Pablo, C. Górriz, C. Sanz, Analysis of the Residuals in Grave Goods From the Vaccaea Era at the Necropolis of "Las Ruedas" in Pintia, Spectroscopy Letters, 45 (2012) 141-145.

[29] C.M. Kraay, The Composition of electrum coinage, Archaeometry, 1 (1958) 21-23.

[30] R. Linke, M. Schreiner, G. Demortier, M. Alram, Determination of the provenance of medieval silver coins: potential and limitations of x-ray analysis using photons, electrons or protons, X-Ray Spectrometry, 32 (2003) 373-380.

[31] L. Torrisi, F. Caridi, L. Giuffrida, A. Torrisi, G. Mondio, T. Serafino, M. Caltabiano, E. Castrizio, E. Paniz, A. Salici, LAMQS analysis applied to ancient Egyptian bronze coins, Nuclear Instruments and Methods in Physics Research Section B: Beam Interactions with Materials and Atoms, 268 (2010) 1657-1664.

[32] M. Ferretti, G. Cristoforetti, S. Legnaioli, V. Palleschi, A. Salvetti, E. Tognoni, E. Console, P. Palaia, In situ study of the Porticello Bronzes by portable X-ray fluorescence and laser-induced breakdown spectroscopy, Spectrochimica Acta Part B: Atomic Spectroscopy, 62 (2007) 1512-1518.

[33] L. Campanella, O.C. Alessandri, M. Ferretti, S. Plattner, The effect of tin on dezincification of archaeological copper alloys, Corrosion Science, 51 (2009) 2183-2191.

[34] E. Babelon, Description historique et chronologique des monnaies de la république romaine vulgairement appelées monnaies consulaires, Paris, 1885-1886.

[35] M.H. Crawford, Roman republican coinage, Cambridge University Press, 1974.

[36] E.A. Sydenham, The Coinage of the Roman Republic, New York, 1952.

[37] D.R. Walker, The metrology of the Roman silver coinage, British Archaeological Reports, 1976.

[38] L. Beck, S. Bosonnet, S. Réveillon, D. Eliot, F. Pilon, Silver surface enrichment of silver–copper alloys: a limitation for the analysis of ancient silver coins by surface techniques, Nuclear Instruments and Methods in Physics Research Section B: Beam Interactions with Materials and Atoms, 226 (2004) 153-162.

[39] R. Gilbert, Stress, paleonutrition, and trace elements, The analysis of prehistoric diets, (1985) 339-358.

[40] A. Sillen, M. Kavanagh, Strontium and paleodietary research: a review, American Journal of Physical Anthropology, 25 (1982) 67-90.

[41] M.A. Kasem, R.E. Russo, M.A. Harith, Influence of biological degradation and environmental effects on the interpretation of archeological bone samples with laser-induced breakdown spectroscopy, J. Anal. At. Spectrom., 26 (2011) 1733-1739.

[42] B.K. Nelson, M.J. DeNiro, M.J. Schoeninger, D.J. De Paolo, P.E. Hare, Effects of diagenesis on strontium, carbon, nitrogen and oxygen concentration and isotopic composition of bone, Geochimica et Cosmochimica Acta, 50 (1986) 1941-1949.

[43] C.M. Nielsen-Marsh, R.E.M. Hedges, Patterns of diagenesis in bone I: The effects of site environments, Journal of Archaeological Science, 27 (2000) 1139-1150.

[44] J.H. Burton, T.D. Price, The ratio of barium to strontium as a paleodietary indicator of consumption of marine resources, Journal of Archaeological Science, 17 (1990) 547-557.

[45] S.J. Haswell, Atomic absorption spectrometry, Elsevier, 1991.

[46] J.E. Cantle, Atomic absorption spectrometry, Elsevier Science Limited, 1982.

[47] A. Bertolini, G. Carelli, F. Francesconi, M. Francesconi, L. Marchesini, P. Marsili, F. Sorrentino, G. Cristoforetti, S. Legnaioli, V. Palleschi, Modì: a new mobile instrument for in situ double-pulse LIBS analysis, Analytical and Bioanalytical Chemistry, 385 (2006) 240-247.

[48] M. Borrini, F. Bartoli, A. Bacci, F. Mallegni, Analisi paleonutrizionale su alcuni campioni dalla mass grave dell'Isola del Lazzaretto Nuovo (Venezia), Archivio per l'antropologia e la etnologia, 140 (2010) 81-91.

[49] J. Cui, L. Zhang, Metallurgical recovery of metals from electronic waste: A review, Journal of hazardous materials, 158 (2008) 228-256.

[50] K. Gloe, P. Muhl, M. Knothe, Recovery of precious metals from electronic scrap, in particular from waste products of the thick-layer technique, Hydrometallurgy, 25 (1990) 99-110.

[51] H.Y. Kang, J.M. Schoenung, Electronic waste recycling: A review of US infrastructure and technology options, Resources, Conservation and Recycling, 45 (2005) 368-400.

[52] J.O. Nriagu, Cupellation: The oldest quantitative chemical process, Journal of chemical education, 62 (1985) 668-674.

[53] M. Balcerzak, Sample digestion methods for the determination of traces of precious metals by spectrometric techniques, Analytical sciences, 18 (2002) 737-750.

[54] A. Martin, S.A. Harbison, An introduction to radiation protection, Environmental Safety Group, Associated Nuclear Services, Epsom, 1986.

[55] A.W. Miziolek, V. Palleschi, I. Schechter, Laser-induced breakdown spectroscopy (LIBS): fundamentals and applications, Cambridge Univ Pr, 2006.

[56] M. Corsi, G. Cristoforetti, V. Palleschi, A. Salvetti, E. Tognoni, A fast and accurate method for the determination of precious alloys caratage by laser induced plasma spectroscopy, The European Physical Journal D-Atomic, Molecular, Optical and Plasma Physics, 13 (2001) 373-377.

[57] A. Jurado-López, M. Luque de Castro, Chemometric approach to laser-induced breakdown analysis of gold alloys, Applied Spectroscopy, 57 (2003) 349-352.

[58] G. Galbács, N. Jedlinszki, G. Cseh, Z. Galbács, L. Túri, Accurate quantitative analysis of gold alloys using multi-pulse laser induced breakdown spectroscopy and a correlation-based calibration method, Spectrochimica Acta Part B: Atomic Spectroscopy, 63 (2008) 591-597.

[59] M. Dzyubenko, S. Kolpakov, D. Kulishenko, A. Priyomko, Rapid analysis of emission spectra for gold alloys, Journal of Applied Spectroscopy, 77 (2010) 279-284.

[60] G. Cristoforetti, S. Legnaioli, V. Palleschi, A. Salvetti, E. Tognoni, Effect of target composition on the emission enhancement observed in Double-Pulse Laser-Induced Breakdown Spectroscopy, Spectrochimica Acta Part B: Atomic Spectroscopy, 63 (2008) 312-323.

[61] F. Sorrentino, G. Carelli, F. Francesconi, M. Francesconi, P. Marsili, G. Cristoforetti, S. Legnaioli, V. Palleschi, E. Tognoni, Fast analysis of complex metallic alloys by double-pulse time-integrated Laser-Induced Breakdown Spectroscopy, Spectrochimica Acta Part B: Atomic Spectroscopy, 64 (2009) 1068-1072.

[62] N. Jedlinszki, G. Galbács, An evaluation of the analytical performance of collinear multi-pulse laser induced breakdown spectroscopy, Microchemical Journal, 97 (2011) 255-263.

[63] G. Amato, G. Cristoforetti, S. Legnaioli, G. Lorenzetti, V. Palleschi, F. Sorrentino, E. Tognoni, Progress towards an unassisted element identification from Laser Induced Breakdown Spectra with automatic ranking techniques inspired by text retrieval, Spectrochimica Acta Part B: Atomic Spectroscopy, 65 (2010) 664-670.

[64] A. Ciucci, V. Palleschi, S. Rastelli, A. Salvetti, D. Singh, E. Tognoni, CF-LIPS: a new approach to LIPS spectra analysis, Laser and Particle Beams, 17 (1999) 793-797.

[65] E. Tognoni, G. Cristoforetti, S. Legnaioli, V. Palleschi, Calibration-free laser-induced breakdown spectroscopy: state of the art, Spectrochimica Acta Part B: Atomic Spectroscopy, 65 (2010) 1-14.

References chapter 8

[1] J.M Lopez-higuera, F. Anabitarte, A. Cobo. La Fotónica en arqueología: su aplicación a la caracterización de pigmentos y materiales. Invited conference on summer courses of University of Cantabria. Ramales de la Victoria, 1st of august 2012

References in alphabetical order

M. Abdelhamid, F. Fortes, J. Laserna, M. Harith, Optical Catapulting Laser Induced Breakdown Spectroscopy (OC-LIBS) And Conventional LIBS: A comparative Study, ICLA, 2011, pp. 55.

G. Abdellatif, H. Imam, A study of the laser plasma parameters at different laser wavelengths, Spectrochimica Acta Part B: Atomic Spectroscopy, 57 (2002) 1155-1165.

R. Aebersold, M. Mann, Mass spectrometry-based proteomics, Nature, 422 (2003) 198-207.

J. Aguilera, C. Aragon, F. Penalba, Plasma shielding effect in laser ablation of metallic samples and its influence on LIBS analysis, Applied surface science, 127 (1998) 309-314.

M.J. Aitken, Thermoluminescence dating, Academic Press London, 1985.

M. Alberghina, R. Barraco, M. Brai, T. Schillaci, L. Tranchina, Comparison of LIBS and μ-XRF measurements on bronze alloys for monitoring plasma effects, IOP Publishing, 2011, pp. 012017.

G. Aldabaldetreku, I. Bikandi, M.Ý.A. Illarramendi, G. Durana, J. Zubia, A comprehensive analysis of scattering in polymer optical fibers, Optics Express, 18 (2010) 24536-24555.

G. Amato, G. Cristoforetti, S. Legnaioli, G. Lorenzetti, V. Palleschi, F. Sorrentino, E. Tognoni, Progress towards an unassisted element identification from Laser Induced Breakdown Spectra with automatic ranking techniques inspired by text retrieval, Spectrochimica Acta Part B: Atomic Spectroscopy, 65 (2010) 664-670.

G. Amato, S. Legnaioli, G. Lorenzetti, V. Palleschi, L. Pardini, F. Rabitti, Element detection relying on information retrieval techniques applied to laser spectroscopy, ACM, 2011, pp. 89-95.

F. Anabitarte, L. Rodriguez-Cobo, M. Lomer, J. Mirapeix, J.M. Lopez-Higuera, A. Cobo, Laser Induced Breakdown Spectroscopy light collector based on coiled plastic optical fiber, in: International conference on Plastic Optical fibers POF, Bilbao, 2011, pp. 315-319.

A. Ancona, V. Spagnolo, P.M. Lugara, M. Ferrara, Optical Sensor for real-time Monitoring of CO2 Laser Welding Process, Applied optics, 40 (2001) 6019-6025.

A. Andreotti, I. Bonaduce, M.P. Colombini, F. Modugno, E. Ribechini, A diagnosis of the yellowing of the marble high reliefs and the black decorations in the chapel of the tomb of Saint Anthony (Padua, Italy), International Journal of Mass Spectrometry, 284 (2009) 123-130.

S.M. Angel, D.N. Stratis, K.L. Eland, T. Lai, M.A. Berg, D.M. Gold, LIBS using dual- and ultra-short laser pulses, Fresenius' journal of analytical chemistry, 369 (2001) 320-327.

L. Angeli, C. Arias, G. Cristoforetti, C. Fabbri, S. Legnaioli, V. Palleschi, G. Radi, A. Salvetti, E. Tognoni, Spectroscopic Techniques Applied to the Study of Italian Painted Neolithic Potteries, Laser Chemistry, 2006 (2006) 1-7.

J.M. Anzano, M.A. Villoria, A. Ruíz-Medina, R.J. Lasheras, Laser-induced breakdown spectroscopy for quantitative spectrochemical analysis of geological materials: Effects of the matrix and simultaneous determination, Analytica chimica acta, 575 (2006) 230-235.

C. Aragon, J. Aguilera, J. Campos, Determination of carbon content in molten steel using laser-induced breakdown spectroscopy, Applied Spectroscopy, 47 (1993) 606-608.

C. Aragon, J.A. Aguilera, F. Penalba, Improvements in quantitative analysis of steel composition by laser-induced breakdown spectroscopy at atmospheric pressure using an infrared Nd: YAG laser, Applied Spectroscopy, 53 (1999) 1259-1267.

R. Arizaga, M. Trivi, H. Rabal, Speckle time evolution characterization by the co-occurrence matrix analysis, Optics & Laser Technology, 31 (1999) 163-169.

E. Babelon, Description historique et chronologique des monnaies de la république romaine vulgairement appelées monnaies consulaires, Paris, 1885-1886.

M. Balcerzak, Sample digestion methods for the determination of traces of precious metals by spectrometric techniques, Analytical sciences, 18 (2002) 737-750.

I. Bassiotis, A. Diamantopoulou, A. Giannoudakos, F. Roubani-Kalantzopoulou, M. Kompitsas, Effects of experimental parameters in quantitative analysis of steel alloy by laser-induced breakdown spectroscopy, Spectrochimica Acta Part B: Atomic Spectroscopy, 56 (2001) 671-683.

H. Bauer, F. Leis, K. Niemax, Laser induced breakdown spectrometry with an echelle spectrometer and intensified charge coupled device detection, Spectrochimica Acta Part B: Atomic Spectroscopy, 53 (1998) 1815-1825.

L. Beck, S. Bosonnet, S. Réveillon, D. Eliot, F. Pilon, Silver surface enrichment of silver–copper alloys: a limitation for the analysis of ancient silver coins by surface techniques, Nuclear Instruments and Methods in Physics Research Section B: Beam Interactions with Materials and Atoms, 226 (2004) 153-162.

B. Beckhoff, N. Langhoff, B. Kanngiefer, R. Wedell, H. Wolff, Handbook of practical X-ray fluorescence analysis, Springer Verlag, 2006.

A. Bertolini, G. Carelli, F. Francesconi, M. Francesconi, L. Marchesini, P. Marsili, F. Sorrentino, G. Cristoforetti, S. Legnaioli, V. Palleschi, Modì: a new mobile instrument for in situ double-pulse LIBS analysis, Analytical and Bioanalytical Chemistry, 385 (2006) 240-247.

S. Besques, Catalogue raisonne des figurines et reliefs en terre-cuite grecs et romains, Editions des Musées nationaux, 1963.

C. Bohling, D. Scheel, K. Hohmann, W. Schade, M. Reuter, G. Holl, Fiber-optic laser sensor for mine detection and verification, Applied optics, 45 (2006) 3817-3825.

O. Borisov, X. Mao, A. Fernandez, M. Caetano, R. Russo, Inductively coupled plasma mass spectrometric study of non-linear calibration behavior during laser ablation of binary Cu-Zn Alloys, Spectrochimica Acta Part B: Atomic Spectroscopy, 54 (1999) 1351-1365.

M. Borrini, F. Bartoli, A. Bacci, F. Mallegni, Analisi paleonutrizionale su alcuni campioni dalla mass grave dell'Isola del Lazzaretto Nuovo (Venezia), Archivio per l'antropologia e la etnologia, 140 (2010) 81-91.

M. Brai, G. Gennaro, T. Schillaci, L. Tranchina, Double pulse laser induced breakdown spectroscopy applied to natural and artificial materials from cultural heritages: A comparison with micro-X-ray fluorescence analysis, Spectrochimica Acta Part B: Atomic Spectroscopy, 64 (2009) 1119-1127.

D. Bulajic, M. Corsi, G. Cristoforetti, S. Legnaioli, V. Palleschi, A. Salvetti, E. Tognoni, A procedure for correcting self-absorption in calibration free-laser induced breakdown spectroscopy, Spectrochimica Acta Part B: Atomic Spectroscopy, 57 (2002) 339-353.

D.A. Burns, E.W. Ciurczak, Handbook of near-infrared analysis, CRC, 2008.

J.H. Burton, T.D. Price, The ratio of barium to strontium as a paleodietary indicator of consumption of marine resources, Journal of Archaeological Science, 17 (1990) 547-557.

L. Cabalin, J. Laserna, Experimental determination of laser induced breakdown thresholds of metals under nanosecond Q-switched laser operation, Spectrochimica Acta Part B: Atomic Spectroscopy, 53 (1998) 723-730.

B. Cagnac, J.C. Pebay-Peyroula, Modern atomic physics: fundamental principles, (1975).

L. Campanella, O.C. Alessandri, M. Ferretti, S. Plattner, The effect of tin on dezincification of archaeological copper alloys, Corrosion Science, 51 (2009) 2183-2191.

L. Campanella, G. Favero, P. Flamini, M. Tomassetti, Prehistoric terracottas from the libyan tadrart acacus, Journal of thermal analysis and calorimetry, 73 (2003) 127-142.

L. Caneve, A. Diamanti, F. Grimaldi, G. Palleschi, V. Spizzichino, F. Valentini, Analysis of fresco by laser induced breakdown spectroscopy, Spectrochimica Acta Part B: Atomic Spectroscopy, 65 (2010) 702-706.

J.E. Cantle, Atomic absorption spectrometry, Elsevier Science Limited, 1982.

J.E. Carranza, E. Gibb, B.W. Smith, D.W. Hahn, J.D. Winefordner, Comparison of nonintensified and intensified CCD detectors for laser-induced breakdown spectroscopy, Applied optics, 42 (2003) 6016-6021.

B. Castle, K. Talabardon, B. Smith, J. Winefordner, Variables influencing the precision of laser-induced breakdown spectroscopy measurements, Applied Spectroscopy, 52 (1998) 649-657.

C. Chaleard, P. Mauchien, N. Andre, J. Uebbing, J. Lacour, C. Geertsen, Correction of Matrix Effects in Quantitative Elemental AnalysisWith Laser Ablation Optical Emission Spectrometry, J. Anal. At. Spectrom., 12 (1997) 183-188.

A. Ciucci, M. Corsi, V. Palleschi, S. Rastelli, A. Salvetti, E. Tognoni, New procedure for quantitative elemental analysis by laser-induced plasma spectroscopy, Applied Spectroscopy, 53 (1999) 960-964.

A. Ciucci, V. Palleschi, S. Rastelli, R. Barbini, F. Colao, R. Fantoni, A. Palucci, S. Ribezzo, H. Van Der Steen, Trace pollutants analysis in soil by a time-resolved laser-induced breakdown spectroscopy technique, Applied Physics B: Lasers and Optics, 63 (1996) 185-190.

A. Ciucci, V. Palleschi, S. Rastelli, A. Salvetti, D. Singh, E. Tognoni, CF-LIPS: a new approach to LIPS spectra analysis, Laser and Particle Beams, 17 (1999) 793-797.

G. Colonna, Bronzi votivi umbro-sabellici a figura umana: Periodo" arcaico", Sansoni, 1970.

S. Conesa, S. Palanco, J. Laserna, Acoustic and optical emission during laser-induced plasma formation, Spectrochimica Acta Part B: Atomic Spectroscopy, 59 (2004) 1395-1401.

M. Corsi, G. Cristoforetti, M. Giuffrida, M. Hidalgo, S. Legnaioli, V. Palleschi, A. Salvetti, E. Tognoni, C. Vallebona, Three-dimensional analysis of laser induced plasmas in single and double pulse configuration, Spectrochimica Acta Part B: Atomic Spectroscopy, 59 (2004) 723-735.

M. Corsi, G. Cristoforetti, M. Hidalgo, S. Legnaioli, V. Palleschi, A. Salvetti, E. Tognoni, C. Vallebona, Double pulse, calibration-free laser-induced breakdown spectroscopy: A new technique for in situ standard-less analysis of polluted soils, Applied geochemistry, 21 (2006) 748-755.

M. Corsi, G. Cristoforetti, V. Palleschi, A. Salvetti, E. Tognoni, A fast and accurate method for the determination of precious alloys caratage by laser induced plasma spectroscopy, The European Physical Journal D-Atomic, Molecular, Optical and Plasma Physics, 13 (2001) 373-377.

C. Cortes, V. Vapnik, Support-vector networks, Machine learning, 20 (1995) 273-297.

M.H. Crawford, Roman republican coinage, Cambridge University Press, 1974.

D. Cremers, J. Barefield, A. Koskelo, Remote elemental analysis by laser-induced breakdown spectroscopy using a fiber-optic cable, Applied Spectroscopy, 49 (1995) 857-860.

D.A. Cremers, L.J. Radziemski, T.R. Loree, Spectrochemical analysis of liquids using the laser spark, Applied Spectroscopy, 38 (1984) 721-729.

D.A. Cremers, L.J. Radziemski, J. Wiley, Handbook of laser-induced breakdown spectroscopy, John Wiley & Sons Ltd., 2006.

N. Cristianini, J. Shawe-Taylor, An introduction to support Vector Machines: and other kernel-based learning methods, Cambridge Univ Pr, 2000.

M. Cristofani, I bronzetti italici del museo di Crotone, Klearkos, 1968.

G. Cristoforetti, A. De Giacomo, M. Dell'Aglio, S. Legnaioli, E. Tognoni, V. Palleschi, N. Omenetto, Local thermodynamic equilibrium in laser-induced breakdown spectroscopy: beyond the McWhirter criterion, Spectrochimica Acta Part B: Atomic Spectroscopy, 65 (2010) 86-95.

G. Cristoforetti, S. Legnaioli, V. Palleschi, A. Salvetti, E. Tognoni, Effect of target composition on the emission enhancement observed in Double-Pulse Laser-Induced Breakdown Spectroscopy, Spectrochimica Acta Part B: Atomic Spectroscopy, 63 (2008) 312-323.

J. Cui, L. Zhang, Metallurgical recovery of metals from electronic waste: A review, Journal of hazardous materials, 158 (2008) 228-256.

J. Cuñat, S. Palanco, F. Carrasco, M. Simon, J. Laserna, Portable instrument and analytical method using laser-induced breakdown spectrometry for in situ characterization of speleothems in karstic caves, J. Anal. At. Spectrom., 20 (2005) 295-300.

J. Diaci, J. Možina, A study of blast waveforms detected simultaneously by a microphone and a laser probe during laser ablation, Applied Physics A: Materials Science & Processing, 55 (1992) 352-358.

W. Ding, A New Method for Image Noise Removal using Chaos-PSO and Nonlinear ICA, Procedia Engineering, 24 (2011) 111-115.

G. Drach, S. Dretler, W. Fair, B. Finlayson, J. Gillenwater, D. Griffith, J. Lingeman, D. Newman, Report of the United States cooperative study of extracorporeal shock wave lithotripsy, The Journal of urology, 135 (1986) 1127.

M. Dzyubenko, S. Kolpakov, D. Kulishenko, A. Priyomko, Rapid analysis of emission spectra for gold alloys, Journal of Applied Spectroscopy, 77 (2010) 279-284.

K.L. Eland, D.N. Stratis, D.M. Gold, S.R. Goode, S.M. Angel, Energy dependence of emission intensity and temperature in a LIBS plasma using femtosecond excitation, Applied Spectroscopy, 55 (2001) 286-291.

G. ElMasry, N. Wang, A. ElSayed, M. Ngadi, Hyperspectral imaging for nondestructive determination of some quality attributes for strawberry, Journal of Food Engineering, 81 (2007) 98-107.

A.P. Engelbrecht, Fundamentals of computational swarm intelligence, Recherche, 67 (2005) 02.

A.S. Eppler, D.A. Cremers, D.D. Hickmott, M.J. Ferris, A.C. Koskelo, Matrix effects in the detection of Pb and Ba in soils using laser-induced breakdown spectroscopy, Applied Spectroscopy, 50 (1996) 1175-1181.

F. Fedele, O. Longo, P. Scarpi, Storie del vino. Homo Edens. Ragioni, miti e pratiche dell'alimentazione nella civiltà del Mediterraneo II, Diapress, Milano, 1991, pp. 35-68.

J.B. Fenn, M. Mann, C.K. Meng, S.F. Wong, C.M. Whitehouse, Electrospray ionization for mass spectrometry of large biomolecules, Science, 246 (1989) 64-71.

J.R. Ferraro, L.J. Basile, Fourier transform infrared spectroscopy, (1985).

M. Ferretti, G. Cristoforetti, S. Legnaioli, V. Palleschi, A. Salvetti, E. Tognoni, E. Console, P. Palaia, In situ study of the Porticello Bronzes by portable X-ray fluorescence and laser-induced breakdown spectroscopy, Spectrochimica Acta Part B: Atomic Spectroscopy, 62 (2007) 1512-1518.

P. Fichet, P. Mauchien, J.F. Wagner, C. Moulin, Quantitative elemental determination in water and oil by laser induced breakdown spectroscopy, Analytica chimica acta, 429 (2001) 269-278.

L. Fornarini, F. Colao, R. Fantoni, V. Lazic, V. Spizzicchino, Calibration analysis of bronze samples by nanosecond laser induced breakdown spectroscopy: A theoretical and experimental approach, Spectrochimica Acta Part B: Atomic Spectroscopy, 60 (2005) 1186-1201.

F. Fortes, J. Laserna, Characteristics of solid aerosols produced by optical catapulting studied by laser-induced breakdown spectroscopy, Applied surface science, 256 (2010) 5924-5928.

M. Gagean, J. Mermet, Study of laser ablation of brass materials using inductively coupled plasma atomic emission spectrometric detection, Spectrochimica Acta Part B: Atomic Spectroscopy, 53 (1998) 581-591.

V.G. Galati, Gli scrittori delle Calabrie:(dizionario bio-bibliografico), Vallecchi, 1928.

G. Galbács, N. Jedlinszki, G. Cseh, Z. Galbács, L. Túri, Accurate quantitative analysis of gold alloys using multi-pulse laser induced breakdown spectroscopy and a correlation-based calibration method, Spectrochimica Acta Part B: Atomic Spectroscopy, 63 (2008) 591-597.

P. García-Allende, J. Mirapeix, O. Conde, A. Cobo, J. López-Higuera, Spectral processing technique based on feature selection and artificial neural networks for arc-welding quality monitoring, NDT & E International, 42 (2009) 56-63.

P.B. Garcia-Allende, F. Anabitarte, O.M. Conde, J. Mirapeix, F.J. Madruga, J.M. Lopez-Higuera, Support vector machines in hyperspectral imaging spectroscopy with application to material identification, Proc. SPIE, 2008, pp. 69661V.

R. Gilbert, Stress, paleonutrition, and trace elements, The analysis of prehistoric diets, (1985) 339-358.

K. Gloe, P. Muhl, M. Knothe, Recovery of precious metals from electronic scrap, in particular from waste products of the thick-layer technique, Hydrometallurgy, 25 (1990) 99-110.

Q. Godoi, F.O. Leme, L.C. Trevizan, I.A. Rufini, D. Santos Jr, F.J. Krug, Laser-induced breakdown spectroscopy and chemometrics for classification of toys relying on toxic elements, Spectrochimica Acta Part B: Atomic Spectroscopy, (2011).

R. González, P. Lucena, L. Tobaria, J. Laserna, Standoff LIBS detection of explosive residues behind a barrier, J. Anal. At. Spectrom., 24 (2009) 1123-1126.

I. Gornushkin, M. Mueller, U. Panne, J. Winefordner, Insights into linear and rank correlation for material identification in laser-induced breakdown spectroscopy and other spectral techniques, Applied Spectroscopy, 62 (2008) 542-553.

I. Gornushkin, U. Panne, J. Winefordner, Linear correlation for identification of materials by laser induced breakdown spectroscopy: Improvement via spectral filtering and masking, Spectrochimica Acta Part B: Atomic Spectroscopy, 64 (2009) 1040-1047.

J.L. Gottfried, F.C. De Lucia, C.A. Munson, A.W. Miziolek, Double-pulse standoff laser-induced breakdown spectroscopy for versatile hazardous materials detection, Spectrochimica Acta Part B: Atomic Spectroscopy, 62 (2007) 1405-1411.

H.R. Griem, Spectral line broadening by plasmas, New York, Academic Press, Inc.(Pure and Applied Physics. Volume 39), 1974. 421 p., 1 (1974).

P.R. Griffiths, J.A. De Haseth, Fourier transform infrared spectrometry, John Wiley & Sons, 2007.

R.L. Grob, E.F. Barry, J. Wiley, Modern practice of gas chromatography, Wiley Online Library, 1985.

P.C. Guida, Bronzetti a figura umana: dalle collezioni dei Civici musei di storia ed arte de Trieste, Electa, 1979.

Q. Guo, H. Yu, Y. Xin, X. Li, X. Li, Experimental study on high alloy steel sample by laser-induced breakdown spectroscopy], Guang pu xue yu guang pu fen xi= Guang pu, 30 (2010) 783.

D.W. Hahn, N. Omenetto, Laser-Induced Breakdown Spectroscopy (LIBS), Part II: Review of Instrumental and Methodological Approaches to Material Analysis and Applications to Different Fields, Applied Spectroscopy, 66 (2012) 347-419.

S. Hamzaoui, R. Khleifia, N. Jaïdane, Z. Ben Lakhdar, Quantitative analysis of pathological nails using laser-induced breakdown spectroscopy (LIBS) technique, Lasers in Medical Science, (2011) 1-5.

S.J. Haswell, Atomic absorption spectrometry, Elsevier, 1991.

G. Hernán Sendra, Activity analysis on dynamic speckle patterns (Análisis de actividad en patrones de speckle dinámico), (2009).

K.O. Hill, G. Meltz, Fiber Bragg grating technology fundamentals and overview, Lightwave Technology, Journal of, 15 (1997) 1263-1276.

I.S. Hornsey, A history of beer and brewing, Royal Society of Chemistry, 2003.

A. Hrdlička, L. Prokeš, A. Staňková, K. Novotný, A. Vitešníková, V. Kanický, V. Otruba, J. Kaiser, J. Novotný, R. Malina, Development of a remote laser-induced breakdown spectroscopy system for investigation of calcified tissue samples, Applied optics, 49 (2010) C16-C20.

A. Hrdlicka, L. Zaorálková, M. Galiová, T. Ctvrtnícková, V. Kanický, V. Otruba, K. Novotný, P. Krásenský, J. Kaiser, R. Malina, Correlation of acoustic and optical emission signals produced at 1064 and 532 nm laser-induced breakdown spectroscopy (LIBS) of glazed wall tiles, Spectrochimica Acta Part B: Atomic Spectroscopy, 64 (2009) 74-78.

Y. Iida, Effects of atmosphere on laser vaporization and excitation processes of solid samples, Spectrochimica Acta Part B: Atomic Spectroscopy, 45 (1990) 1353-1367.

J. Izquierdo, I. Montalvo, R. Pérez, V.S. Fuertes, Design optimization of wastewater collection networks by PSO, Computers & Mathematics with Applications, 56 (2008) 777-784.

J.F. James, R. Sternberg, The design of optical spectrometers, London: Chapman and Hall, 1969, 1 (1969).

N. Jedlinszki, G. Galbács, An evaluation of the analytical performance of collinear multi-pulse laser induced breakdown spectroscopy, Microchemical Journal, 97 (2011) 255-263.

W. Johannowsky, M. Merolla, Materiali di età arcaica dalla Campania, G. Macchiaroli, 1983.

I.T. Jolliffe, MyiLibrary, Principal component analysis, Wiley Online Library, 2002.

A. Jurado-López, M. Luque de Castro, Chemometric approach to laser-induced breakdown analysis of gold alloys, Applied Spectroscopy, 57 (2003) 349-352.

E.R. Kaal, M. Kurano, H.G. Janssen, Hyphenation of aqueous liquid chromatography to pyrolysis-gas chromatography and mass spectrometry for the comprehensive characterization of water-soluble polymers, Journal of Chromatography A, 1186 (2008) 222-227.

H.Y. Kang, J.M. Schoenung, Electronic waste recycling: A review of US infrastructure and technology options, Resources, Conservation and Recycling, 45 (2005) 368-400.

M.A. Kasem, R.E. Russo, M.A. Harith, Influence of biological degradation and environmental effects on the interpretation of archeological bone samples with laser-induced breakdown spectroscopy, J. Anal. At. Spectrom., 26 (2011) 1733-1739.

R. Kashyap, Fiber bragg gratings, Academic Pr, 1999.

B. Kearton, Y. Mattley, Laser-induced breakdown spectroscopy: Sparking new applications, Nature Photonics, 2 (2008) 537-540.

J.M. Keller, A Fuzzy^-Nearest Neighbor Algorithm JAMES M. KELLER, MICHAEL R. GRAY, and JAMES A. GIVENS, JR, IEEE Transactions on Systems, Man, and Cybernetics, 15 (1985) 581.

J. Kennedy, R. Eberhart, Particle swarm optimization, IEEE, 1995, pp. 1942-1948 vol. 1944.

W. Koechner, Solid-state laser engineering, Springer Verlag, 2006.

S. Konorov, A. Fedotov, O. Kolevatova, V. Beloglazov, N. Skibina, A. Shcherbakov, E. Wintner, A. Zheltikov, Laser breakdown with millijoule trains of picosecond pulses transmitted through a hollow-core photonic-crystal fiber, Journal of Physics D: Applied Physics, 36 (2003) 1375.

J.M.D. Kowalczyk, J. Perkins, J. Kaneshiro, N. Gaillard, Y. Chang, A. DeAngelis, S.A. Mallory, D. Bates, E. Miller, Measurement of the sodium concentration in CIGS solar cells via laser induced breakdown spectroscopy, IEEE, 2010, pp. 001742-001744.

C.M. Kraay, The Composition of electrum coinage, Archaeometry, 1 (1958) 21-23.

R. Krasniker, V. Bulatov, I. Schechter, Study of matrix effects in laser plasma spectroscopy by shock wave propagation, Spectrochimica Acta Part B: Atomic Spectroscopy, 56 (2001) 609-618.

J. Lancaster, The physics of welding, Physics in Technology, 15 (1984) 73-79.

Y. Langeron, M. Doussot, D. Hewson, J. Duchêne, Classifying NIR spectra of textile products with kernel methods, Engineering Applications of Artificial Intelligence, 20 (2007) 415-427.

J. Laserna, S. Palanco, Spectral analysis of the acoustic emission of laser-produced plasmas, Optical Society of America, 2002.

V. Lazic, F. Colao, R. Fantoni, V. Spizzicchino, Recognition of archeological materials underwater by laser induced breakdown spectroscopy, Spectrochimica Acta Part B: Atomic Spectroscopy, 60 (2005) 1014-1024.

V. Lazic, A. Palucci, S. Jovicevic, M. Carapanese, C. Poggi, E. Buono, Detection of explosives at trace levels by laser-induced breakdown spectroscopy (LIBS), Proc. SPIE, 2010, pp. 76650V.

B. Le Drogoff, J. Margot, M. Chaker, M. Sabsabi, O. Barthelemy, T. Johnston, S. Laville, F. Vidal, Y. Von Kaenel, Temporal characterization of femtosecond laser pulses induced plasma for spectrochemical analysis of aluminum alloys, Spectrochimica Acta Part B: Atomic Spectroscopy, 56 (2001) 987-1002.

W.B. Lee, J. Wu, Y.I. Lee, J. Sneddon, Recent applications of laser-induced breakdown spectrometry: A review of material approaches, Applied Spectroscopy Reviews, 39 (2004) 27-97.

Y.I. Lee, S.P. Sawan, T.L. Thiem, Y.Y. Teng, J. Sneddon, Interaction of a laser beam with metals. Part II: Space-resolved studies of laser-ablated plasma emission, Applied Spectroscopy, 46 (1992) 436-441.

H. Lindner, K.H. Loper, D.W. Hahn, K. Niemax, The influence of laser-particle interaction in laser induced breakdown spectroscopy and laser ablation inductively coupled plasma spectrometry, Spectrochimica Acta Part B: Atomic Spectroscopy, (2011).

R. Linke, M. Schreiner, G. Demortier, M. Alram, Determination of the provenance of medieval silver coins: potential and limitations of x-ray analysis using photons, electrons or protons, X-Ray Spectrometry, 32 (2003) 373-380.

X.Y. Liu, W.J. Zhang, Recent developments in biomedicine fields for laser induced breakdown spectroscopy, Journal of Biomedical Science, 1 (2008).

J.M López-higuera, F. Anabitarte, A. Cobo. La Fotónica en arqueología: su aplicación a la caracterización de pigmentos y materiales. Invited conference on summer courses of University of Cantabria. Ramales de la Victoria, 1st of august 2012

J.M. López-Higuera, L. Rodriguez Cobo, A. Quintela Incera, A. Cobo, Fiber Optic Sensors in Structural Health Monitoring, Journal of Lightwave Technology, 29 (2011) 587-608.

C. Lopez-Moreno, S. Palanco, J.J. Laserna, F. DeLucia Jr, A.W. Miziolek, J. Rose, R.A. Walters, A.I. Whitehouse, Test of a stand-off laser-induced breakdown spectroscopy sensor for the detection of explosive residues on solid surfaces, J. Anal. At. Spectrom., 21 (2005) 55-60.

M. Losada, I. Garcés, J. Mateo, I. Salinas, J. Lou, J. Zubia, Mode coupling contribution to radiation losses in curvatures for high and low numerical aperture plastic optical fibers, Lightwave Technology, Journal of, 20 (2002) 1160-1164.

J. Madejova, FTIR techniques in clay mineral studies, Vibrational Spectroscopy, 31 (2003) 1-10.

G. Maetzke, La collezione del Museo Archeologico Nazionale di Chiusi', Studi Etruschi, 25 (1957) 489-523.

X. Mao, W.T. Chan, M. Caetano, M.A. Shannon, R.E. Russo, Preferential vaporization and plasma shielding during nano-second laser ablation, Applied surface science, 96 (1996) 126-130.

X. Mao, A. Ciocan, O. Borisov, R. Russo, Laser ablation processes investigated using inductively coupled plasma-atomic emission spectroscopy (ICP-AES), Applied surface science, 127 (1998) 262-268.

P. Maravelaki, V. Zafiropulos, V. Kilikoglou, M. Kalaitzaki, C. Fotakis, Laser-induced breakdown spectroscopy as a diagnostic technique for the laser cleaning of marble, Spectrochimica Acta Part B: Atomic Spectroscopy, 52 (1997) 41-53.

B.J. Marquardt, S.R. Goode, S.M. Angel, In situ determination of lead in paint by laser-induced breakdown spectroscopy using a fiber-optic probe, Analytical Chemistry, 68 (1996) 977-981.

A. Martin, S.A. Harbison, An introduction to radiation protection, Environmental Safety Group, Associated Nuclear Services, Epsom, 1986.

P.E. McGovern, D.L. Glusker, L.J. Exner, M.M. Voigt, Neolithic resinated wine, Nature, 381 (1996) 480-481.

K. Melessanaki, M. Mateo, S.C. Ferrence, P.P. Betancourt, D. Anglos, The application of LIBS for the analysis of archaeological ceramic and metal artifacts, Applied surface science, 197 (2002) 156-163.

M. Minoja, Il Museo Archeologico dell'Antica Capua, Napoli, 1995, pp. 27-29.

J. Mirapeix, A. Cobo, D. González, J. López-Higuera, Plasma spectroscopy analysis technique based on optimization algorithms and spectral synthesis for arc-welding quality assurance, Optics Express, 15 (2007) 1884-1897.

A.W. Miziolek, V. Palleschi, I. Schechter, Laser-induced breakdown spectroscopy (LIBS): fundamentals and applications, Cambridge Univ Pr, 2006.

A. Montaser, D. Golightly, Inductively coupled plasmas in analytical atomic spectrometry, (1987).

R.A. Multari, D.A. Cremers, M.L. Bostian, Use of laser-induced breakdown spectroscopy for the differentiation of pathogens and viruses on substrates, Applied optics, 51 (2012) B57-B64.

R.A. Multari, L.E. Foster, D.A. Cremers, M.J. Ferris, Effect of sampling geometry on elemental emissions in laser-induced breakdown spectroscopy, Applied Spectroscopy, 50 (1996) 1483-1499.

T.W. Murray, J.W. Wagner, Laser generation of acoustic waves in the ablative regime, Journal of applied physics, 85 (1999) 2031.

S. Nakamura, Y. Ito, T. Nakabayashi, M. Watanabe, T. Inoue, A. Matsunawa, Analysis of optical and acoustic emissions during CO 2 laser welding of a stainless steel, ICALEO'97: Laser Materials Processing., 83 (1997).

P.S. Nayak, B. Singh, Instrumental characterization of clay by XRF, XRD and FTIR, Bulletin of Materials Science, 30 (2007) 235-238.

B.K. Nelson, M.J. DeNiro, M.J. Schoeninger, D.J. De Paolo, P.E. Hare, Effects of diagenesis on strontium, carbon, nitrogen and oxygen concentration and isotopic composition of bone, Geochimica et Cosmochimica Acta, 50 (1986) 1941-1949.

C.M. Nielsen-Marsh, R.E.M. Hedges, Patterns of diagenesis in bone I: The effects of site environments, Journal of Archaeological Science, 27 (2000) 1139-1150.

K. Norrish, B. Chappell, X-ray fluorescence spectrometry, Physical methods in determinative mineralogy, (1977) 201-272.

J.O. Nriagu, Cupellation: The oldest quantitative chemical process, Journal of chemical education, 62 (1985) 668-674.

I. Osticioli, N.F.C. Mendes, S. Porcinai, A. Cagnini, E. Castellucci, Spectroscopic analysis of works of art using a single LIBS and pulsed Raman setup, Analytical and Bioanalytical Chemistry, 394 (2009) 1033-1041.

A. Othonos, Fiber bragg gratings, Review of Scientific Instruments, 68 (1997) 4309.

S. Palanco, J. Laserna, Spectral analysis of the acoustic emission of laser-produced plasmas, Applied optics, 42 (2003) 6078-6084.

G. Pianu, Il bucchero, Edipuglia srl, 2000.

C.F. Poole, S.K. Poole, Chromatography today, Elsevier Science Publishers, 1991.

A. Prieto, M. Avella, M. González, J. Jiménez, F. Romero, R. De Pablo, C. Górriz, C. Sanz, Analysis of the Residuals in Grave Goods From the Vaccaea Era at the Necropolis of “Las Ruedas” in Pintia, Spectroscopy Letters, 45 (2012) 141-145.

M. provinciale sannitico di Campobasso, A. Di Niro, Piccoli bronzi figurati nel museo di Campobasso, P. Laveglia, 1978.

E.W. Psenner, G. Ciurletti, I bronzetti figurati antichi del Trentino, Provincia Autonoma, Assessorato alle attività culturali, 1983.

P. Pudil, J. Novovicová, J. Kittler, Floating search methods in feature selection, Pattern recognition letters, 15 (1994) 1119-1125.

A. Rai, F. Yueh, J. Singh, Laser-induced breakdown spectroscopy of molten aluminum alloy, Applied optics, 42 (2003) 2078-2084.

A.K. Rai, H. Zhang, F.Y. Yueh, J.P. Singh, A. Weisburg, Parametric study of a fiber-optic laser-induced breakdown spectroscopy probe for analysis of aluminum alloys, Spectrochimica Acta Part B: Atomic Spectroscopy, 56 (2001) 2371-2383.

N.K. Rai, A. Rai, LIBS--an efficient approach for the determination of Cr in industrial wastewater, Journal of hazardous materials, 150 (2008) 835-838.

S. Rai, A.K. Rai, Characterization of organic materials by LIBS for exploration of correlation between molecular and elemental LIBS signals, AIP Advances, 1 (2011) 042103-042103-042111.

Y. Ralchenko, NIST atomic spectra database, Memorie della Societa Astronomica Italiana Supplementi, 8 (2005) 96.

S.J. Rehse, Q. Mohaidat, S. Palchaudhuri, Laser-Induced Breakdown Spectroscopy (LIBS) for the Rapid Field Identification and Classification of Pathogenic Bacteria, Optical Society of America, 2010.

C. Riedo, D. Scalarone, O. Chiantore, Advances in identification of plant gums in cultural heritage by thermally assisted hydrolysis and methylation, Analytical and Bioanalytical Chemistry, 396 (2010) 1559-1569.

H. Rolland, Bronzes antiques de Haute Provence, Recherche, 67 (1965) 02.

N. Roussopoulos, S. Kelley, F. Vincent, Nearest neighbor queries, ACM, 1995, pp. 71-79.

Z. Rui, L. Zhong-Cheng, H. Bing, Z. Hong-Chao, X. Rong-Qing, L. Jian, N. Xiao-Wu, Mechanism of laser-induced plasma shock wave evolution in air, Chinese Physics B, 18 (2009) 1877.

E. Runge, Spectrochemical analysis using a pulsed laser source, Spectrochimica Acta, 20 (1964) 733-736.

R. Russo, X. Mao, O. Borisov, H. Liu, Influence of wavelength on fractionation in laser ablation ICP-MS, J. Anal. At. Spectrom., 15 (2000) 1115-1120.

R.E. Russo, X. Mao, H. Liu, J. Gonzalez, S.S. Mao, Laser ablation in analytical chemistry-a review, Talanta, 57 (2002) 425-451.

B. Sallé, D.A. Cremers, S. Maurice, R.C. Wiens, Laser-induced breakdown spectroscopy for space exploration applications: Influence of the ambient pressure on the calibration curves prepared from soil and clay samples, Spectrochimica Acta Part B: Atomic Spectroscopy, 60 (2005) 479-490.

B. Salle, D.A. Cremers, S. Maurice, R.C. Wiens, P. Fichet, Evaluation of a compact spectrograph for in-situ and stand-off laser-induced breakdown spectroscopy analyses of geological samples on Mars missions, Spectrochimica Acta Part B: Atomic Spectroscopy, 60 (2005) 805-815.

A. Sarkar, V.M. Telmore, D. Alamelu, S.K. Aggarwal, Laser induced breakdown spectroscopic quantification of platinum group metals in simulated high level nuclear waste, J. Anal. At. Spectrom., 24 (2009) 1545-1550.

R. Sattmann, V. Sturm, R. Noll, Laser-induced breakdown spectroscopy of steel samples using multiple Q-switch Nd: YAG laser pulses, Journal of Physics D: Applied Physics, 28 (1995) 2181.

J. Scaffidi, W. Pearman, J.C. Carter, B.W. Colston, S.M. Angel, Temporal dependence of the enhancement of material removal in femtosecond-nanosecond dual-pulse laser-induced breakdown spectroscopy, Applied optics, 43 (2004) 6492-6499.

R.H. Scott, V.A. Fassel, R.N. Kniseley, D.E. Nixon, Inductively coupled plasma-optical emission analytical spectrometry, Analytical Chemistry, 46 (1974) 75-80.

W. Sdorra, K. Niemax, Basic investigations for laser microanalysis: III. Application of different buffer gases for laser-produced sample plumes, Microchimica Acta, 107 (1992) 319-327.

L. Sedov, Similarity methods and dimensional analysis in mechanics, Moscow Izdatel Nauka, 1 (1977).

A. Semerok, C. Dutouquet, Ultrashort double pulse laser ablation of metals, Thin Solid Films, 453 (2004) 501-505.

Y. Shi, R.C. Eberhart, Empirical study of particle swarm optimization, IEEE, 1999.

A. Sillen, M. Kavanagh, Strontium and paleodietary research: a review, American Journal of Physical Anthropology, 25 (1982) 67-90.

J.P. Singh, Laser-induced breakdown spectroscopy, Elsevier Science, 2007.

J.B. Sirven, B. Bousquet, L. Canioni, L. Sarger, S. Tellier, M. Potin-Gautier, I.L. Hecho, Qualitative and quantitative investigation of chromium-polluted soils by laser-induced breakdown spectroscopy combined with neural networks analysis, Analytical and Bioanalytical Chemistry, 385 (2006) 256-262.

F. Sorrentino, G. Carelli, F. Francesconi, M. Francesconi, P. Marsili, G. Cristoforetti, S. Legnaioli, V. Palleschi, E. Tognoni, Fast analysis of complex metallic alloys by double-pulse time-integrated Laser-Induced Breakdown Spectroscopy, Spectrochimica Acta Part B: Atomic Spectroscopy, 64 (2009) 1068-1072.

W. Spillman Jr, B. Kline, L. Maurice, P. Fuhr, Statistical-mode sensor for fiber optic vibration sensing uses, Applied optics, 28 (1989) 3166-3176.

R. Srinivasan, B. Braren, Ultraviolet laser ablation of organic polymers, Chemical Reviews, 89 (1989) 1303-1316.

R. Srinivasan, B. Braren, R. Dreyfus, L. Hadel, D. Seeger, Mechanism of the ultraviolet laser ablation of polymethyl methacrylate at 193 and 248 nm: laser-induced fluorescence analysis, chemical analysis, and doping studies, JOSA B, 3 (1986) 785-791.

C. Stauter, P. Gerard, J. Fontaine, T. Engel, Laser ablation acoustical monitoring, Applied surface science, 109 (1997) 174-178.

L. St-Onge, V. Detalle, M. Sabsabi, Enhanced laser-induced breakdown spectroscopy using the combination of fourth-harmonic and fundamental Nd: YAG laser pulses, Spectrochimica Acta Part B: Atomic Spectroscopy, 57 (2002) 121-135.

L. St-Onge, E. Kwong, M. Sabsabi, E. Vadas, Quantitative analysis of pharmaceutical products by laser-induced breakdown spectroscopy, Spectrochimica Acta Part B: Atomic Spectroscopy, 57 (2002) 1131-1140.

L. St-Onge, M. Sabsabi, P. Cielo, Analysis of solids using laser-induced plasma spectroscopy in double-pulse mode, Spectrochimica Acta Part B: Atomic Spectroscopy, 53 (1998) 407-415.

D.N. Stratis, K.L. Eland, S.M. Angel, Enhancement of aluminum, titanium, and iron in glass using pre-ablation spark dual-pulse LIBS, Applied Spectroscopy, 54 (2000) 1719-1726.

D.N. Stratis, K.L. Eland, S.M. Angel, Effect of pulse delay time on a pre-ablation dual-pulse LIBS plasma, Applied Spectroscopy, 55 (2001) 1297-1303.

B. Stuart, Infrared spectroscopy, Wiley Online Library, 2004.

V. Sturm, L. Peter, R. Noll, Steel analysis with laser-induced breakdown spectrometry in the vacuum ultraviolet, Applied Spectroscopy, 54 (2000) 1275-1278.

J.A.K. Suykens, J. Vandewalle, Least squares support vector machine classifiers, Neural processing letters, 9 (1999) 293-300.

E.A. Sydenham, The Coinage of the Roman Republic, New York, 1952.

C. Tameze, R. Vincelette, N. Melikechi, V. Zeljkovic, E. Izquierdo, Empirical analysis of LIBS images for ovarian cancer detection, IEEE, 2007, pp. 76-76.

G.A. Theriault, S. Bodensteiner, S.H. Lieberman, A real-time fiber-optic LIBS probe for the in situ delineation of metals in soils, Field Analytical Chemistry & Technology, 2 (1998) 117-125.

E. Tognoni, G. Cristoforetti, S. Legnaioli, V. Palleschi, Calibration-free laser-induced breakdown spectroscopy: state of the art, Spectrochimica Acta Part B: Atomic Spectroscopy, 65 (2010) 1-14.

E. Tognoni, G. Cristoforetti, S. Legnaioli, V. Palleschi, A. Salvetti, M. Mueller, U. Panne, I. Gornushkin, A numerical study of expected accuracy and precision in Calibration-Free Laser-Induced Breakdown Spectroscopy in the assumption of ideal analytical plasma, Spectrochimica Acta Part B: Atomic Spectroscopy, 62 (2007) 1287-1302.

L. Torrisi, F. Caridi, L. Giuffrida, A. Torrisi, G. Mondio, T. Serafino, M. Caltabiano, E. Castrizio, E. Paniz, A. Salici, LAMQS analysis applied to ancient Egyptian bronze coins, Nuclear Instruments and Methods in Physics Research Section B: Beam Interactions with Materials and Atoms, 268 (2010) 1657-1664.

L.C. Trevizan, D. Santos, R.E. Samad, N.D. Vieira, L.C. Nunes, I.A. Rufini, F.J. Krug, Evaluation of laser induced breakdown spectroscopy for the determination of micronutrients in plant materials, Spectrochimica Acta Part B: Atomic Spectroscopy, 64 (2009) 369-377.

J. Uebbing, J. Brust, W. Sdorra, F. Leis, K. Niemax, Reheating of a laser-produced plasma by a second pulse laser, Applied Spectroscopy, 45 (1991) 1419-1423.

J. Vadillo, J. Fernandez Romero, C. Rodriguez, J. Laserna, Effect of plasma shielding on laser ablation rate of pure metals at reduced pressure, Surface and interface analysis, 27 (1999) 1009-1015.

D. Van de Meent, S.C. Brown, R.P. Philp, B.R.T. Simoneit, Pyrolysis-high resolution gas chromatography and pyrolysis gas chromatography-mass spectrometry of kerogens and kerogen precursors, Geochimica et Cosmochimica Acta, 44 (1980) 999-1013.

V.N. Vapnik, The nature of statistical learning theory, Springer Verlag, 2000.

D.R. Walker, The metrology of the Roman silver coinage, British Archaeological Reports, 1976.

R.H. Wang, B. Fang, Emotion Fusion Recognition for Intelligent Surveillance with PSO-CSVM, Advanced Materials Research, 225 (2011) 51-56.

K. Watkins, C. Curran, J.M. Lee, Two new mechanisms for laser cleaning using Nd: YAG sources, Journal of cultural Heritage, 4 (2003) 59-64.

A. Whitehouse, J. Young, I. Botheroyd, S. Lawson, C. Evans, J. Wright, Remote material analysis of nuclear power station steam generator tubes by laser-induced breakdown spectroscopy, Spectrochimica Acta Part B: Atomic Spectroscopy, 56 (2001) 821-830.

J.D. Winefordner, I.B. Gornushkin, T. Correll, E. Gibb, B.W. Smith, N. Omenetto, Comparing several atomic spectrometric methods to the super stars: special emphasis on laser induced breakdown spectrometry, LIBS, a future super star, J. Anal. At. Spectrom., 19 (2004) 1061-1083.

R. Wisbrun, I. Schechter, R. Niessner, H. Schroeder, K.L. Kompa, Detector for trace elemental analysis of solid environmental samples by laser plasma spectroscopy, Analytical Chemistry, 66 (1994) 2964-2975.

S. Wold, K. Esbensen, P. Geladi, Principal component analysis, Chemometrics and intelligent laboratory systems, 2 (1987) 37-52.

B. Yegnanarayana, Artificial neural networks, PHI Learning Pvt. Ltd., 2004.

H. Yu, J. Yang, A direct LDA algorithm for high-dimensional data-with application to face recognition, Pattern recognition, 34 (2001) 2067.

Y.B. Zel'Dovich, Y.P. Raizer, Physics of shock waves and high-temperature hydrodynamic phenomena, Dover Pubns, 2002.

X. Zeng, X. Mao, R. Greif, R. Russo, Experimental investigation of ablation efficiency and plasma expansion during femtosecond and nanosecond laser ablation of silicon, Applied Physics A: Materials Science & Processing, 80 (2005) 237-241.

R. Zhang, J. Ma, An improved SVM method P-SVM for classification of remotely sensed data, International Journal of Remote Sensing, 29 (2008) 6029-6036.

S. Zhen-gang, L. Qin-zi, Edge detection for Medical Image based on PSO Algorithm, IEEE, 2010, pp. 84-87.

G. Zhitao, Y. Jinli, G. Junhua, Design and research of RFID microstrip antenna based on improved PSO neural networks, IEEE, 2010, pp. 251-254.

N.B. Zorov, A.A. Gorbatenko, T.A. Labutin, A.M. Popov, A review of normalization techniques in analytical atomic spectrometry with laser sampling: From single to multivariate correction, Spectrochimica Acta Part B: Atomic Spectroscopy, 65 (2010) 642-657.

List of publications

Close related with the PhD work

Journals

1. F. Anabitarte, A. Cobo, J.M. López-Higuera; 'Laser Induced Breakdown Spectroscopy; fundamentals, applications and challenges'; ISRN Spectroscopy; ISSN: 2090-8776; accepted on 01/10/2012.

2. A. Foresta, F. Anabitarte García, S. Legnaioli, G. Lorenzetti, D. Diaz Pace, L. Pardini, V. Palleschi; 'Análisis LIBS de doce estatuillas de bronce expuestas en el Museo Arqueológico Nacional de Crotona'; Óptica Pura y Aplicada, Vol.45, Nº 3, pp. 277-286; ISSN: 2171-8814; 01/09/2012.

3. L. Pardini, A. El Hassan, M. Ferretti, A. Foresta, S. Legnaioli, G. G. Lorenzetti, E. Nebbia, F. Catalli, M.A. Harith, D. Diaz Pace, F. Anabitarte Garcia, M. Scuotto, V. Palleschi; 'X-Ray Fluorescence and Laser-Induced Breakdown Spectroscopy analysis of Roman silver denarii'; Spectrochimica Acta Part B: Atomic Spectroscopy, Vol.74, pp. 156-161; ISSN: 0584-8547; 01/09/2012.

4. F. Anabitarte, J. Mirapeix, O.M. Conde, J.M. López-Higuera, A. Cobo; 'Sensor for the detection of protective coating traces on boron steel with Aluminium-Silicon covering by means of laser-induced breakdown spectroscopy and support vector machines'; IEEE Sensors Journal, Vol.12, Nº 1, pp. 64-70; ISSN: 1530-437X; 01/06/2012.

5. S. Legnaioli, G. Lorenzetti, L. Pardini, V. Palleschi, D.M. Diaz Pace, F. Anabitarte Garcia, R. Grassi, F. Sorrentino, G. Carelli, M. Francesconi, F. Francesconi, R. Borgogni; 'Laser-induced breakdown spectroscopy application to control of the process of precious metal recovery and recycling'; Spectrochimica Acta Part B: Atomic Spectroscopy, Vol.71, pp. 123-126; ISSN:0584-8547; 01/06/2012.

6. S. Legnaioli, F. Anabitarte Garcia, A. Andreotti, E. Bramanti, D. Diaz Pace, S. Formola, G. Lorenzetti, M. Martini, L. Pardini, E. Ribechini, E. Sibilia, R. Spiniello, V. Palleschi; 'Multi-technique study of a ceramic archaeological artifact and its content'; Spectrochimica acta part A: Molecular and Biomolecular Spectroscopy. ; ISSN: 1386-1425; accepted on 03/04/2012.

International conferences

7. F. Anabitarte, L. Rodríguez-Cobo, C. Galíndez, A. Ullan, A. Cobo; 'Focal beam position detection in a laser Induced Breakdown Spectroscopy system by using a Fiber Bragg Grating sensor'; OFS'22 (22nd International Conference on Optical Fiber Sensors), Beijing, China; 15/10/2012.

8. Francisco Anabitarte, Luis Rodriguez-Cobo, Mauro Lomer, Jesus Mirapeix, Jose Miguel Lopez-Higuera, Adolfo Cobo; 'Laser Induced Breakdown Spectroscopy light collector based on coiled plastic optical fiber'; POF 2011 (The 20th International Conference on Plastic Optical Fibers), Bilbao, Spain, pp. 315-319; 14/09/2011.

9. Francisco Anabitarte, Jesus Mirapeix, Olga M. Conde, Ana M. Cubillas, Luis Rodriguez-Cobo, Carlos Galindez and Adolfo Cobo; 'Automatic classification of steel plates based on Laser Induced Breakdown Spectroscopy and Support Vector Machines'; EWOFS'10, Oporto, Portugal, pp. 765347-1/765347-4; ISBN: 9780819480835; ISSN: 0277-786X; 08/09/2010.

National conferences

10. Luis Rodriguez-Cobo, Francisco Anabitarte, Jesús Mirapeix, José Miguel López-Higuera, Adolfo Cobo; 'Acoustic Detection of laser-induced plasma emission by means of a fiber-Bragg grating sensor'; OPTOEL'11 (VII Reunión Española de Optoelectrónica), Santander; ISBN: 978-84-86116-31-6; 29/06/2011.

Other contributions

Other contributions in journals

11. Olga M. Conde, Lucía Uriarte, Pilar B. García-Allende, Ana M. Cubillas, F. Anabitarte, Jose M. Lopez-Higuera; 'Spectral and Optimized Marks for Qualitative Material Discrimination'; IEEE Sensors Journal, Vol.12, Nº 1, pp. 230-236; ISSN: 1530-437X; 01/01/2012

12. J. Mirapeix, R. Ruiz-Lombera, J.J. Valdiande, L. Rodriguez-Cobo, F. Anabitarte and A. Cobo; 'Defect detection with CCD-spectrometer and photodiode-based arc-welding monitoring systems'; Journal of Materials Processing Technology, Vol 211, pp. 2132-2139; ISSN: 0924-0136; 27/07/2011.

Other contributions in international conferences

13. C.A. Galíndez, L. Rodriguez-Cobo, F. Anabitarte, J.M. Lopez-Higuera; 'Integral temperature hybrid laser sensor'; OFS'22 (22nd International Conference on Optical Fiber Sensors), Beijing, China; 15/10/2012.

14. Olga M. Conde, Lucía Uriarte, Pilar B. García-Allende, Ana M. Cubillas, F. Anabitarte, Jose M. Lopez-Higuera; 'Spectral marks for qualitative discriminant analysis'; EWOFS'10, Oporto, Portugal, pp. 76531J-1/76531J-4; ISBN: 9780819480835; ISSN: 0277-786X; 08/09/2010.

15. M.A. Quintela, A. Quintela, N. Becue, J.M. Lazaro, F. Anabitarte J.M. Lopez-Higuera; 'Tunable fiber laser using concatenated non-adiabatic single-mode fiber tapers'; OFS'19 (19th International Conference on Optical fiber Sensors), Perth, Western Australia, pp. 700453-1/700453-4; ISBN: 978-0-8194-7205; ISSN: 0277-786X; 14/04/2008.

16. Pilar Beatriz García-Allende, Francisco Anabitarte, Olga Maria Conde, Jesus Mirapeix, Francisco J. Madruga, Jose Miguel Lopez-Higuera; 'Support Vector Machines in Hyperspectral imaging spectroscopy with application to material identification'; Defense and Security 2008: Sensor Data Exploitation, Target

Recognition, and Information Fusion, Data Mining, and Information Networks Security Technologies, Orlando, Florida, USA, pp. 69661V-1 / 69661V-11; ISBN: 978-0-8194-7176-5; ISSN: 0277-786X; 17/03/2008.

17. Pilar Beatriz Garcia-Allende, Francisco Anabitarte, Olga Maria Conde, Francisco J. Madruga, Mauro Lomer, Jose Miguel Lopez-Higuera; 'Infrared Imaging spectroscopic system based on a PGP spectrograph and a monochrome infrared camera'; Defense and Security 2008: Infrared, Tactical, and Laser Sensors and Systems, Orlando, Florida, USA, pp. 694118-1 / 694118-10; ISBN: 978-0-8194-7175-8; ISSN: 0277-786X; 17/03/2008.

Other contributions on national conferences

18. Jesús Mirapeix, Pilar Beatriz García-Allende, Olga M. Conde, Francisco Anabitarte, Luis Rodríguez-Cobo, José Miguel López-Higuera, Adolfo Cobo; 'Evaluación de la calidad de soldadura mediante algoritmos de selección de características y de optimización'; OPTOEL'11 (VII Reunión Española de Optoelectrónica), Santander; ISBN: 978-84-86116-31-6; 29/06/2011.

19. Jesús Mirapeix, Rubén Ruiz, José J. Valdiande, Luis Rodríguez-Cobo, F. Anabitarte, J.M. López-Higuera, A. Cobo; 'Estudio comparativo entre sistemas de monitorización on-line basados en espectrómetros y fotodiodos para la detección en línea de defectos de soldadura'; OPTOEL'11 (VII Reunión Española de Optoelectrónica), Santander; ISBN: 978-84-86116-31-6; 29/06/2011.

Submitted contributions

1. Francisco Anabitarte, Luis Rodríguez-Cobo, José-Miguel López-Higuera and Adolfo Cobo. ‘Normalization of LIBS spectra using a plastic optical fiber light collector and acoustic sensor device’. Submitted to Applied Optics.

2. F. Anabitarte, L. Rodriguez-Cobo, A. Cobo and J. M. Lopez-Higuera. ‘Laser Induced Breakdown Spectroscopy induced shockwave detection by means of a Fiber Bragg Grating Transducer’. Submitted to Spectrochimica Acta Part B: Atomic Spectroscopy.

Part V

Resumen, objetivos y conclusiones

Este apartado contiene un resumen del trabajo llevado a cabo en esta Tesis, expone los objetivos que se pretenden alcanzar y finalmente muestra las conclusiones que se han alcanzado al analizar el trabajo llevado a cabo

UNIVERSIDAD DE CANTABRIA

ESCUELA TÉCNICA SUPERIOR DE INGENIEROS INDUSTRIALES Y DE TELECOMUNICACIÓN

TESIS DOCTORAL

Desarrollo de nuevos dispositivos y técnicas para espectroscopía inducida por láser

Autor: **FRANCISCO ANABITARTE GARCÍA**
Director: **JOSÉ MIGUEL LÓPEZ HIGUERA**
ADOLFO COBO GARCÍA

SANTANDER, 2012

Resumen y objetivos

La interacción entre luz y materia puede aportar importante información sobre la naturaleza de esta materia. La espectroscopía es la ciencia que analiza el contenido espectral de la luz después de dicha interacción, y puede aportar una importante información para la caracterización de un amplio rango de materiales diferentes en diversos estados.

Laser Induced Breakdown Spectroscopy (LIBS) es un tipo de espectroscopía laser dentro del amplio abanico que abarca este tipo de técnicas. LIBS usa un pulso laser de corta duración y alta energía para vaporizar e ionizar una pequeña cantidad de la muestra, creando un plasma formado por este material ablacionado. Este gas ionizado emite luz durante su periodo de vida y la luz emitida durante el proceso de enfriamiento contiene las características espectrales de todos los elementos químicos que componen la muestra, permitiendo su identificación.

LIBS permite trabajar con muestras en cualquier estado (sólidos, líquidos o gases) sin preparación de la muestra o con una preparación muy sencilla y la detección de todos los elementos químicos es posible, así como su análisis cuantitativo, todo ello con un análisis rápido que proporciona incluso la capacidad de análisis in-situ. LIBS ablaciona la muestra, pero el cráter generado tiene solo unas pocas micras de diámetro, por lo que se considera una técnica microdestructiva con capacidad de analizar muestras valiosas sin dañarlas. Estas características y los desarrollos de todos los dispositivos que componen un sistema LIBS explica el creciente interés del mundo científico e industrial en LIBS, a pesar de que los componentes del sistema son todavía caros y que otras técnicas ofrecen mejores límites de detección y un análisis cuantitativo más preciso.

El presente trabajo no pretende incluir un análisis exhaustivo sobre los procesos físicos relacionados con esta técnica espectral. De hecho, este trabajo emplea los conocimientos ya adquiridos en LIBS durante su desarrollo para unir este campo con otros diferentes, como pueden ser los sensores basados en fibra óptica o los algoritmos de clasificación. Además de esta unión entre diferentes campos de

investigación, LIBS será empleado en diferentes aplicaciones reales, en ámbitos tan diferentes como la clasificación de aceros industriales, la detección de metales preciosos en residuos industriales o el análisis de muestras arqueológicas de diferente índole. Concretamente, los objetivos de esta tesis son los siguientes.

1. Diseñar y desarrollar nuevos sensores basados en fibra óptica. Estos sensores se emplearán para medir la onda de choque generada por el plasma en su proceso de expansión. Estos sensores estarán basados en diferentes tecnologías como los Fiber Bragg Gratings (FBG) o emplearán efectos como la interferometría speckle en fibra óptica. Además de esto se diseñará un sensor híbrido capaz de detectar y cuantificar la energía de la onda de choque y capturar la luz del plasma al mismo tiempo. Esta energía de la onda de choque aporta información sobre el proceso de expansión del plasma y sus características y puede ser útil para normalizar la emisión del plasma y mejorar el análisis cuantitativo. Otro sistema que será desarrollado pretende medir la distancia entre la lente de focalización del láser y la muestra. Este parámetro varía la energía de la onda de choque, y por tanto este tipo de sensores puede cuantificar esta distancia y corregir errores de focalización.

2. Aplicar diferentes algoritmos a espectros LIBS. Un grupo de algoritmos serán clasificadores que permiten distinguir entre diferentes materiales empleando los espectros generados por un sistema LIBS sin requerir ningún tipo de análisis ni cualitativo ni cuantitativo de la muestra. Esto permite eliminar la indeterminación debida a las imprecisiones de los sistemas LIBS para generar análisis cuantitativos de precisión. El segundo grupo de algoritmos supone un nuevo avance en el análisis semi-cuantitativo. Un algoritmo basado en Particle Swarm Optimization (PSO) será empleado para llevar a cabo un análisis semi-cuantitativo de un amplio rango de muestras diferentes.

3. Emplear LIBS para aplicaciones reales. LIBS será empleado para aplicaciones relacionadas con dos campos; la arqueología y la industria. Este trabajo expone propuestas para detectar metales preciosos en residuos industriales o para analizar diferentes muestras arqueológicas, todo ello basado en sistemas LIBS.

Conclusiones

Los capítulos de esta Tesis has descrito los trabajos llevados a cabo durante este periodo, revisando los resultados obtenidos y discutiéndolos. Estos trabajos están relacionados con los objetivos expuestos anteriormente.

El primero de estos objetivos se centra en la detección de la onda de choque generada por la expansión del plasma empleando dispositivos basados en Fibra Óptica. El capítulo 4 de este documento está relacionado con este objetivo. La primera parte de este capítulo ha mostrado dispositivos basados en FBG's para llevar a cabo esta detección. Este transductor ha demostrado su capacidad para detectar y cuantificar la energía de esta onda de choque y su rendimiento ha sido comparado con el de un micrófono estándar, un dispositivo empleado anteriormente para este propósito. Además el dispositivo ha demostrado su utilidad para la detección de errores de focalización del láser sobre la superficie de la muestra.

La segunda parte de este capítulo presenta un transductor basado en fibra óptica de plástico enrollada, que emplea interferometría speckle para cuantificar la energía de la onda de choque y capturar la emisión luminosa del plasma debido a su forma, todo ello al mismo tiempo. La medida de la energía de la onda de choque ha sido empleada además para normalizar el espectro luminoso adquirido con el objeto de mejorar un posterior análisis cuantitativo.

El segundo objetivo de esta Tesis, el empleo de algoritmos para el procesado automático de espectros LIBS, está desarrollado en el capítulo 5 del presente documento. Por una parte un algoritmo basado en Análisis de Componentes Principales (PCA), que permite eliminar la información redundante de los espectros LIBS, ha sido empleado para datar un conjunto de estatuas de bronce, obteniendo una gran correlación con el análisis tipológico y estilístico llevado a cabo previamente. Este uso de PCA puede evitar llevar a cabo un análisis cuantitativo y cualitativo, ambos más laboriosos y complejos, obteniendo buenos resultados. La segunda parte de este capítulo aplica un algoritmo de clasificación basado en Máquinas de Vectores Soporte (SVM) para la detección de impurezas en aceros industriales. En este caso los aceros industriales analizados son almacenados con

una capa protectora antioxidante compuesta de aluminio y silicio que debe ser eliminada antes de soldar diferentes láminas para evitar soldaduras frágiles. Este clasificador ha permitido la detección de estas impurezas con un rendimiento notable, empleando los espectros LIBS directamente y evitando un análisis cuantitativo o cualitativo. Esto conlleva que sea una herramienta rápida que permite detectar las impurezas en tiempo real, algo importante para este tipo de aplicación.

La última parte de este capítulo describe una nueva herramienta para el análisis cuantitativo basado en LIBS. El algoritmo presentado está basado en PSO y permite un análisis semi-cuantitativo que ha sido probado con diferentes muestras. Todo esto es el primer paso para una nueva herramienta con la capacidad para realizar un análisis cuantitativo más preciso, lo que siempre ha sido un reto para la espectroscopía LIBS.

Finalmente, el capítulo 6 está imbricado con el tercer objetivo y describe aplicaciones reales de LIBS. LIBS ha sido empleado con diversas muestras arqueológicas, desde un vaso cerámico a denarios romanos, pasando por huesos de fallecidos en Venecia durante la epidemia de peste. En el análisis del vaso cerámico, LIBS se ha empleado junto a otras técnicas espectroscópicas permitiendo realizar, junto a un análisis tipológico y estilístico siempre necesario para estas muestras, la autenticación del mismo y un análisis del contenido de vaso durante su periodo de uso. Este tipo de análisis múltiples empleando diversas técnicas pueden sumar la fortaleza de cada una para generar una enorme cantidad de información útil sobre el objeto bajo análisis.

En cuanto a los denarios romanos, LIBS se ha empleado desde otro punto de vista. La naturaleza de estas muestras no aconseja el uso de LIBS por su carácter microdestructivo y otras técnicas como la Fluorescencia de rayos-X (XRF) pueden ser más adecuadas. Sin embargo XRF no puede realizar un análisis en profundidad de la muestra, y está demostrado que la composición superficial de estas muestras metálicas puede variar con respecto a la composición interna por diversos procesos de envejecimiento. Por este motivo, un pequeño grupo de monedas ha sido analizado en profundidad con LIBS para certificar que la composición superficial no altera los resultados del análisis XRF. Una vez LIBS ha certificado que el análisis

XRF es válido, las demás muestras pueden ser analizadas con el sistema XRF. Por tanto, LIBS se ha empleado como una herramienta de validación para esta aplicación en concreto.

El último conjunto de muestras arqueológicas analizado está compuesto por un conjunto de huesos de personas fallecidas durante una epidemia de peste en Venecia en el siglo XVI. Los ratios entre diferentes elementos químicos presentes en los huesos pueden ser un indicativo de la dieta seguida por el fallecido durante su vida, y esta dieta puede aportar información sobre la procedencia y modo de vida de dicha persona. Estos huesos han sido analizados con un set-up LIBS para analizar los ratios entre estos elementos y los resultados se han comparado con los ratios calculados con Inductively Coupled plasma – Optical Emission Spectrometry (ICP-OES), una técnica que da unos resultados precisos para estos análisis. Los resultados han sido similares, lo que demuestra la viabilidad del empleo de LIBS para este propósito. Los resultados aportados por ICP-OES son muy precisos, pero la preparación de las muestras es compleja y esta técnica no permite un análisis en profundidad, que sí ha sido realizado con LIBS, lo que son ventajas que justifican el empleo de LIBS.

La última aplicación que muestra este capítulo está relacionada con otro campo diferente, en este caso con la detección de metales preciosos en residuos industriales. Este tipo de análisis se lleva a cabo con XRF, pero la instrumentación es cara y el análisis continuo con rayos-X no es seguro en laboratorio para los operarios. El trabajo desarrollado demuestra que LIBS puede ser una herramienta válida para esta aplicación, y LIBS emplea una instrumentación más económica y es inocua para los operarios.

Para concluir, esta Tesis demuestra que LIBS es una técnica espectroscópica con un futuro prometedor en un amplio rango de aplicaciones. Campos tan diferentes como los sensores de Fibra Óptica o los algoritmos de clasificación pueden ser unidos a los análisis y sistemas LIBS más tradicionales obteniendo nuevas herramientas para mejorar las prestaciones de esta técnica espectroscópica.